Introduction to parton distributions in perturbative QCD

FYSV447 (Jyväskylä Summer School 2018)

Lecturer: Hannu Paukkunen, office FL311

Assistant: Topi Löytäinen, office FL353

Lectures: 13.8–17.8 (Monday to Friday), 9-11, FYS3

Exercises: 14.8 & 16.8 (Tuesday + Thursday), 15-17, FYS3

The parton distributions are:

- **a fundamental measurement**
  — a challenge to understand by non-perturbative QCD.
- **a necessary evil**
  — an essential input to perturbative calculations of signal and background at hadron colliders.

Jon Pumplin

Contents

1 Deeply inelastic scattering and the parton model

1.1 General structure

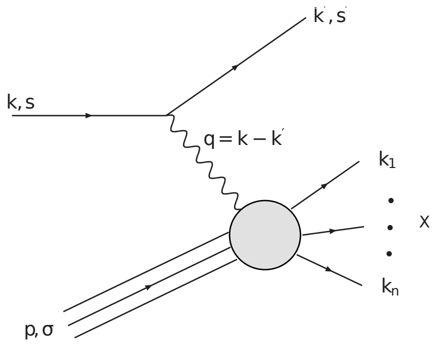

Figure 1: Schematic picture of the deeply inelastic scattering. The variables k and P denote the incoming momenta, whereas k' and $k_1, \ldots, k_n$ are all outgoing. The spin states are marked by s, s' and σ.

In the deeply inelastic scattering (DIS) a lepton projectile hits a target nucleon (here we will implicitly think of a proton target, but in general is can be any hadron) breaking it apart to a state X consisting of a plethora of various particles with invariant mass $M_X^2 \gg M^2$, where M denotes the rest mass of the nucleon. In the simplest case the lepton is an electron or muon and the interaction is dominantly mediated by exchanging a virtual photon, as illustrated in Fig. 1. In the target rest frame, the four-momenta of the particles can be chosen as

$$\begin{aligned} k &= (E, \mathbf{k}) &&= (E, 0, 0, E) \\ k' &= (E', \mathbf{k}') &&= (E', E'\sin\theta\cos\phi, E'\sin\theta\sin\phi, E'\cos\theta) \\ P &= (P^0, \mathbf{P}) &&= (M, 0, 0, 0) \\ q &= (\nu, \mathbf{q}) &&= (E - E', \mathbf{k} - \mathbf{k}'), \end{aligned} \tag{1}$$

where we have neglected the lepton mass m_ℓ. The standard invariant DIS-variables are

$$\begin{aligned} Q^2 &\equiv -q^2 = 4EE'\sin^2(\theta/2) && (\textbf{Virtuality}) \\ x &\equiv \frac{Q^2}{2P\cdot q} = \frac{Q^2}{2M\nu} && (\textbf{Bjorken x}) \\ y &\equiv \frac{P\cdot q}{P\cdot k} = \frac{\nu}{E} && (\textbf{Inelasticity}), \end{aligned} \tag{2}$$

where the latter equalities refer to the target rest frame. The invariant mass W of the final state X is

$$W^2 \equiv (P+q)^2 = M^2 + Q^2\frac{1-x}{x}\,. \tag{3}$$

For lepton-proton scattering we have the condition $W^2 \geq M^2_{\text{proton}}$ following from the baryon-number conservation. From Eq. (3) we see that (for a proton target) $W^2 = M^2_{\text{proton}}$ when $x = 1$. That is, $x = 1$ corresponds to an elastic scattering. The differential, spin-independent cross-section for this process can be written as

$$d\sigma = \frac{1}{4\sqrt{(k\cdot p)^2 - m_\ell^2 M^2}} \frac{d^3\mathbf{k}'}{(2\pi)^3 2E'} \sum_n \int \prod_{i=1}^{n} \frac{d^3\mathbf{k_i}}{(2\pi)^3 2k_i^0} (2\pi)^4 \delta^{(4)}(P + k - k' - \sum_{j=1}^{n} k_j)\overline{|M_n|^2} \tag{4}$$

where the matrix element is

$$M_n = \left[\overline{u}(k', s')(-ie\gamma^\mu)u(k, s)\right] \left(-\frac{ig_{\mu\nu}}{q^2}\right) \langle n, \mathrm{out}|e\hat{J}^\nu(0)|(P, \sigma), \mathrm{in}\rangle \,. \tag{5}$$

Squaring and averaging over the spins,

$$\begin{aligned}\overline{|M_n|^2} = \frac{e^4}{q^4}\, &\underbrace{\frac{1}{2}\sum_{s,s'} \left[\overline{u}(k', s')\gamma^\mu u(k, s)\right] \left[\overline{u}(k', s')\gamma^\nu u(k, s)\right]^*}_{L^{\mu\nu}} \\ &\times \frac{1}{2}\sum_\sigma \langle n, \mathrm{out}|\hat{J}_\mu(0)|(P, \sigma), \mathrm{in}\rangle \langle n, \mathrm{out}|\hat{J}_\nu(0)|(P, \sigma), \mathrm{in}\rangle^*\end{aligned} \tag{6}$$

such that

$4\pi M W_{\mu\nu}$ “hadronic tensor“

$$d\sigma = \frac{1}{2s}\frac{e^4}{q^4}\frac{d^3\mathbf{k}'}{(2\pi)^3 2E'} L^{\mu\nu} \times \boxed{\begin{aligned}&\frac{1}{2}\sum_\sigma \sum_n \int \prod_{i=1}^n \frac{d^3\mathbf{k_i}}{(2\pi)^3 2k_i^0}(2\pi)^4 \delta^{(4)}(P + q - \sum_{j=1}^n k_j) \\ &\langle n, \mathrm{out}|\hat{J}_\mu(0)|(P, \sigma), \mathrm{in}\rangle \langle n, \mathrm{out}|\hat{J}_\nu(0)|(P, \sigma), \mathrm{in}\rangle^* \,.\end{aligned}} \tag{7}$$

That is, we can write the cross section as

$$d\sigma = \frac{4\pi M}{2s}\frac{e^4}{q^4}\frac{d^3\mathbf{k}'}{(2\pi)^3 2E'} L^{\mu\nu} W_{\mu\nu} \tag{8}$$

where e is the QED coupling constant and

$$L^{\mu\nu} \equiv \frac{1}{2}\mathrm{Tr}[\not{k}'\gamma^\mu \not{k}\gamma^\nu] = 2\left[k'^\mu k^\nu + k^\mu k'^\nu - (k \cdot k')g^{\mu\nu}\right] \tag{9}$$

$$\begin{aligned}4\pi M W_{\mu\nu} \equiv\ &\frac{1}{2}\sum_n \sum_\sigma \prod_{i=1}^n \frac{d^3\mathbf{k_i}}{(2\pi)^3 2k_i^0}(2\pi)^4 \delta^{(4)}(P + q - \sum_{j=1}^n k_j) \\ &\langle n, \mathrm{out}|\hat{J}_\mu(0)|(P, \sigma), \mathrm{in}\rangle \langle n, \mathrm{out}|\hat{J}_\nu(0)|(P, \sigma), \mathrm{in}\rangle^*\end{aligned} \tag{10}$$

are the leptonic and hadronic tensors. In contrast to the leptonic tensor $L^{\mu\nu}$, the non-perturbative nature of QCD makes it impossible to compute $W_{\mu\nu}$ directly but its general form can nevertheless be written down without much further input. Indeed, since $L^{\mu\nu}$ is real and symmetric under interchange of indices, the relevant part of the hadronic tensor should satisfy $W_{\mu\nu} = W^*_{\mu\nu} = W_{\nu\mu}$. A further restriction is provided by the Ward identity $q^\mu W_{\mu\nu} = q^\nu W_{\mu\nu} = 0$. The general expression satisfying these conditions can be written as

$$W_{\mu\nu} = -W_1\left(g_{\mu\nu} - \frac{q_\mu q_\nu}{q^2}\right) + \frac{W_2}{M^2}\left(P_\mu - \frac{P \cdot q}{q^2}q_\mu\right)\left(P_\nu - \frac{P \cdot q}{q^2}q_\nu\right), \tag{11}$$

where W_1 and W_2 are, *a priori* unknown coefficients. They can only depend on the momenta P and q, and thus (for Lorentz invariance), on x, Q^2 (neglecting M^2). It is traditional to define the dimensionless structure functions

$$F_1(x, Q^2) \equiv M W_1 \qquad F_2(x, Q^2) \equiv \nu W_2, \tag{12}$$

which, in the $M^2 \ll Q^2$ limit, can be projected from the hadronic tensor as

$$\begin{aligned}
\frac{F_2}{x} &= \left(-g^{\mu\nu} + \frac{12x^2}{Q^2}P^\mu P^\nu\right) MW_{\mu\nu} \qquad (13)\\
F_1 &= \left(-\frac{1}{2}g^{\mu\nu} + \frac{2x^2}{Q^2}P^\mu P^\nu\right) MW_{\mu\nu} = \frac{F_2}{2x} - \left(\frac{4x^2}{Q^2}P^\mu P^\nu\right) MW_{\mu\nu}\,,
\end{aligned}$$

where the proton mass M has been neglected in comparison to Q^2. In terms of the structure functions F_1 and F_2 the cross-section in Eq. (8) can expressed in an invariant way

$$\frac{d^2\sigma}{dxdQ^2} = \frac{4\pi\alpha_{\rm em}^2}{Q^4}\frac{1}{x}\left[xy^2F_1 + F_2\left(1 - y - \frac{xyM^2}{s-M^2}\right)\right], \qquad (14)$$

where $s \equiv (P+k)^2$ denotes the center-of-mass energy, and $\alpha_{\rm em} \equiv e^2/4\pi$ stands for the QED fine-structure constant. Often, the data are presented as **reduced cross sections**, defined as

$$d\sigma_{\rm reduced} \equiv \frac{xQ^4}{2\pi\alpha_{\rm em}^2 Y_+}\frac{d^2\sigma}{dxdQ^2} = F_2 - \frac{y^2}{Y_+}F_{\rm L},$$

where $Y_+ \equiv 1 + (1-y)^2$, and $F_{\rm L} \equiv F_2 - 2xF_1$ is the **longitudinal structure function**. At high Q^2 also a third structure function F_3 appears due to exchange of a Z boson.

1.2 Parton model

The parton model [1, 2] can be motivated by considering the DIS not in the target-rest-frame but in the electron-proton center-of-mass system. In such a frame, the nucleon appears Lorentz contracted, and the time dilatation slows down the intrinsic interaction rate of the fundamental constituents of the nucleon, the partons. During the short period it takes for the electron to traverse across the nucleon, the state of the nucleon wave function can thus be envisioned as being frozen to a superposition of free partons collinear with the nucleon. Mathematically, the parton model is defined by the relation

$$d\sigma_{\rm parton\ model} = \sum_q \int_0^1 d\xi d\hat{\sigma}_0^q(\xi P) f_q(\xi), \qquad (15)$$

where $\hat{\sigma}_0^q(\xi P)$ is the leading order (Born) cross-section for the electron-parton scattering, with the parton carrying a momentum $p = \xi P$. The functions $f_q(\xi)$ are called **parton distributions**, and represent the number density of partons of **flavor** q in the nucleon.

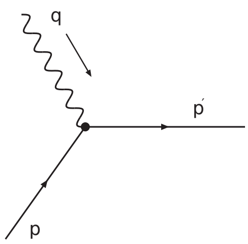

Figure 2: The leading-order diagram for photon-quark interaction.

$$d\hat{\sigma}_0^q(p = \xi P) = \frac{1}{2\hat{s}}\frac{d^3\mathbf{k}'}{(2\pi)^3 2E'}\int \frac{d^3\mathbf{p}'}{(2\pi)^3 2p'^0}(2\pi)^4\delta^{(4)}(p + k - k' - p')\overline{|M_0|^2} \qquad (16)$$

where the leading-order matrix element is

$$M_0 = \left[\overline{u}(k', s'_\ell)(-ie\gamma^\mu)u(k, s_\ell)\right]\left(-\frac{ig_{\mu\nu}}{q^2}\right)\left[\overline{u}(p', s'_q)(-iee_q\gamma^\nu)u(p, s_q)\right] . \tag{17}$$

Squaring & summing,

$$\overline{|M_n|^2} = \frac{e^4}{q^4}\underbrace{\frac{1}{2}\sum_{s_\ell, s'_\ell}\left[\overline{u}(k', s'_\ell)\gamma^\mu u(k, s_\ell)\right]\left[\overline{u}(k', s'_\ell)\gamma^\nu u(k, s_\ell)\right]^*}_{L^{\mu\nu}} \tag{18}$$
$$\times \frac{e_q^2}{2}\sum_{s_q, s'_q}\left[\overline{u}(p', s'_q)\gamma^\mu u(p, s_q)\right]\left[\overline{u}(p', s'_q)\gamma^\nu u(p, s_q)\right]^*$$

such that

$$d\hat{\sigma}_0^q(p = \xi P) = \frac{1}{2\hat{s}}\frac{e^4}{q^4}\frac{d^3\mathbf{k}'}{(2\pi)^3 2E'}L^{\mu\nu} \times \int \frac{d^3\mathbf{p}'}{(2\pi)^3 2p'^0}(2\pi)^4\delta^{(4)}(p + k - k' - p')\frac{e_q^2}{2}\mathrm{Tr}[\not{p}'\gamma^\mu \not{p}\gamma^\nu] . \tag{19}$$

Using the δ-function identity

$$\int \frac{d^3\mathbf{p}'}{2p'^0} = \int d^4p'\theta(p'^0)\delta(p'^2)$$

we get

$$\longrightarrow 4\pi M\hat{W}^q_{\mu\nu} \text{ “quark tensor“}$$

$$d\hat{\sigma}_0^q(p = \xi P) = \frac{1}{2\hat{s}}\frac{e^4}{q^4}\frac{d^3\mathbf{k}'}{(2\pi)^3 2E'}L^{\mu\nu} \times \boxed{\frac{2\pi x}{Q^2}\frac{e_q^2}{2}\mathrm{Tr}[\not{p}'\gamma^\mu \not{p}\gamma^\nu]\delta(\xi - x)} .$$

Using Eq. (15) and noting that $\hat{s} = \xi s$,

$$d\sigma = \sum_q \int d\xi \left[\frac{1}{2\hat{s}}\frac{e^4}{q^4}\frac{d^3\mathbf{k}'}{(2\pi)^3 2E'}L^{\mu\nu}(4\pi M)\hat{W}^q_{\mu\nu}\right] f_q(\xi) \tag{20}$$

$$= \frac{1}{2s}\frac{e^4}{q^4}\frac{d^3\mathbf{k}'}{(2\pi)^3 2E'}L^{\mu\nu} \times \sum_q \int \frac{d\xi}{\xi}(4\pi M)\hat{W}^q_{\mu\nu}f_q(\xi) \tag{21}$$

Comparing now with Eq. (7), we see that the hadronic tensor $W_{\mu\nu}$ in parton model becomes

$$W_{\mu\nu} = \sum_q \int_0^1 \frac{d\xi}{\xi}\hat{W}^q_{\mu\nu}f_q(\xi), \tag{22}$$

where the quark tensor $\hat{W}^q_{\mu\nu}$ is

$$4\pi M\hat{W}^q_{\mu\nu} = \frac{e_q^2}{2}\frac{2\pi x}{Q^2}\mathrm{Tr}[\not{p}'\gamma^\mu \not{p}\gamma^\nu]\delta(\xi - x). \tag{23}$$

From Eq. (13) we see that in order to get $F_{1,2}$, we need the contractions with $g_{\mu\nu}$ and $P_\mu P_\nu$:

$$g_{\mu\nu}\,\mathrm{Tr}[\not{p}'\gamma^\mu \not{p}\gamma^\nu] = -4Q^2 \qquad P_\mu P_\nu\,\mathrm{Tr}[\not{p}'\gamma^\mu \not{p}\gamma^\nu] = 0, \tag{24}$$

so that

$$-g_{\mu\nu}(M\hat{W}^q_{\mu\nu}) = e_q^2 x\delta(\xi - x) \qquad P^\mu P^\nu(M\hat{W}^q_{\mu\nu}) = 0. \tag{25}$$

Consequently, using Eq. (13), the parton model predictions for the structure functions reduce to an electric-charge-weighted sum of the quark distributions,

$$\frac{F_2}{x} = -g^{\mu\nu}(MW_{\mu\nu}) = \sum_q \int_0^1 \frac{d\xi}{\xi}(-g^{\mu\nu}M\hat{W}^q_{\mu\nu})f_q(\xi) = \sum_q e_q^2 f_q(x), \tag{26}$$

$$2xF_1(x) = F_2(x) = \sum_q e_q^2 x f_q(x), \tag{27}$$

and the cross-section in Eq. (14) can be written as

$$\frac{d^2\sigma}{dxdQ^2} = \frac{d^2\hat{\sigma}_0}{dxdQ^2}\sum_q e_q^2 f_q(x), \tag{28}$$

where $\hat{\sigma_0}$ denotes the partonic Born cross-section

$$\frac{d^2\hat{\sigma}_0}{dxdQ^2} \equiv \frac{4\pi\alpha_{\rm em}^2}{Q^4}\left[\frac{y^2}{2} + \left(1 - y - \frac{xyM^2}{s-M^2}\right)\right]. \tag{29}$$

It is a prediction of the parton model that the structure functions $F_{1,2}$ are only functions of x, and should not depend on Q^2 in the $Q^2 \gg M^2$ limit. This phenomenon, termed as **Bjorken-scaling**, was indeed observed in the early SLAC experiments providing direct evidence about the inner constituents of the nucleon. Later experiments which have covered a larger domain in the (x, Q^2)-plane have revealed, however, that the Q^2-independence of the structure functions $F_{1,2}$, although a good first approximation, is not exact. Such deviations are clear e.g. in Fig. 3 and Fig. 4, which show some experimental data for the proton structure function F_2. These **scaling violations**, as they are nowadays called, can however be fully explained by QCD dynamics — by the so-called DGLAP equations.

2 DGLAP evolution equations: resummation of leading logarithms

2.1 Origin of the scaling violations

Due to the inclusive nature of the deeply inelastic scattering nothing forbids having additional QCD particles in the final state. First such corrections to the Born-level matrix element originate from a radiation of a real gluon as shown in Fig. 5. Both of these diagrams are divergent as the intermediate quark propagators are close to being on-shell:

$$\begin{aligned}(p-k)^2 &= -2p^0k^0\,(1-\cos\theta) \ \to 0,\\ \left(p'+k\right)^2 &= -2p'^0k^0\left(1-\cos\theta'\right) \to 0\,,\end{aligned}$$

for massless quarks. This can happen either if the momentum of the emitted particle goes to zero, $k^0, p'^0 \to 0$, or if the emission is collinear with the incoming or the outgoing quark $\theta, \theta' \to 0$. These are archetypes of **infrared** and **collinear** singularities, respectively. There are also same kind of divergences stemming from the virtual corrections, and it turns out that all but the collinear divergence related to the gluon radiation from the *incoming quark* will eventually cancel. In what follows, we will see how to extract these divergences and how their resummation gives rise to the partonic DGLAP evolution — the Q^2-dependence of the parton distributions observed in the experiments (e.g. in Figure 3).

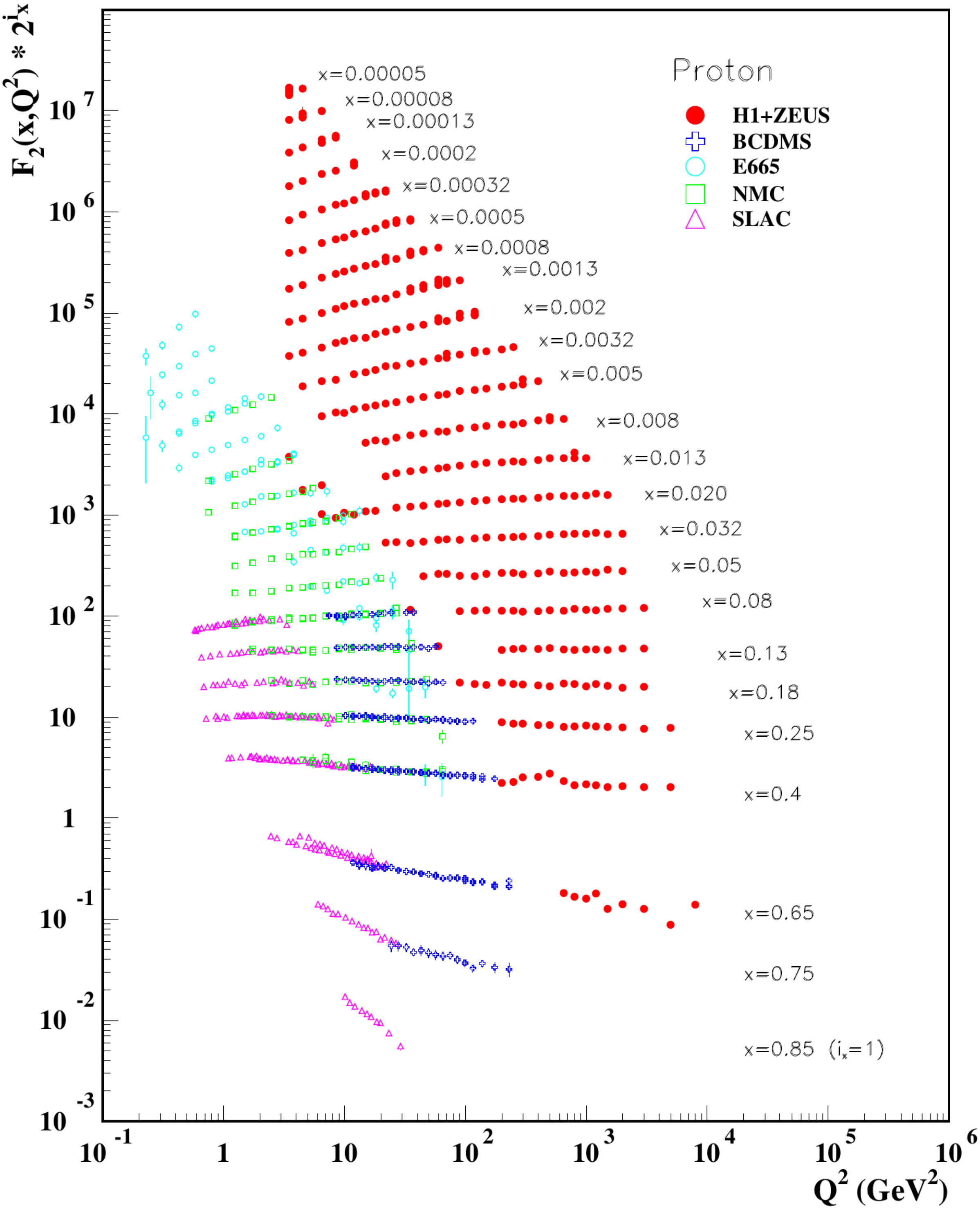

Figure 3: Experimental data for proton structure function F_2. Figure from Ref. [3].

2.2 One gluon emission

The partonic DIS cross section with one extra gluon emission can be written as

$$d\hat{\sigma}^{\ell q\to\ell qg} = \frac{1}{2\hat{s}}\frac{d^3\mathbf{k}'}{(2\pi)^3 2E'}\int\frac{d^3\mathbf{p}'}{(2\pi)^3 2p'^0}\frac{d^3\mathbf{k}}{(2\pi)^3 2k^0}(2\pi)^4\delta^{(4)}(p+q-p'-k)\overline{|\mathcal{M}|^2} \tag{30}$$

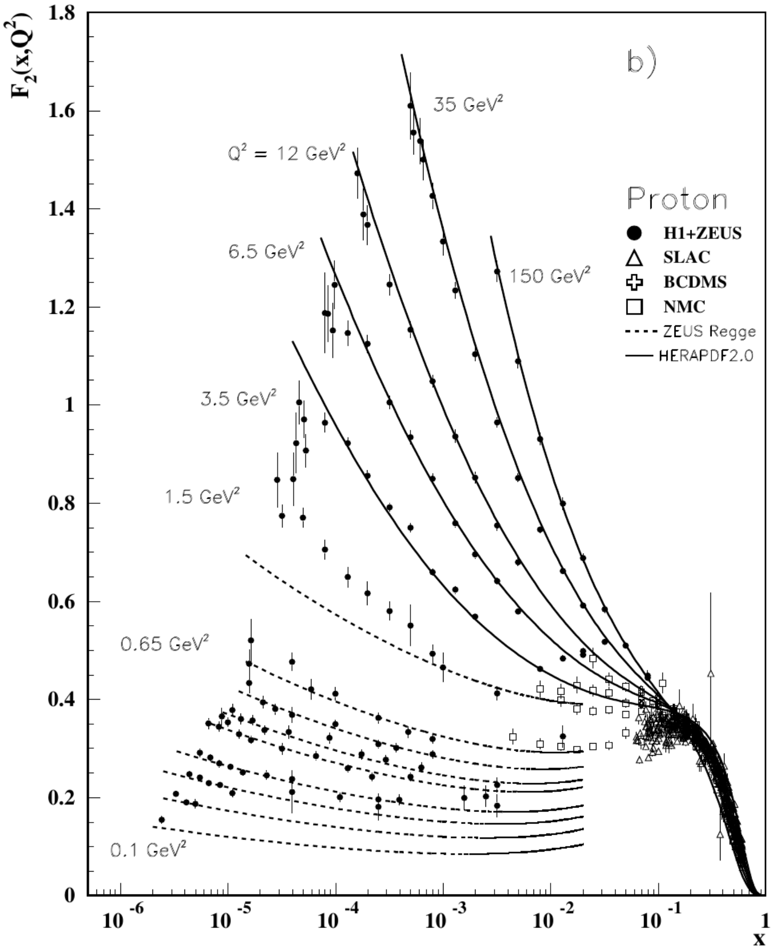

Figure 4: Experimental data for proton structure function F_2. Figure from Ref. [3].

where the matrix element is

$$i\mathcal{M} = \left[\overline{u}(k', s'_\ell)(ie\gamma^\mu)u(k, s_\ell)\right]\left(-\frac{ig_{\mu\nu}}{q^2}\right)\left[\overline{u}(p', s_{p'})(iee_q\gamma^\mu)\frac{i(\not{p}-\not{k})}{(p-k)^2}(ig_s t^a_{ij}\not{\epsilon}_\lambda)u(p, s_p)\right. \tag{31}$$
$$\left. + \, \overline{u}(p', s_{p'})(ig_s t^a_{ij}\not{\epsilon}_\lambda)\frac{i(\not{p}'+\not{k})}{(p'+k)^2}(iee_q\gamma^\mu)u(p, s_p)\right].$$

We write squared and spin/colour summed matrix element as

$$|\mathcal{M}|^2 = \frac{e^4}{q^4}L_{\mu\nu}\mathcal{M}^{\mu\nu}_{\gamma * q\to qg} \tag{32}$$

with

$$\mathcal{M}^{\mu\nu}_{\gamma * q\to qg} = g_s^2 e_q^2 \frac{1}{2}\sum_{\text{spins}}\frac{1}{3}\sum_{\text{colours}} t^a_{ij}(t^a_{ij})^*\left\{\frac{1}{(p-k)^4}\text{Tr}\left[\not{p}'\gamma^\mu(\not{p}-\not{k})\not{\epsilon}_\lambda\not{p}\not{\epsilon}^*_\lambda(\not{p}-\not{k})\gamma^\nu\right]\right. \tag{33}$$
$$+\frac{1}{(p'+k)^4}\text{Tr}\left[\not{p}'\not{\epsilon}_\lambda(\not{p}'+\not{k})\gamma^\mu\not{p}\gamma^\nu(\not{p}'+\not{k})\not{\epsilon}^*_\lambda\right]$$
$$\left.+\frac{2}{(p-k)^2(p'+k)^2}\text{Tr}\left[\not{p}'\gamma^\mu(\not{p}-\not{k})\not{\epsilon}_\lambda\not{p}\gamma^\nu(\not{p}'+\not{k})\not{\epsilon}^*_\lambda\right]\right\}.$$

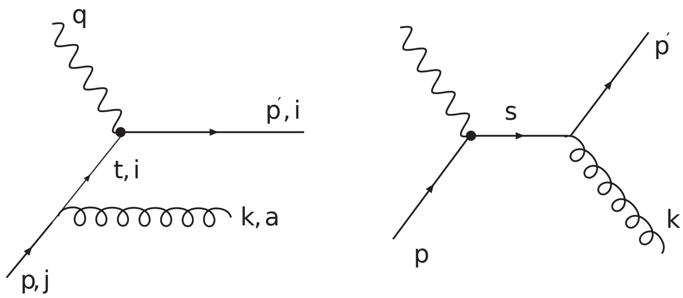

Figure 5: Real gluon radiation. The letter i, j, a are the color indices.

Rather than drawing graphs for matrix elements, for the rest of this Chapter, we will draw the graphs in the cut diagram notation (see e.g. [4]) directly for the cross-sections. The square of the diagrams in Fig. 5 can be represented as four cut diagrams shown in Fig. 6. Although the

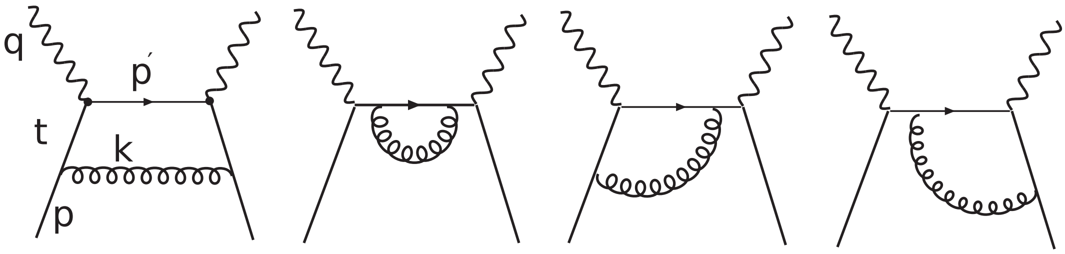

Figure 6: Diagrams representing the $\gamma^* q \to qg$ process. It should be understood that the parton lines in the middle are real, on-shell particles.

full squared matrix element is certainly gauge invariant, the contribution of an individual graph depends on the choice of gauge. Here, we'll be mostly interested in the collinear singularities and, as it turns out, it is advantageous to perform the calculations in an **axial gauge**, as it is the first diagram alone in Fig. 6 that is responsible for collinearly divergent behaviour. We'll call this type of graph as a **ladder diagram**.

2.2.1 Axial gauge

The class of axial gauges is specified by a gauge-fixing term $-\left(n \cdot G\right)^2/(2\xi)$ in the QCD Lagrangian where G denotes the gluon field, n is an arbitrary four-vector and ξ is a gauge parameter. The gluon propagator in this gauge is

$$D_{\mu\nu}(k) \quad = \quad \frac{-i}{k^2 + i\epsilon}\left[g_{\mu\nu} - \frac{k_\mu n_\nu + k_\nu n_\mu}{k \cdot n} + \frac{\xi k^2 + n^2}{(k \cdot n)^2} k_\mu k_\nu\right]. \tag{34}$$

The sum over the two physical polarization states $\epsilon^{\lambda_{1,2}}(k)$ ($k^2 = 0$), obeying $k \cdot \epsilon^{\lambda_i}(k) = 0$ and $n \cdot \epsilon^{\lambda_i}(k) = 0$, normalized by $\epsilon^{\lambda_i}(k) \cdot \epsilon^{\lambda_i}(k) = -1$, reads

$$\sum_\lambda \epsilon_\mu^\lambda(k) \epsilon_\nu^{*\lambda}(k) \quad = \quad -g_{\mu\nu} + \frac{k_\mu n_\nu + k_\nu n_\mu}{(k \cdot n)} - \frac{n^2 k_\mu k_\nu}{(k \cdot n)^2}. \tag{35}$$

Usually, it is convenient to choose $\xi = 0$ and $n^2 = 0$ which specifies a **light-cone gauge**. The axial gauges are sometimes called **physical gauges**: the reason for this is most distinct in the light-cone gauge as any propagator in a Feynman diagram can be replaced by the polarization sum over the physical states:

$$D_{\mu\nu}(k) = \frac{i}{k^2} \sum_{\lambda} \epsilon_{\mu}^{\lambda}(k) \epsilon_{\nu}^{*\lambda}(k). \tag{36}$$

A convenient choice for the light-like axial vector n ($n = 0$) in the present problem is

$$n \equiv q + \eta p, \qquad \eta \equiv \frac{-q^2}{2p \cdot q}. \tag{37}$$

2.2.2 Sudakov decomposition

In extracting the dominant part of the squared matrix elements, it is convenient to parametrize the momenta of the outgoing partons by a Sudakov decomposition [5],

$$k = (1-z)p + \beta n + k_{\perp}, \qquad \beta = \frac{-k_{\perp}^2}{2(1-z)p \cdot q}, \tag{38}$$

where $k_{\perp}$ is a space-like 4-vector orthogonal to n and p: $k_T^2 < 0$, $n \cdot k_T = p \cdot k_T = 0$. For example, the momenta can be parametrized as,

$$\begin{aligned}
p &= (\frac{\xi}{2x}Q, 0, 0, \frac{\xi}{2x}Q) \\
n &= (Q/2, 0, 0, -Q/2) \\
q &= (0, 0, 0, -Q) \\
k_{\perp} &= (0, \mathbf{k}_{\perp}, 0) \\
k &= \left(\frac{Q}{2} \left[(1-z)\frac{\xi}{x} + \frac{-k_{\perp}^2}{Q^2} \frac{x}{\xi(1-z)} \right], \mathbf{k}_{\perp}, \frac{Q}{2} \left[(1-z)\frac{\xi}{x} - \frac{-k_{\perp}^2}{Q^2} \frac{x}{\xi(1-z)} \right] \right)
\end{aligned} \tag{39}$$

where $Q = \sqrt{Q^2}$. In such a frame the interpretation of $k_{\perp}^2 = -\mathbf{k}_{\perp}^2$ as the transverse momentum is evident. In these coordinates,

$$t^2 = (p-k)^2 = k_{\perp}^2/(1-z),$$

which suggests that the collinear divergences should be found by looking for the $k_{\perp}^2 \to 0$ limit.

2.2.3 Evaluation of the ladder diagram

The part of $(\mathcal{M}_{\gamma * q \to qg})_{\mu\nu}$ corresponding to the first diagram in Fig. 6 reads

$$(\mathcal{M}_{\gamma * q \to qg}^{\text{Ladder}})_{\mu\nu} = C_F g_s^2 \frac{e_q^2}{2} \sum_{\text{pol}} \frac{1}{t^4} \text{Tr} \left[\not{p}' \gamma_{\mu} \not{t} \not{\epsilon} \not{p} \not{\epsilon}^* \not{t} \gamma_{\nu} \right], \quad t = p - k \tag{40}$$

where the color factor $C_F = 4/3$ arises from (see Fig. 5)

$$\frac{1}{3} \sum_{i,j,a} t_{ij}^a (t_{ij}^a)^* = \frac{1}{3} \sum_a \text{Tr}(t^a t^a) = \frac{4}{3} = C_F.$$

Using the polarization sum Eq. (35) we find

$$\sum_{\rm pol} \not\epsilon \not p \not\epsilon^* = \frac{2}{1-z} \left(\not k + \beta \not n\right), \tag{41}$$

and after a short calculation

$$\not t \left(\not k + \beta \not n\right) \not t = \left(\frac{1+z^2}{1-z}\right) (-k_\perp^2) \not p + \mathcal{O}(\not k_\perp k_\perp^2), \tag{42}$$

where the remaining terms are higher order in $k_\perp$ and will not contribute to the collinear divergence. In total,

$$(\mathcal{M}^{\rm Ladder}_{\gamma * q \to qg})^2_{\mu\nu} = g_s^2 C_F \frac{2(1-z)}{-k_\perp^2} \left(\frac{1+z^2}{1-z}\right) \times \frac{e_q^2}{2} {\rm Tr}\left[\not p' \gamma_\mu \not p \gamma_\nu\right] + \cdots . \tag{43}$$

It is essential that the last combination of terms is nothing but the squared matrix element in the Born approximation, see Eq. (19). Supplying the phase-space element in the Sudakov variables

$$\frac{d^3\mathbf{k}}{(2\pi)^3 2k^0} = \frac{1}{16\pi^2} \frac{dz}{1-z} d\mathbf{k}_\perp^\mathbf{2}, \tag{44}$$

one obtains

$$\frac{d^3\mathbf{k}}{(2\pi)^3 2k^0} (\mathcal{M}^{\rm Ladder}_{\gamma * q \to qg})^2_{\mu\nu} = \frac{d\mathbf{k}_\perp^\mathbf{2}}{\mathbf{k}_\perp^\mathbf{2}} dz \left(\frac{\alpha_s}{2\pi}\right) P_{qq}(z) \times \frac{e_q^2}{2} {\rm Tr}\left[\not p' \gamma_\mu \not p \gamma_\nu\right] + \cdots , \tag{45}$$

where

$$P_{qq}(z) \equiv C_F \left(\frac{1+z^2}{1-z}\right) \tag{46}$$

is the so-called *Altarelli-Parisi splitting function* associated with the unpolarized quark → quark transition. In the collinear limit, the variable z is readily interpreted as the momentum fraction of the incoming quark left after emitting a gluon. The contribution to the quark tensor $\hat{W}^q_{\mu\nu}$ is

$$\begin{aligned} 4\pi M \hat{W}^q_{\mu\nu} &= \int \frac{d^3\mathbf{p}'}{(2\pi)^3 2p'^0} \int \frac{d^3\mathbf{k}}{(2\pi)^3 2k^0} (\mathcal{M}^{\rm Ladder}_{\gamma * q \to qg})^2_{\mu\nu} (2\pi)^4 \delta^{(4)}(p+q-k-p') \\ &= 2\pi \int \frac{d^3\mathbf{k}}{(2\pi)^3 2k^0} (\mathcal{M}^{\rm Ladder}_{\gamma * q \to qg})^2_{\mu\nu}\, \delta(p'^2) \theta(p'^0). \end{aligned}$$

The on-shell condition $p'^2 = 0$ appearing in the δ function above is now

$$0 = p'^2 = (p+q-k)^2 = -Q^2 \left(1 - \frac{z\xi}{x}\right) - \frac{\mathbf{k}_\perp^\mathbf{2}}{1-z} \left(1 - \frac{x}{\xi}\right) . \tag{47}$$

Solving this for ξ yields two solutions, which in $\mathbf{k}_\perp^\mathbf{2} \to 0$ limit behave as

$$\xi_+ = \frac{x}{z} \left(1 + \frac{\mathbf{k}_\perp^\mathbf{2}}{Q^2}\right) + \mathcal{O}(\mathbf{k}_\perp^\mathbf{4}), \quad \xi_- = \frac{\mathbf{k}_\perp^\mathbf{2}}{Q^2} \frac{x}{1-z} + \mathcal{O}(\mathbf{k}_\perp^\mathbf{4}) . \tag{48}$$

The latter one does not give rise to a collinear pole as the quark propagator behaves as $1/t^2 = (1-z)/k_\perp^2 \to x/(\xi Q^2)$, $x < \xi < 1$. Thus, we identify $\xi = \xi_+$, and neglecting all $\mathcal{O}(k_\perp^2)$ terms which would cancel the collinear singularity in Eq. (45),

$$p'^2 \approx Q^2 \left(\frac{\xi z}{x} - 1\right) \tag{49}$$

and

$$g_{\mu\nu}\,\mathrm{Tr}[\not p'\gamma^\mu\not p\gamma^\nu] \approx -4Q^2\frac{\xi}{x} \qquad P_\mu P_\nu\,\mathrm{Tr}[\not p'\gamma^\mu\not p\gamma^\nu] = 0. \tag{50}$$

Thus, the dominant $\mathcal{O}(\alpha_s)$ piece in the quark tensor is

$$-g^{\mu\nu}M\hat{W}^q_{\mu\nu} = e_q^2\left[\left(\frac{\alpha_s}{2\pi}\right)\int\frac{dz}{z}P_{qq}(z)\int\frac{d\mathbf{k}_\perp^2}{\mathbf{k}_\perp^2}\right]\xi\delta\left(\xi-\frac{x}{z}+\mathcal{O}(\mathbf{k}_\perp^2)\right)+\cdots\,, \tag{51}$$

which contributes to the hadronic tensor by

$$-g^{\mu\nu}MW_{\mu\nu} = \sum_q\int\frac{d\xi}{\xi}(-g^{\mu\nu}M\hat{W}^q_{\mu\nu})f_q\left(\xi\right) = \sum_q e_q^2\left[\left(\frac{\alpha_s}{2\pi}\right)\int_x^1\frac{dz}{z}P_{qq}(z)\int_0^{\mathbf{k}^2_{\perp\max}}\frac{d\mathbf{k}_\perp^2}{\mathbf{k}_\perp^2}\right]f_q\left(\frac{x}{z}\right)+\cdots\,. \tag{52}$$

The upper integration limits for $\mathbf{k}_\perp^2$ and z can be found by requirement $p'^0 > 0$,

$$p'^0 = p^0+q^0-k^0 = \frac{\sqrt{Q^2}}{2}\left[\frac{z\xi}{x}-\frac{\mathbf{k}_\perp^2}{Q^2}\frac{x}{\xi(1-z)}\right]\geq 0\,, \tag{53}$$

which, in the limit $\xi = x/z$ gives

$$\mathbf{k}_\perp^2 \leq \frac{1-z}{z}Q^2 = \mathbf{k}^2_{\perp\max}, \quad z\leq\frac{Q^2}{Q^2+\mathbf{k}_\perp^2} = 1-\frac{\mathbf{k}_\perp^2}{Q^2}+\mathcal{O}(\mathbf{k}_\perp^4) \tag{54}$$

The minimum $\mathbf{k}_\perp^2$ is zero, so $z<1$. As anticipated, the expression in Eq. (52) is divergent in $\mathbf{k}_\perp^2\to 0$, and $z\to 1$ limits. We may regulate the integrals by introducing a small cut-off mass m for $\mathbf{k}_\perp^2$,

$$\int_x^{1-\frac{m^2}{Q^2}}\frac{dz}{z}P_{qq}(z)\int_{m^2}^{\mathbf{k}^2_{\perp\max}}\frac{d\mathbf{k}_\perp^2}{\mathbf{k}_\perp^2}f_q\left(\frac{x}{z}\right) = \int_x^{1-\frac{m^2}{Q^2}}\frac{dz}{z}P_{qq}(z)\log\left(\frac{Q^2}{m^2}\frac{1-z}{z}\right)f_q\left(\frac{x}{z}\right)\,. \tag{55}$$

The singularity at $z=1$ can be written in terms of distributions:

$$\begin{aligned}
&\log\left(\frac{Q^2}{m^2}\right)\int_0^{1-\frac{m^2}{Q^2}}\left[\frac{1+z^2}{1-z}\right]\left[\frac{1}{z}f_q\left(\frac{x}{z}\right)-f_q\left(x\right)+f_q\left(x\right)\right]\\
=&\log\left(\frac{Q^2}{m^2}\right)\int_0^1\left[\frac{1+z^2}{1-z}\right]\left[\frac{1}{z}f_q\left(\frac{x}{z}\right)-f_q\left(x\right)\right]+\left[2\log^2\left(\frac{Q^2}{m^2}\right)-\frac{3}{2}\log\left(\frac{Q^2}{m^2}\right)\right]f(x)\\
=&\log\left(\frac{Q^2}{m^2}\right)\int_0^1\frac{dz}{z}\left(\frac{1+z^2}{1-z}\right)_+f_q\left(\frac{x}{z}\right)+\left[2\log^2\left(\frac{Q^2}{m^2}\right)-\frac{3}{2}\log\left(\frac{Q^2}{m^2}\right)\right]f(x)\,,
\end{aligned} \tag{56}$$

where we have used **plus distributions**,

$$\begin{aligned}
\int_0^1 dzh(z)\left(\frac{1+z^2}{1-z}\right)_+ &= \int_0^1 dz\left(\frac{1+z^2}{1-z}\right)\left[h(z)-h(1)\right]\,,\\
\int_0^{x<1} dzh(z)\left(\frac{1+z^2}{1-z}\right)_+ &= \int_0^x dz\left(\frac{1+z^2}{1-z}\right)h(z).
\end{aligned} \tag{57}$$

All but the first term in Eq. (56) including the rest of Eq. (55), are either finite or correspond to $z\to 1$ singularity (when the emitted gluon is arbitrarily soft). It so happens that the $z\to 1$ divergences will cancel against virtual corrections. However, the division in Eq. (56) to plus distribution and $\log(Q^2/m^2)$ terms is not unique, and from the current calculation it is impossible to say what the "correct" splitting function P_{qq} would be. We shall return to this in Section 2.6, and for the moment we simply write the dominant correction to the hadronic tensor in the collinear limit as

$$-g^{\mu\nu}MW_{\mu\nu}=\sum_q\int\frac{d\xi}{\xi}(-g^{\mu\nu}M\hat{W}^q_{\mu\nu})=\left(\frac{\alpha_s}{2\pi}\right)\log\left(\frac{Q^2}{m^2}\right)\sum_q e_q^2\int_x^1\frac{dz}{z}P_{qq}(z)f_q\left(\frac{x}{z}\right)+\cdots. \tag{58}$$

Comparing with the parton-model expression Eq. (26), we immediately see that the contribution to the DIS cross-section is proportional to the partonic cross section $d^2\hat{\sigma}_0$, and adding this and the LO result, we have

$$\frac{d^2\sigma}{dxdQ^2}\stackrel{\text{LL}}{=}\frac{d^2\hat{\sigma}_0}{dxdQ^2}\sum_q e_q^2\left[1+\left(\frac{\alpha_s}{2\pi}\right)\log\left(\frac{Q^2}{m^2}\right)P_{qq}\right]\otimes f_q, \tag{59}$$

where the designation LL means that we kept only the leading logarithmic contribution, and the shorthand notation $\otimes$ stands for the convolution

$$\begin{aligned}P_{qq}\otimes f_q &\equiv \int_x^1\frac{dz}{z}P_{qq}(z)f_q\left(\frac{x}{z}\right) = f_q\otimes P_{qq},\\ 1\otimes f_q &\equiv \int_x^1\frac{dz}{z}\delta(1-z)f_q\left(\frac{x}{z}\right)=f_q(x).\end{aligned} \tag{60}$$

Since the left-hand side of Eq. (59) is a measurable, finite, quantity the non-perturbative parton density f_q is inevitably intertwined with the arbitrary cut-off scale m^2 such that the cross-section is finite.

2.3 Multiple gluon emissions

Based on the previous section, it is natural to expect to find two similar collinear divergences as in Eq. (59) if double gluon emission, shown in Fig. 7, is considered. This is indeed the case and employing the method introduced earlier one can extract an $\alpha_s^2\log^2(Q^2/m^2)$ contribution to cross-section Eq. (59). This is how it goes.

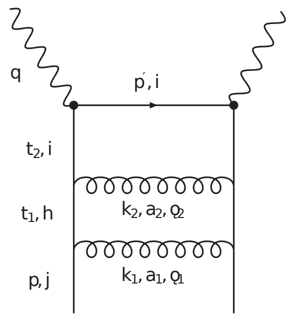

Figure 7: Ladder graph for two-gluon emission. Momenta of the produced gluons with polarizations ϵ_1,ϵ_2 are denoted by k_1,k_2, and the intermediate quark momenta are $t_1\equiv p-k_1$, $t_2\equiv p-k_1-k_2$. The color indices are denoted by i,j,h,a_1,a_2.

The squared and spin-summed matrix element for the ladder diagram in Fig. 7 reads

$$|\mathcal{M}^{\rm Ladder}_{\gamma * q\to q,2g}|^2_{\mu\nu} \;=\; g_s^4\frac{e_q^2}{2}C_F^2\sum_{\rm pol}\frac{1}{t_1^4t_2^4}{\rm Tr}\left[\not p'\gamma_\mu \not t_2\not\epsilon_2\not t_1\not\epsilon_1\not p\not\epsilon_1^*\not t_1\not\epsilon_2^*\not t_2\gamma_\nu\right] \tag{61}$$

where the color factor $C_F^2 = (4/3)^2$ arises in the following way (summation over all indices is implicit):

$$\begin{aligned}
&\frac{1}{3}(t^{a_2}_{ih}t^{a_1}_{hj})(t^{a_2}_{is}t^{a_1}_{sj})^* = \frac{1}{3}(t^{a_2}_{ih}t^{a_1}_{hj})(t^{a_2}_{si}t^{a_1}_{js})\\
=\;& \frac{1}{3}(t^{a_1}t^{a_1})_{hs}(t^{a_2}t^{a_2})_{sh}\\
=\;& \frac{1}{3}{\rm Tr}(t^{a_1}t^{a_1})\frac{1}{3}{\rm Tr}(t^{a_2}t^{a_2}) = \left(\frac{4}{3}\right)\left(\frac{4}{3}\right) = C_F^2,
\end{aligned} \tag{62}$$

where I used $(t^at^a)_{hs} = (1/3)\,\delta_{hs}$. Introducing the Sudakov decomposition for the lower gluon momentum

$$k_1 \;=\; (1-z_1)p+\beta_1 n + k_{1\perp}, \qquad \beta_1 = \frac{-k_{1\perp}^2}{2(1-z_1)p\cdot q}, \tag{63}$$

one immediately obtains, reading from the preceding calculation, that

$$\sum_{{\rm pol}_1}\not t_1\not\epsilon_1\not p\not\epsilon_1^*\not t_1 = \frac{2}{1-z_1}\left(\frac{1+z_1^2}{1-z_1}\right)(-k_{1\perp}^2)\not p+\ldots, \tag{64}$$

where I have again omitted the terms higher order in $k_{1\perp}$. In the same way, writing the Sudakov decomposition for the upper gluon momentum as

$$k_2 = z_1(1-z_2)p+\beta_2 n+k_{2\perp}, \qquad \beta_2 = \frac{-k_{2\perp}^2}{2z_1(1-z_2)p\cdot q}, \tag{65}$$

and dropping terms higher order in $k_{1\perp}$ and $k_{2\perp}$, one finds the leading contribution

$$\sum_{{\rm pol}_2}\not t_2\not\epsilon_2\not p\not\epsilon_2^*\not t_2 = \frac{2}{1-z_2}\left(\frac{1+z_2^2}{1-z_2}\right)(-k_{2\perp}^2)\not p+\ldots. \tag{66}$$

Thus, the squared matrix element (61) acquires a form

$$\begin{aligned}
|\mathcal{M}^{\rm Ladder}_{\gamma * q\to q,2g}|^2_{\mu\nu} \;=\;& g_s^4\frac{-k_{1\perp}^2}{t_1^4}\left[\frac{2P_{qq}(z_1)}{1-z_1}\right]\frac{-k_{2\perp}^2}{t_2^4}\left[\frac{2P_{qq}(z_2)}{1-z_2}\right]\\
&\frac{e_q^2}{2}{\rm Tr}\left[\not p'\gamma_\mu\not p\gamma_\nu\right]+\cdots,
\end{aligned} \tag{67}$$

where the last factor is again the Born matrix-element that has penetrated through the calculation. If there were not the factors $t_{1,2}^4$ in the denominator, the leading factors for both emitted gluons would be identical. However,

$$\begin{aligned}
t_1^2 \;&=\; \frac{k_{1\perp}^2}{1-z_1}\\
t_2^2 \;&=\; \frac{k_{2\perp}^2}{1-z_2}+\frac{1-z_1(1-z_2)}{1-z_1}k_{1\perp}^2+k_{1\perp}\cdot k_{2\perp},
\end{aligned} \tag{68}$$

where the latter one looks bad. In the region of phase space where $-k_{1\perp}^2 < -k_{2\perp}^2$ one can power expand Eq. (67) in $k_{1\perp}^2/k_{2\perp}^2$, schematically

$$|\mathcal{M}^{\text{Ladder}}_{\gamma * q \to q, 2g}|^2_{\mu\nu} \propto \frac{1}{k_{1\perp}^2}\frac{1}{k_{2\perp}^2}\left[1 + A\left(\frac{k_{1\perp}^2}{k_{2\perp}^2}\right) + B\left(\frac{k_{1\perp}^2}{k_{2\perp}^2}\right)^2 + \ldots\right] \tag{69}$$

where the odd powers of $k_{1\perp}$ are absent as they would vanish upon integration. Whereas the integration over the first term gives the leading double logarithm,

$$\int_{m^2}^{Q^2} \frac{d\mathbf{k}_{2\perp}^2}{\mathbf{k}_{2\perp}^2} \int_{m^2}^{\mathbf{k}_{2\perp}^2} \frac{d\mathbf{k}_{1\perp}^2}{\mathbf{k}_{1\perp}^2} = \frac{1}{2!}\log^2\left(\frac{Q^2}{m^2}\right), \tag{70}$$

the rest can give only a single logarithm. In the opposite transverse momentum ordering $-k_{1\perp}^2 > -k_{2\perp}^2$, one again obtains only single logarithms. Thus, the leading contribution stems

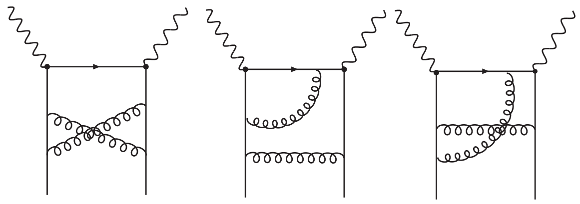

Figure 8: Diagrams for two-gluon emission that do not contain double-logarithms.

from the transverse momentum ordering $-k_{1\perp}^2 < -k_{2\perp}^2$. In fact, from Eq. (70) we see that the dominant region is $-k_{1\perp}^2 \ll -k_{2\perp}^2$ for the emitted gluons. In total,

$$\begin{aligned}|\mathcal{M}^{\text{Ladder}}_{\gamma * q \to q, 2g}|^2_{\mu\nu} \overset{\text{LL}}{=}\ & \frac{1-z_1}{-k_{1\perp}^2}\left[2g_s^2 P_{qq}(z_1)\right]\frac{1-z_2}{-k_{2\perp}^2}\left[2g_s^2 P_{qq}(z_2)\right] \\ & \frac{e_q^2}{2}\text{Tr}\left[\not{p}'\gamma_\mu \not{p}\gamma_\nu\right],\end{aligned} \tag{71}$$

Following the same steps as earlier, we find

$$\begin{aligned}-g^{\mu\nu} M\hat{W}^{q\to q,2g}_{\mu\nu} &= e_q^2 \quad \frac{1}{2}\left[\frac{\alpha_s}{2\pi}\log\left(\frac{Q^2}{m^2}\right)\right]^2 \int \frac{dz_2}{z_2}P_{qq}(z_2)\int\frac{dz_1}{z_1}P_{qq}(z_1) \\ & \quad \xi\delta\left(\xi - \frac{x}{z_1 z_2}\right),\end{aligned} \tag{72}$$

which contributes to the hadronic tensor by

$$-g^{\mu\nu} M\hat{W}_{\mu\nu} \quad = \quad \sum_q e_q^2 \frac{1}{2}\left[\frac{\alpha_s}{2\pi}\log\left(\frac{Q^2}{m^2}\right)\right]^2 P_{qq}\otimes P_{qq}\otimes f_q. \tag{73}$$

The convolution between three objects above is defined by

$$P_{qq}\otimes P_{qq}\otimes f_q = \int_x^1 \frac{dz_2}{z_2}P_{qq}(z_2)\int_{x/z_2}^1 \frac{dz_1}{z_1}P_{qq}(z_1) f_q\left(\frac{x}{z_1 z_2}\right), \tag{74}$$

with obvious extension to convolutions between an arbitrary number of functions. Thus, to $\mathcal{O}(\alpha_s^2)$, the leading logarithms organize themselves as

$$\frac{d^2\sigma}{dxdQ^2} \stackrel{\text{LL}}{=} \frac{d^2\hat{\sigma}_0}{dxdQ^2} \sum_q e_q^2 \left[1 + \left(\frac{\alpha_s}{2\pi}\right) \log\left(\frac{Q^2}{m^2}\right) P_{qq} \right. \\ \left. + \frac{1}{2}\left(\frac{\alpha_s}{2\pi}\right)^2 \log^2\left(\frac{Q^2}{m^2}\right) P_{qq} \otimes P_{qq} \right] \otimes f_q. \tag{75}$$

Based on a similar reasoning as in the end of the previous subsection, the diagrams like those in Fig. 8 cannot contain $\mathcal{O}(\alpha_s^2 \log^2(Q^2/m^2))$ terms in the axial gauge — it is the ladder diagram in Fig. 7 alone that gives the leading logarithmic singularity.

The generalization to an arbitrary number of collinear gluon emissions from the initial quark is now quite straightforward: For n emitted gluons the leading logarithms originate from the region of the phase space where the transverse momenta are **strongly ordered**

$$-k_{1\perp}^2 \ll -k_{2\perp}^2 \ll \cdots \ll -k_{n-1\perp}^2 \ll -k_{n\perp}^2 \ll Q^2,$$

and the longitudinal momenta ordered as (the quark loses momentum as gluons are emitted)

$$1 \geq z_1 \geq z_2 \geq \cdots \geq z_n \geq x\,.$$

The contribution to the DIS cross-section is

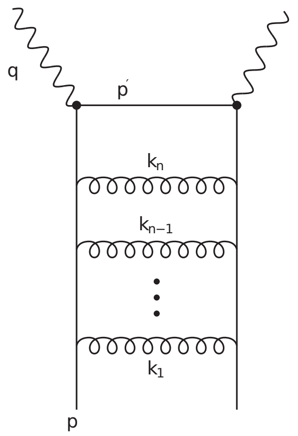

Figure 9: Ladder graph for n-gluon emission.

$$\frac{d^2\hat{\sigma}_0}{dxdQ^2} \sum_q e_q^2 \frac{1}{n!}\left(\frac{\alpha_s}{2\pi}\right)^n \log^n\left(\frac{Q^2}{m^2}\right) \underbrace{P_{qq} \otimes P_{qq} \otimes \cdots \otimes P_{qq}}_{n\,\text{times}} \otimes f_q. \tag{76}$$

Thus, the leading logarithm contributions to the DIS cross-section constitute a series which is formally an exponential

$$\frac{d^2\sigma}{dxdQ^2} \stackrel{\text{LL}}{=} \frac{d^2\hat{\sigma}_0}{dxdQ^2} \sum_q e_q^2 \exp\left[\frac{\alpha_s}{2\pi} \log\left(\frac{Q^2}{m^2}\right) P_{qq}\right] \otimes f_q. \tag{77}$$

Comparing this expression to the corresponding parton model prediction, given in Eq. (28), one can see that the resummation of the leading logarithms is equivalent to replacing the Q^2-independent parton distribution function a scale-dependent one,

$$f_q(x) \to f_q(x, Q^2) \equiv \exp\left[\frac{\alpha_s}{2\pi}\log\left(\frac{Q^2}{m^2}\right)P_{qq}\right]\otimes f_q. \tag{78}$$

To distinguish between the scale-dependent (measurable) and scale-independent (unmeasurable) PDFs, the latter are often called **bare distributions**. During the rest of these lectures, we shall adopt this convention and write $f_q = f_q^{\text{bare}}$. Taking the Q^2-derivative we see that $f_q(x, Q^2)$ satisfies the following integro-differential equation

$$Q^2\frac{\partial}{\partial Q^2}f_q(x, Q^2) = \frac{\alpha_s}{2\pi}P_{qq}\otimes f_q(x, Q^2), \tag{79}$$

which is an archetype of the **Dokshitzer-Gribov-Lipatov-Altarelli-Parisi evolution equations** [6, 7, 8, 9], or just **DGLAP equations** in brief.

2.4 More splitting functions

The gluon emission discussed above is, of course, only one possibility among other QCD-interactions. For example, from $\mathcal{O}(\alpha_s)$ onwards, also gluon-initiated subprocesses contribute to the deeply inelastic cross-section. The simplest such diagram is shown in Fig. 10. As in the

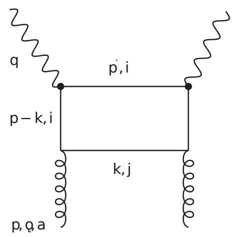

Figure 10: A gluon-initiated ladder diagram.

case of gluon radiation graphs discussed in the preceding sections, also this diagram — and in the axial gauge this ladder-type diagram only — gives a collinear divergence. Extracting this divergence goes as in the previous section. The result is,

$$\frac{d^2\hat{\sigma}_0}{dxdQ^2}\sum_q e_q^2\left(\frac{\alpha_s}{2\pi}\right)\log\left(\frac{Q^2}{m^2}\right)P_{qg}\otimes f_g^{\text{bare}}, \tag{80}$$

where

$$P_{qg}(z) \equiv T_R\left[z^2 + (1-z)^2\right] \tag{81}$$

is the splitting function for a gluon→quark transition and f_g is the parton distribution function for the gluons. This is obviously of the same form as what we had for the gluon radiation.

Having now considered two different ladder vertices, we can also pile them on top of each other to form a parton ladder like the one in Fig. 11 below. The leading contribution to the DIS cross section from this diagram is

$$\frac{d^2\hat{\sigma}_0}{dxdQ^2}\sum_q e_q^2\frac{1}{2}\left(\frac{\alpha_s}{2\pi}\right)^2\log^2\left(\frac{Q^2}{m^2}\right)P_{qq}\otimes P_{qg}\otimes f_g^{\text{bare}}.$$

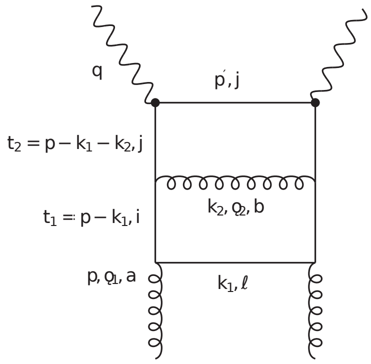

Figure 11: Another gluon-initiated ladder diagram.

The story continues with vertical gluon lines as in the diagram of Fig. 12. This leads to a

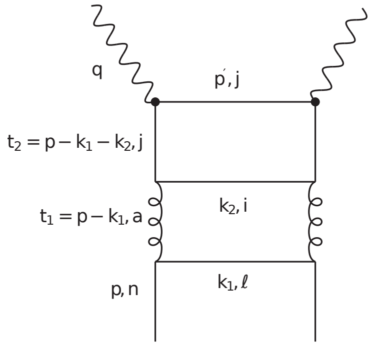

Figure 12: Ladder diagram with gluon as a vertical line.

contribution

$$\frac{d^2\hat{\sigma}_0}{dxdQ^2}\sum_{q,q'} e_q^2 \frac{1}{2}\left(\frac{\alpha_s}{2\pi}\right)^2 \log^2\left(\frac{Q^2}{m^2}\right) P_{qg}\otimes P_{gq'}\otimes f_{q'}^{\mathrm{bare}}\,,$$

where

$$P_{gq}(z) \equiv C_F\left[\frac{1+(1-z)^2}{z}\right] \tag{82}$$

is the splitting function for the quark→gluon transition. Not that here, the flavour of the incoming quark may change, and thus the summation runs over q (the quark on which the photon collides) and q' (the incoming quark).

There is still one more splitting function — namely that related to the 3-gluon vertex. This is involved e.g. in the ladder diagram depicted in Fig. 13. The leading contribution of this diagram in the DIS cross section is

$$\frac{d^2\hat{\sigma}_0}{dxdQ^2}\sum_{q} e_q^2 \frac{1}{2}\left(\frac{\alpha_s}{2\pi}\right)^2 \log^2\left(\frac{Q^2}{m^2}\right) P_{qg}\otimes P_{gg}\otimes f_{g}^{\mathrm{bare}},$$

with

$$P_{gg}(z) \equiv 2C_G\left[\frac{1-z}{z}+\frac{z}{1-z}+z(1-z)\right], \qquad C_G = 3. \tag{83}$$

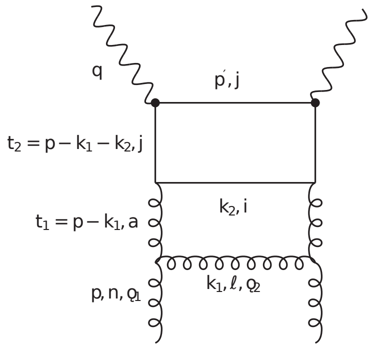

Figure 13: A ladder diagram from which one can compute sthe plitting function for gluon→gluon transition.

From now on, one can pretty much see how this goes on: each additional ladder-compartment in which parton of flavor i transforms to j, effectively just increments the power of $\alpha_s \log Q^2/m^2$ by one unit and adds the corresponding splitting function P_{ij} to the convolution integral. The possible building blocks for constructing the ladders are displayed in Fig. 14 together with the characteristic splitting functions. In Eq. (78) we defined the scale-dependent quark PDFs solely in terms of quark-to-quark splittings P_{qq}. However, clearly we should account not only for those, but rather for all possible parton ladders — also the gluon-triggered ones — when defining the scale-dependent quark densities. Therefore, we define the scale-dependent parton distributions as a sum of all possible ladders that end up with the specific parton i:

$$
\begin{aligned}
f_i(x, Q^2) = f_i^{\mathrm{bare}} &+ \frac{1}{1!}\left(\frac{\alpha_s}{2\pi}\right)\log\left(\frac{Q^2}{m^2}\right)\sum_j P_{ij}\otimes f_j^{\mathrm{bare}} \\
&+ \frac{1}{2!}\left(\frac{\alpha_s}{2\pi}\right)^2\log^2\left(\frac{Q^2}{m^2}\right)\sum_{jk} P_{ij}\otimes P_{jk}\otimes f_k^{\mathrm{bare}} \\
&+ \frac{1}{3!}\left(\frac{\alpha_s}{2\pi}\right)^3\log^3\left(\frac{Q^2}{m^2}\right)\sum_{jkn} P_{ij}\otimes P_{jk}\otimes P_{kn}\otimes f_n^{\mathrm{bare}} + \\
&+ \frac{1}{4!}\left(\frac{\alpha_s}{2\pi}\right)^4\log^4\left(\frac{Q^2}{m^2}\right)\sum_{jknm} P_{ij}\otimes P_{jk}\otimes P_{kn}\otimes P_{nm}\otimes f_m^{\mathrm{bare}} + \cdots
\end{aligned}
\tag{84}
$$

$$C_F = 4/3, \quad T_R = 1/2, \quad C_G = 3$$

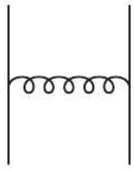

$$P_{qq}(z) = C_F \frac{1+z^2}{1-z}$$

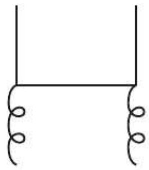

$$P_{qg}(z) = T_R \left[z^2 + (1-z)^2\right]$$

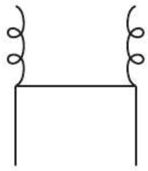

$$P_{gq}(z) = C_F \frac{1+(1-z)^2}{z}$$

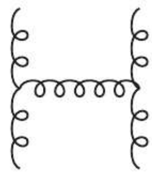

$$P_{gg}(z) = 2C_G \left[\frac{z}{1-z} + \frac{1-z}{z} + z(1-z)\right]$$

Figure 14: Unpolarized splitting functions.

Taking a Q^2 derivative gives

$$\begin{aligned}
Q^2 \frac{f_i(x,Q^2)}{dQ^2} &= \left(\frac{\alpha_s}{2\pi}\right) \sum_j P_{ij} \otimes f_j^{\text{bare}} \\
&+ \frac{1}{1!}\left(\frac{\alpha_s}{2\pi}\right)^2 \log\left(\frac{Q^2}{m^2}\right) \sum_{jk} P_{ij} \otimes P_{jk} \otimes f_k^{\text{bare}} \\
&+ \frac{1}{2!}\left(\frac{\alpha_s}{2\pi}\right)^3 \log^2\left(\frac{Q^2}{m^2}\right) \sum_{jkn} P_{ij} \otimes P_{jk} \otimes P_{kn} \otimes f_n^{\text{bare}} + \\
&+ \frac{1}{3!}\left(\frac{\alpha_s}{2\pi}\right)^4 \log^3\left(\frac{Q^2}{m^2}\right) \sum_{jknm} P_{ij} \otimes P_{jk} \otimes P_{kn} \otimes P_{nm} \otimes f_m^{\text{bare}} + \cdots \\
&= \left(\frac{\alpha_s}{2\pi}\right) \sum_j P_{ij} \otimes \Bigg[f_j^{\text{bare}} + \frac{1}{1!}\left(\frac{\alpha_s}{2\pi}\right) \log\left(\frac{Q^2}{m^2}\right) \sum_k P_{jk} \otimes f_k^{\text{bare}} \\
&+ \frac{1}{2!}\left(\frac{\alpha_s}{2\pi}\right)^2 \log^2\left(\frac{Q^2}{m^2}\right) \sum_{kn} P_{jk} \otimes P_{kn} \otimes f_n^{\text{bare}} + \\
&+ \frac{1}{3!}\left(\frac{\alpha_s}{2\pi}\right)^3 \log^3\left(\frac{Q^2}{m^2}\right) \sum_{knm} P_{jk} \otimes P_{kn} \otimes P_{nm} \otimes f_m^{\text{bare}} + \cdots \Bigg]
\end{aligned} \tag{85}$$

The term in square brackets is just $f_j(x, Q^2)$ and thus the full DGLAP equations read

$$Q^2 \frac{f_i(x, Q^2)}{dQ^2} = \frac{\alpha_s}{2\pi} \sum_j \int_x^1 \frac{dz}{z} P_{ij}(z) f_j\left(\frac{x}{z}, Q^2\right) . \tag{86}$$

2.5 Incorporating the running coupling

In the derivation of Eq. (86) the strong coupling α_s has been taken as a fixed constant. In order to incorporate the effects of running coupling we should consider the renormalization of the ladder vertices. As the vertical lines in the parton ladder are somewhat virtual, the loop corrections will lead to logarithmic terms $\log(\Lambda^2/\mathbf{k}_\perp^2)$, where Λ^2 is some UV cut off, which are absorbed into the definition of running coupling,

$$\begin{aligned}
\alpha_s(\mu^2) &= \frac{\alpha_s^0}{1 - \frac{\alpha_s^0}{4\pi}\beta_0 \log\left(\frac{\Lambda^2}{\mu^2}\right)} = \alpha_s^0 \left[1 + \frac{\alpha_s^0}{4\pi}\beta_0 \log\left(\frac{\Lambda^2}{\mu^2}\right) + \cdots\right], \\
&= \frac{4\pi}{\beta_0 \log\left(\mu^2/\Lambda_{\text{QCD}}^2\right)}
\end{aligned} \tag{87}$$

where $\beta_0 = \dfrac{11}{3}C_G - \dfrac{4}{3}T_R n_f$, and $\Lambda_{\text{QCD}} \approx 200\,\text{MeV}$ is the QCD scale parameter. In what follows, for each ladder vertex, we will take $\mathbf{k}_\perp^2$ of the emitted parton as the argument of α_s. Doing otherwise would leave explicit $\mathbf{k}_\perp^2$-dependent logarithms in the cross-sections. However, when the scale μ is identified as $\mathbf{k}_\perp^2$, also these logarithms can be resummed: In each ladder vertex we change $\alpha_s \to \alpha_s(\mathbf{k}_\perp^2)$, and do the nested transverse momentum integrals like (70) by a change of variables

$$\kappa(\mathbf{k}_\perp^2) \equiv \frac{2}{\beta_0} \log\left[\frac{\alpha_s(m^2)}{\alpha_s(\mathbf{k}_\perp^2)}\right] = \frac{2}{\beta_0} \log\left[\frac{\log(\mathbf{k}_\perp^2/\Lambda_{\text{QCD}}^2)}{\log(m^2/\Lambda_{\text{QCD}}^2)}\right], \tag{88}$$

such that

$$\begin{aligned}
&\int_{m^2}^{Q^2} \frac{d\mathbf{k}_{2\perp}^2}{\mathbf{k}_{2\perp}^2} \frac{\alpha_s(\mathbf{k}_{2\perp}^2)}{2\pi} \int_{m^2}^{\mathbf{k}_{2\perp}^2} \frac{d\mathbf{k}_{1\perp}^2}{\mathbf{k}_{1\perp}^2} \frac{\alpha_s(\mathbf{k}_{1\perp}^2)}{2\pi} \\
&= \int_0^{\kappa(Q^2)} d\kappa(\mathbf{k}_{2\perp}^2) \int_0^{\kappa(\mathbf{k}_{2\perp}^2)} d\kappa(\mathbf{k}_{1\perp}^2) \\
&= \frac{1}{2}\kappa^2(Q^2).
\end{aligned} \tag{89}$$

Our definition of the scale-dependent PDFs would then become

$$\begin{aligned}
f_i(x, Q^2) = f_i^{\text{bare}} &+ \frac{1}{1!}\kappa(Q^2) \sum_j P_{ij} \otimes f_j^{\text{bare}} \\
&+ \frac{1}{2!}\kappa^2(Q^2) \sum_{jk} P_{ij} \otimes P_{jk} \otimes f_k^{\text{bare}} \\
&+ \frac{1}{3!}\kappa^3(Q^2) \sum_{jkn} P_{ij} \otimes P_{jk} \otimes P_{kn} \otimes f_n^{\text{bare}} + \\
&+ \frac{1}{4!}\kappa^4(Q^2) \sum_{jknm} P_{ij} \otimes P_{jk} \otimes P_{kn} \otimes P_{nm} \otimes f_m^{\text{bare}} + \cdots
\end{aligned} \tag{90}$$

Taking a Q^2 derivative gives

$$
\begin{aligned}
Q^2 \frac{f_i(x,Q^2)}{dQ^2} = \frac{\alpha_s(Q^2)}{2\pi} \sum_j P_{ij} \otimes \Bigg[& f_j^{\rm bare} + \frac{1}{1!}\kappa(Q^2)\log\left(\frac{Q^2}{m^2}\right) \sum_k P_{jk} \otimes f_k^{\rm bare} \\
& + \frac{1}{2!}\kappa^2(Q^2) \sum_{kn} P_{jk} \otimes P_{kn} \otimes f_n^{\rm bare} + \\
& + \frac{1}{3!}\kappa^3(Q^2) \sum_{knm} P_{jk} \otimes P_{kn} \otimes P_{nm} \otimes f_m^{\rm bare} + \cdots \Bigg]
\end{aligned}
$$

The term in square brackets is just $f_j(x, Q^2)$ and thus the DGLAP equations with running coupling read

$$
Q^2 \frac{f_i(x,Q^2)}{dQ^2} = \frac{\alpha_s(Q^2)}{2\pi} \sum_j \int_x^1 \frac{dz}{z} P_{ij}(z) f_j\left(\frac{x}{z}, Q^2\right) . \tag{91}
$$

In summary, the leading collinear singularities in the perturbative Feynman-diagram expansion can be factored to the scale-dependent parton distributions $f_i(x, Q^2)$ such that the parton model prediction for the DIS cross-section stays formally intact, but the parton densities no longer respect the Bjorken-scaling but are Q^2-dependent. In principle, by experimentally measuring cross sections at given Q^2 one can unfold the PDFs at this scale. The Q^2 dependence of PDFs — and thereby also the Q^2 dependence of cross sections — is then predicted by QCD via Eq. (91). Also the interpretation of the parton distributions as simple number densities upgrades to being number densities with transverse momentum up to Q^2. This and further extensions to the simple parton model are often referred to as **pQCD-improved parton model**.

2.6 Virtual corrections to P_{qq} and P_{gg}

The splitting functions $P_{qq}(z)$ and $P_{gg}(z)$ obtained from real emisson only, contain $1/(1-z)$-poles making the convolution integrals divergent. However, the contributions from the emitted gluons being "reabsorbed“ by the quark or gluon that emitted it in the first place, diverges similarly. While it is possible to calculate these virtual corrections directly by a similar Sudakov technique that we have used to evaluate the real diagrams, it's a bit awkward (and regulating the loop integrals with a cut-off mass is not Lorentz invariant). However, the effect of these loop corrections to the splitting functions can be deduced from sum rules.

At this point, it is convenient to introduce the concepts of **valence** (sometimes also called **non-singlet**) $V_i(x, Q^2)$ and **singlet** $\Sigma(x, Q^2)$ distributions,

$$
V_i(x,Q^2) = f_i(x,Q^2) - f_{\bar{i}}(x,Q^2), \;\; i \neq g \, . \tag{92}
$$

$$
\Sigma(x,Q^2) = \sum_{i=q} \left[f_i(x,Q^2) + f_{\bar{i}}(x,Q^2) \right] . \tag{93}
$$

The DGLAP equations for these combinations become

$$
Q^2 \frac{V_i(x,Q^2)}{dQ^2} = \frac{\alpha_s(Q^2)}{2\pi} \int_x^1 \frac{dz}{z} P_{qq}(z) V_i\left(\frac{x}{z}, Q^2\right) . \tag{94}
$$

$$
Q^2 \frac{\Sigma(x,Q^2)}{dQ^2} = \frac{\alpha_s(Q^2)}{2\pi} \int_x^1 \frac{dz}{z} \left[P_{qq}(z)\Sigma\left(\frac{x}{z}, Q^2\right) + 2n_f P_{qg}(z) f_g\left(\frac{x}{z}, Q^2\right) \right] , \tag{95}
$$

where n_f refers to the number of active flavours.

Let us now consider the integral

$$\int_0^1 dx V_i(x, Q^2)\,. \tag{96}$$

This counts the number of valence quarks, and it should be independent of Q^2 since the flavour of the quark does not alter by gluon emission, and every gluons splitting generates both a quark and an antiquark. Indeed, for a proton,

$$\int_0^1 dx V_u(x, Q^2) = 2, \qquad \int_0^1 dx V_d(x, Q^2) = 1\,. \tag{97}$$

Thus, we must have

$$\frac{d}{dQ^2}\int_0^1 dx V_i(x, Q^2) = 0\,. \tag{98}$$

By using Eq. (94), we find

$$\int_0^1 dz P_{qq}(z) \int_0^1 dx V_i(x, Q^2) = 0\,. \tag{99}$$

Since the latter integral is in general non-zero, we see that

$$\int_0^1 dz P_{qq}(z) = 0\,. \tag{100}$$

The contribution of virtual corrections in $P_{qq}(z)$ must be proportional to $\delta(1-z)$ (virtual corrections do not affect the kinematics of the process) such that the complete $P_{qq}(z)$ should be of the from

$$P_{qq}(z) = C_F \frac{1+z^2}{1-z} + A\delta(1-z)\,. \tag{101}$$

The requirement that the integral over $P_{qq}(z)$ gives zero then indicates

$$P_{qq}(z) = C_F \left[\frac{1+z^2}{1-z}\right]_+ = C_F \frac{1+z^2}{1-z} - \delta(1-z)\int_0^1 dy C_F \frac{1+y^2}{1-y}\,. \tag{102}$$

That is, P_{qq} is not a function, but rather a distribution (pure plus distribution).

Another important sum rule is that of the total momentum. As the total momentum of the hadron is carried by its constituent partons, we must have

$$\int_0^1 dx x \left[\sum_{i=q,\bar{q},g} f_i(x, Q^2)\right] = 1\,. \tag{103}$$

Also this must be independent of the scale Q^2. Proceeding as above, we obtain two equations,

$$\int_0^1 dz z \left[P_{qq}(z) + P_{gq}(z)\right] = 0 \tag{104}$$

$$\int_0^1 dz z \left[P_{gg}(z) + 2n_f P_{qg}(z)\right] = 0\,. \tag{105}$$

With the P_{qq} of Eq. (102) the first of these equations is satisfied automatically. From the second one we can obtain, as above, the contribution of virtual corrections to P_{gg}. It's a simple exercise in integration to show that the full P_{gg} must be

$$P_{gg}(z) = 2C_A \left[\frac{z}{(1-z)_+} + \frac{1-z}{z} + z(1-z)\right] + \delta(1-z)\left[\frac{11C_A - 2n_f}{6}\right]\,. \tag{106}$$

3 Higher orders, factorization, universality, schemes & scales

3.1 Higher orders

When building the parton ladder, we systematically retained only terms of the form $\alpha_s^n \log^n(Q^2/m^2)$, discarding all contributions which are suppressed by additional powers of α_s. This the leading logarithmic approximation. However, if one keeps track also of the non-leading contributions

$$\alpha_s^{n+1} \log^n(Q^2/m^2),\ \alpha_s^{n+2} \log^n(Q^2/m^2), \ldots$$

one finds that the splitting functions P_{ij} actually constitute a power series in α_s,

$$P_{ij}(z) = \left(\frac{\alpha_s}{2\pi}\right) P_{ij}^{(1)}(z) + \left(\frac{\alpha_s}{2\pi}\right)^2 P_{ij}^{(2)}(z) + \left(\frac{\alpha_s}{2\pi}\right)^2 P_{ij}^{(3)}(z) + \ldots. \tag{107}$$

Of these, $P^{(2)}$ have been known since 1980's [14, 15] and also $P^{(3)}$ have been computed already 15 years ago [16, 17]. Also parts of $P^{(4)}$ are known [18] (incredible!). While the kernels $P_{ij}^{(1)}$ are unique, the higher order splitting functions $P_{ij}^{(n)}$, $n > 1$ are not unique but they are scheme dependent. We will soon return to this point.

One might expect that towards higher orders in α_s the corrections would become smaller. However, a difficulty appears. At small-x limit, the 1- and 2-loop quark-to-gluon and gluon-to-gluon splitting functions go as

$$P_{gq}^{(1)}(x) \xrightarrow{x\to 0} \frac{2C_F}{x}, \quad P_{gq}^{(2)}(x) \xrightarrow{x\to 0} \frac{9C_FC_A - 40C_FT_f}{9x} \tag{108}$$

$$P_{gg}^{(1)}(x) \xrightarrow{x\to 0} \frac{2C_A}{x}, \quad P_{gg}^{(2)}(x) \xrightarrow{x\to 0} \frac{12C_FT_f - 46C_AT_f}{9x} \tag{109}$$

That is, both behave as $\sim 1/x$ and the perturbative stability appears reasonable. However, at 3-loop level, the leading behaviour gets logarithmically enhanced,

$$P_{ij}^{(3)}(x) \xrightarrow{x\to 0} \sim \frac{1}{x}\log(x)\,, \tag{110}$$

which appears to destroy the perturbative convergence of the expansion at low Q^2. Figure 15 illustrates the situation. Since $\alpha_s(Q^2) \to 0$ as $Q^2 \to \infty$, at high Q^2 the prefactor $\alpha_s^3(Q^2)$ becomes suppressed, so this is a small-x and small-Q^2 issue. The effect of $\log x$ enhancement in the splitting functions is to make the Q^2 evolution faster and faster towards small x. For fixed Q^2 (above the parametrization scale) the quark and gluon distributions thus become increasingly steeper functions of x. Importantly, there are now some evidence that such a steep growth is not compatible with the experimental data [20], indicating that also the $\log x$ terms in the splitting functions should be resummed (achieved by the duality between the DGLAP and the BFKL equations). In particular, the difficulty of the fixed-order predictions is to describe properly the turnover towards small x at fixed Q^2. Figure 16 shows some examples and how the situation improves upon performing the small-x resummations.

3.2 Factorization & universality

We have seen that, when extracting the divergent logarithms from the parton ladders, a multiplicative front factor that coincides with the leading order cross-section for photon-quark scattering, was always found. This continues to be true in higher-order calculations, and order

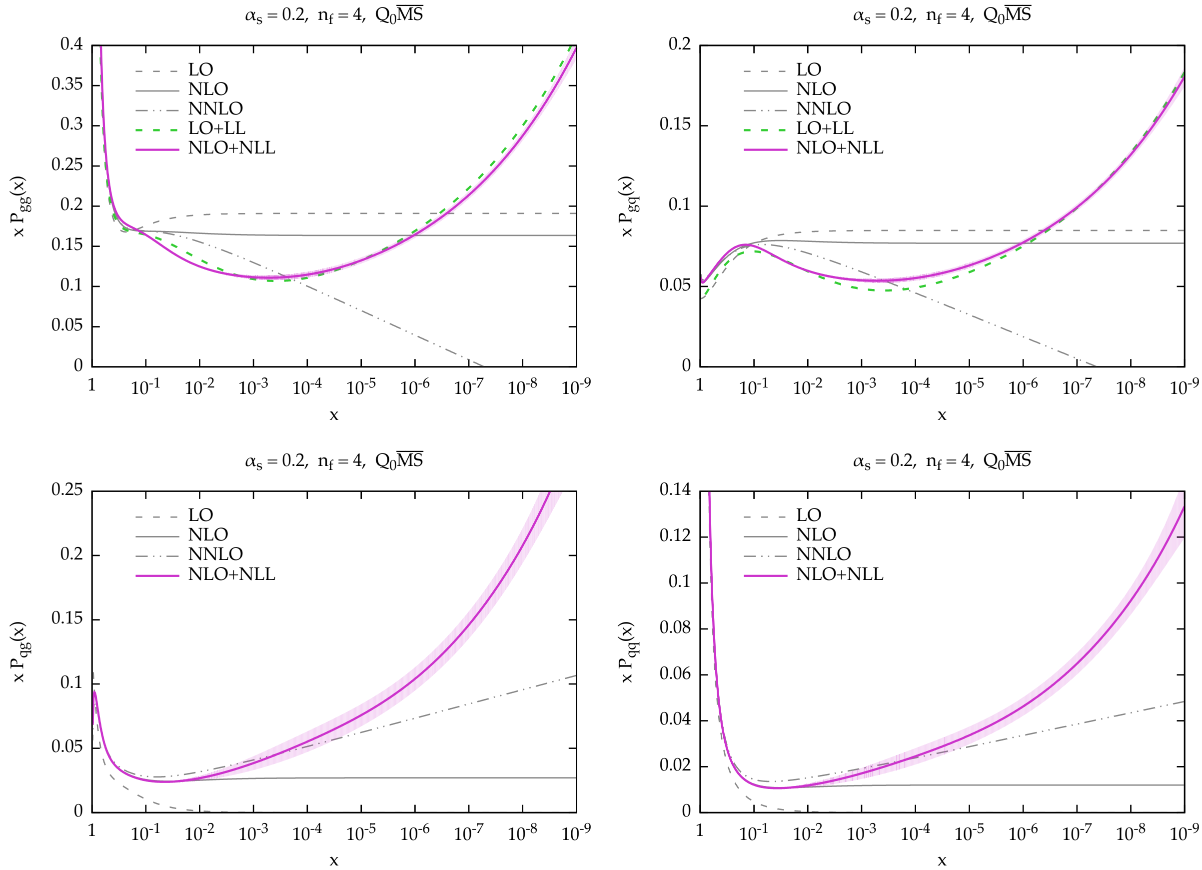

Figure 15: Perturbative behaviour of splitting functions. Figure from Ref. [19].

by order in perturbative calculations, the divergent logarithms can be systematically factored apart from the finite perturbative parton-level pieces:

$$
\begin{aligned}
d\sigma = & \sum_i \left[d\hat{\sigma}_i^{(0)} + \left(\frac{\alpha_s}{2\pi}\right) d\hat{\sigma}_i^{(1)} + \left(\frac{\alpha_s}{2\pi}\right)^2 d\hat{\sigma}_i^{(2)} + \ldots \right] \otimes \\
& \Bigg\{ f_i + \frac{1}{1!}\left(\frac{\alpha_s}{2\pi}\right) \log\left(\frac{Q^2}{m^2}\right) \sum_j P_{ij}^{(1)} \otimes f_j + \frac{1}{2!}\left(\frac{\alpha_s}{2\pi}\right)^2 \log^2\left(\frac{Q^2}{m^2}\right) \sum_{jk} P_{ij}^{(1)} \otimes P_{jk}^{(1)} \otimes f_k + \ldots \\
& \quad + \frac{1}{1!}\left(\frac{\alpha_s}{2\pi}\right)^2 \log\left(\frac{Q^2}{m^2}\right) \sum_j P_{ij}^{(2)} \otimes f_j + \frac{1}{2!}\left(\frac{\alpha_s}{2\pi}\right)^4 \log^2\left(\frac{Q^2}{m^2}\right) \sum_{jk} P_{ij}^{(2)} \otimes P_{jk}^{(2)} \otimes f_k + \ldots \\
& \quad + \frac{1}{1!}\left(\frac{\alpha_s}{2\pi}\right)^3 \log^2\left(\frac{Q^2}{m^2}\right) \sum_{jk} P_{ij}^{(1)} \otimes P_{jk}^{(2)} \otimes f_k + \ldots \Bigg\}, \\
= & \sum_i d\hat{\sigma}_i \otimes f_i(Q^2) \,.
\end{aligned} \tag{111}
$$

In other words, to all orders in perturbation theory, the DIS cross section retains its simple form in which the partonic "cross section" $d\hat{\sigma}_i$ are convoluted with the scale-dependent PDFs. This remarkable property is known as **collinear factorization** [22, 23]. However, this is not the final truth, but a more complete treatment indicates that the factorization is subject to power

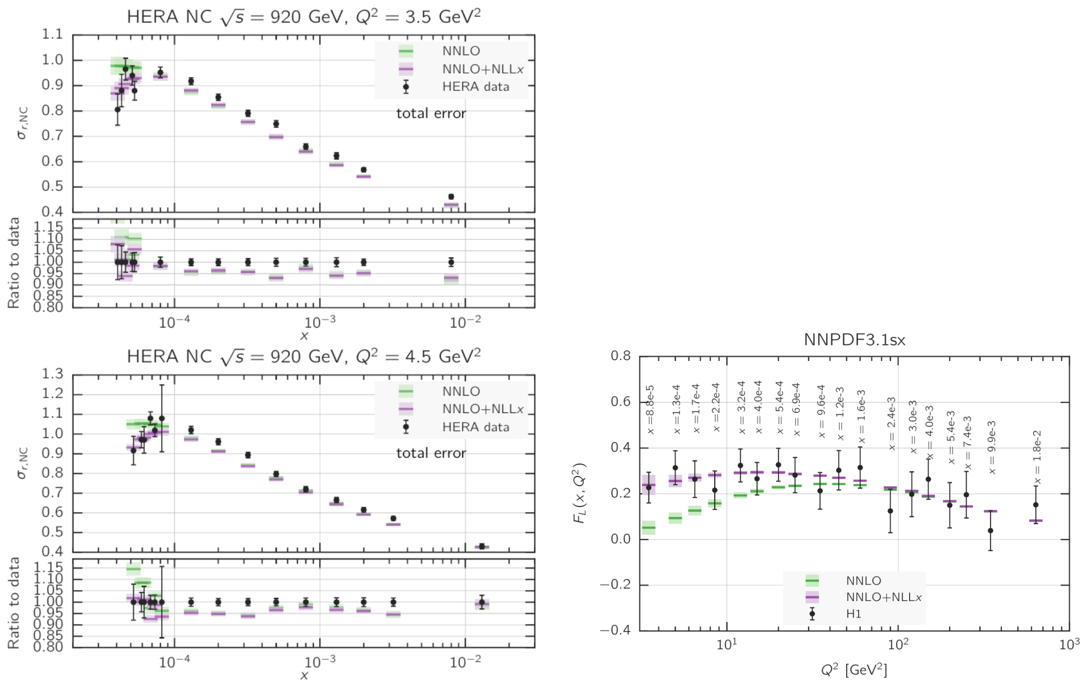

Figure 16: HERA data vs. NNLO fit. Figure from Ref. [21].

corrections $\mathcal{O}\left(\Lambda^2_{\rm QCD}/Q^2\right)^n$ which should become important at small Q^2. Such terms appear, for example, if one accounts for the fact that the partons are not exactly collinear with the parent nucleon, but are allowed to carry some "primordial" transverse momentum $\mathbf{k}_\perp$. More generally, such terms arise form multi-parton interactions.

Although we have here considered only the deeply inelastic scattering, the underlying physics is shared in variety of other processes involving hadrons in the initial state — the structure of the collinear singularities is the same. For example, for a generic inclusive observable $\mathcal{O}$ in proton-proton collisions (say, at the LHC), we have

$$d\sigma^{\rm p+p\rightarrow \mathcal{O}+X} = \sum_{ij} f_i(Q^2) \otimes d\hat{\sigma}_{ij}^{\rm p+p\rightarrow \mathcal{O}+X} \otimes f_j(Q^2)\,, \tag{112}$$

where the PDFs $f_j(Q^2)$ are defined as exactly the same infinite series as in DIS. In other words, the parton densities are independent of the actual hard process, **universal**. For example in the Drell-Yan production of dileptons in nucleon-nucleon collisions, the leading logarithms originate from diagrams like that in Fig. 17. The formal proofs for factorization are highly technical and mathematically demanding. Therefore, there are only few processes for which such all-order proofs actually exists [23], but it is typically assumed that for hadronic interactions that are "hard enough" (involve a large invariant scale), the factorization holds. An integral part of the LHC physics is based on this assumption.

3.3 Scheme dependence of PDFs

In preceding sections we defined the PDFs including only $\log(Q^2/m^2)$ type of terms. However, this definition of PDFs is not unique. Starting from parton densities $f_i(x, Q^2)$ we may define

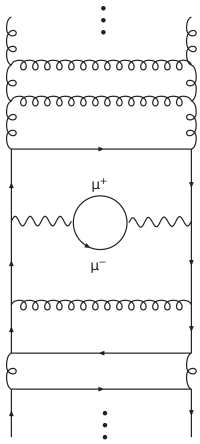

Figure 17: Ladder-type diagram that gives rise to a leading logarithmic terms (in axial gauge) for Drell-Yan dilepton production.

another version $f'_i(x,Q^2)$ by

$$f'_i(x,Q^2) \equiv \sum_j C_{ij} \otimes f_j(Q^2), \tag{113}$$

where

$$C_{ij}(z) = \delta_{ij}\delta(1-z) + \frac{\alpha_s}{2\pi} C^{(1)}_{ij}(z) + \left(\frac{\alpha_s}{2\pi}\right)^2 C^{(2)}_{ij}(z) + \ldots .. \tag{114}$$

In terms of the primed PDFs, the cross-section can be written as

$$\sigma = \hat{\sigma}_i \otimes f_i = \hat{\sigma}_i \otimes C^{-1}_{ij} \otimes f'_j = \hat{\sigma}'_i \otimes f'_i,$$

where, in the last step, we defined $\hat{\sigma}'_j \equiv \hat{\sigma}_i \otimes C^{-1}_{ij}$. Here, C^{-1}_{ij} should be understood as a "perturbative inverse"

$$C^{-1}_{ij}(z) = \delta_{ij}\delta(1-z) - \frac{\alpha_s}{2\pi} C^{(1)}_{ij}(z) + \cdots , \tag{115}$$

such that the primed coefficient function becomes

$$\hat{\sigma}'_i \equiv \hat{\sigma}_j \otimes C^{-1}_{ji} = \hat{\sigma}^{(0)}_i + \frac{\alpha_s}{2\pi}\left[\hat{\sigma}^{(1)}_i - \sum_j \hat{\sigma}^{(0)}_j \otimes C^{(1)}_{ji}\right] + \cdots . \tag{116}$$

We see that, by a choosing C_{ij} suitably, we could e.g. eliminate the $\mathcal{O}(\alpha_s)$ contributions in DIS altogether. Using the definition Eq. (84) in Eq. (113), and keeping only the $C^{(1)}_{ij}$ and $P^{(1)}_{ij}$ term for simplicity, we see that the definition of PDFs (in terms of the bare) PDFs will, in general, include also other than logarithmic terms:

$$f'_i(x,Q^2) = f^{\text{bare}}_i + \left(\frac{\alpha_s}{2\pi}\right)\left[\frac{1}{1!}\log\left(\frac{Q^2}{m^2}\right) P^{(1)}_{ij} + C^{(1)}_{ij}\right] \otimes f^{\text{bare}}_j + \cdots . \tag{117}$$

A similar reshuffling implies that f'_i obey the DGLAP equations with splitting functions

$$P'_{ij} = C_{ik} \otimes P_{k\ell} \otimes C^{-1}_{\ell j} + \frac{dC_{ik}}{d\log Q^2} C^{-1}_{kj} . \tag{118}$$

In other words the definition of PDFs can involve also other than $\log(Q^2/m^2)$ type of terms and, beyond leading order, the perturbative coefficients functions $\hat{\sigma}_i$, and the splitting functions P_{ij} depend also on exact definition of the PDFs. This is known as **factorization scheme dependence**. In essence, defining a scheme is a statement of how certain finite part of the calculations are distributed among PDFs, partonic cross sections, and splitting functions. Formally, the predictions for physical, measurable cross-sections are independent of the chosen scheme, up to corrections which are suppressed by one more power in α_s than to what the computation was performed. Indeed, to $\mathcal{O}(\alpha_s)$,

$$\begin{aligned}
\hat{\sigma}'_i \otimes f'_i &= \left\{ \hat{\sigma}_i^{(0)} + \frac{\alpha_s}{2\pi} \left[\hat{\sigma}_i^{(1)} - \hat{\sigma}_j^{(0)} \otimes C_{ji}^{(1)} \right] \right\} \otimes \left[\delta_{ik} + \frac{\alpha_s}{2\pi} C_{ik}^{(1)} \right] \otimes f_k \qquad (119) \\
&= \sigma_i^{(0)} \otimes f_i + \frac{\alpha_s}{2\pi} \hat{\sigma}_i^{(1)} \otimes f_i - \frac{\alpha_s}{2\pi} \hat{\sigma}_j^{(0)} \otimes C_{jk}^{(1)} \otimes f_k + \frac{\alpha_s}{2\pi} \sigma_i^{(0)} \otimes C_{ik}^{(1)} \otimes f_k + \mathcal{O}(\alpha_s^2) \\
&= \sigma_i^{(0)} \otimes f_i + \frac{\alpha_s}{2\pi} \hat{\sigma}_i^{(1)} \otimes f_i + \mathcal{O}(\alpha_s^2) = \hat{\sigma}_i \otimes f_i + \mathcal{O}(\alpha_s^2) \,.
\end{aligned}$$

3.4 Factorization scale

There is a similar ambiguity in choosing the scale argument of $f_q(Q^2)$ in Eq. (111). This is because, based on DGLAP equation, different scale choices are perturbatively related. Indeed, we can express the PDFs at scale Q^2 with the aid of PDFs at another scale Q_f^2 as

$$\begin{aligned}
f_i(x, Q^2) &= f_i(x, Q_f^2) + \frac{\alpha_s}{2\pi} \log\left(Q^2/Q_f^2\right) P_{ij} \otimes f_j(Q_f^2) \qquad (120) \\
&+ \frac{1}{2} \left(\frac{\alpha_s}{2\pi}\right)^2 \log^2\left(Q^2/Q_f^2\right) P_{ij} \otimes P_{jk} \otimes f_k(Q_f^2) \\
&+ \ldots \\
&= \sum_j D_{ij}(Q^2/Q_f^2) \otimes f_j(Q_f^2) \,.
\end{aligned}$$

Defining now

$$\hat{\sigma}_j(Q^2, Q_f^2) \equiv \hat{\sigma}_i(Q^2) \otimes D_{ij}(Q^2/Q_f^2) = \hat{\sigma}_j^{(0)} + \frac{\alpha_s}{2\pi} \left[\hat{\sigma}_j^{(1)} + \log\left(Q^2/Q_f^2\right) \hat{\sigma}_i^{(0)} \otimes P_{ij} \right] + \cdots \qquad (121)$$

the factorization formula (111) becomes

$$\sigma = \hat{\sigma}_i \otimes f_i(Q^2) = \hat{\sigma}_i \otimes D_{ij}(Q^2/Q_f^2) \otimes f_j(Q_f^2) = \hat{\sigma}_j(Q^2/Q_f^2) \otimes f_j(Q_f^2)$$

The arbitrary scale Q_f^2 is called the **factorization scale**, which we are free to choose. Choosing a certain factorization scale is a statement of how the logarithmic transverse-momentum integrals are distributed: Earlier we absorbed the contribution

$$\int_{m^2}^{Q^2} \frac{d\mathbf{k}_\perp^2}{\mathbf{k}_\perp^2} = \log\left(Q^2/m^2\right) \,,$$

into the definition of PDFs $f_i(Q^2)$. However, we can equally write

$$\int_{m^2}^{Q^2} \frac{d\mathbf{k}_\perp^2}{\mathbf{k}_\perp^2} = \int_{m^2}^{Q_f^2} \frac{d\mathbf{k}_\perp^2}{\mathbf{k}_\perp^2} + \int_{Q_f^2}^{Q^2} \frac{d\mathbf{k}_\perp^2}{\mathbf{k}_\perp^2} = \log\left(Q_f^2/m^2\right) + \log\left(Q^2/Q_f^2\right) \,,$$

and absorb only the first $\log\left(Q_f^2/m^2\right)$ term into the defition of PDFs $f_i(Q_f^2)$. The latter term will then appear in the partonic cross sections as in Eq. (121). Formally the physical cross sections do not depend on this choice, the differences between two choices being suppressed by one more power in α_s than to what $\hat{\sigma}_j$ was computed to. If Q_f^2 is very different from Q^2, the log $\left(Q^2/Q_f^2\right)$ term can become large. Thus, the only possibility that really makes sense is to choose $Q_f^2 \sim Q^2$. The sensitivity of the cross section to the variation of the factorization scale is often taken as a guideline of the missing higher-order corrections.

3.5 Definition of PDFs in dimensional regularization

In previous section we have argued that before introducing the scale-dependent PDFs, the structure function F_2 to $\mathcal{O}(\alpha_s)$ is of the form

$$\begin{aligned}\frac{F_2(x,Q^2)}{x} = \sum_{q,\bar{q}} e_q^2 \Bigg\{ &\left[1 + \left(\frac{\alpha_s}{2\pi}\right) \log\left(\frac{Q^2}{m^2}\right) P_{qq} + h'^q\right] \otimes f_q \\ &+ \left[\left(\frac{\alpha_s}{2\pi}\right) \log\left(\frac{Q^2}{m^2}\right) P_{qg} + h'^g\right] \otimes f_g \Bigg\} ,\end{aligned} \tag{122}$$

where the functions h^i (often called **coefficient functions** or **Wilson coefficients**) contain all the finite pieces of the calculation. Rather than introducing a mass scale to regulate the collinear and infrared divergences, the standard procedure to regulate the divergent integrals is to work at $4+\epsilon$ dimensions, in which the strong coupling constant is replaced by

$$g_s \to g_s \mu_s^{\epsilon/2},$$

where the scale μ_s is arbitrary. In this case, before introducing the scale-dependent PDFs, the structure function F_2 to $\mathcal{O}(\alpha_s)$ is of the form

$$\begin{aligned}\frac{F_2(x,Q^2)}{x} = \sum_{q,\bar{q}} e_q^2 \Bigg\{ &\left[1 - \left(\frac{\alpha_s}{2\pi}\right) \left[\frac{1}{\hat{\epsilon}} + \log\left(\frac{\mu_s^2}{Q^2}\right)\right] P_{qq} + h^q\right] \otimes f_q \\ &- \left[\left(\frac{\alpha_s}{2\pi}\right) \left[\frac{1}{\hat{\epsilon}} + \log\left(\frac{\mu_s^2}{Q^2}\right)\right] P_{qg} + h^g\right] \otimes f_g \Bigg\} ,\end{aligned} \tag{123}$$

where $1/\hat{\epsilon} = 1/\epsilon + \log(4\pi) - \gamma_E$. We see that the $\log(Q^2/m^2)$ type of divergences are now represented by poles at $\epsilon = 0$,

$$\log\left(\frac{Q^2}{m^2}\right) \Leftrightarrow -\left[\frac{1}{\hat{\epsilon}} + \log\left(\frac{\mu_s^2}{Q^2}\right)\right] . \tag{124}$$

The finite pieces h^i and h'^i are in general different due to a different regularization procedure. Based on what was just said on the scheme and factorization-scale dependence, we now understand that the general $\mathcal{O}(\alpha_s)$ definition of scale-dependent PDFs at factorization scale μ^2 can be written as

$$f_q(x,\mu^2) = \left[1 + \left(\frac{\alpha_s}{2\pi}\right) [L] P_{qq} + f^{qq}_{\text{scheme}}\right] \otimes f_q + \left[\left(\frac{\alpha_s}{2\pi}\right) [L] P_{qg} + f^{qg}_{\text{scheme}}\right] \otimes f_g \tag{125}$$

$$f_g(x,\mu^2) = \left[1 + \left(\frac{\alpha_s}{2\pi}\right) [L] P_{gg} + f^{gg}_{\text{scheme}}\right] \otimes f_g + \left[\left(\frac{\alpha_s}{2\pi}\right) [L] P_{gq} + f^{gq}_{\text{scheme}}\right] \otimes f_q \tag{126}$$

where

$$[L] = \log\left(\frac{\mu^2}{m^2}\right), \text{ or } [L] = -\left[\frac{1}{\hat{\epsilon}} + \log\left(\frac{\mu_s^2}{\mu^2}\right)\right] . \tag{127}$$

or, equivalently,

$$f_q = \left[1 - \left(\frac{\alpha_s}{2\pi}\right)[L]P_{qq} - f^{qq}_{\text{scheme}}\right] \otimes f_q(x,\mu^2) - \left[\left(\frac{\alpha_s}{2\pi}\right)[L]P_{qg} + f^{qg}_{\text{scheme}}\right] \otimes f_g(x,\mu^2)$$

$$f_g = \left[1 - \left(\frac{\alpha_s}{2\pi}\right)[L]P_{gg} - f^{gg}_{\text{scheme}}\right] \otimes f_g(x,\mu^2) - \left[\left(\frac{\alpha_s}{2\pi}\right)[L]P_{gq} + f^{gq}_{\text{scheme}}\right] \otimes f_q(x,\mu^2)$$

Here, the arbitrary functions f^{ij}_{scheme} define the **factorization scheme** and the arbitrary scale μ^2 is called the **factorization scale**. In terms of these scale-dependent PDFs, the structure function F_2 can be written as

$$\begin{aligned}\frac{F_2(x,Q^2)}{x} = \sum_{q,\bar{q}} e_q^2 \Bigg\{ &\left[1 + \left(\frac{\alpha_s}{2\pi}\right)\log\left(\frac{Q^2}{\mu^2}\right)P_{qq} + \left(h^q - f^{qq}_{\text{scheme}}\right)\right] \otimes f_q(\mu^2) \\ &+ \left[\left(\frac{\alpha_s}{2\pi}\right)\log\left(\frac{Q^2}{\mu^2}\right)P_{qg} + \left(h^g - f^{qg}_{\text{scheme}}\right)\right] \otimes f_g(\mu^2)\Bigg\},\end{aligned} \tag{128}$$

from which we see that the scheme dependence also affects the coefficient functions, as was already discussed. Today, it is almost exclusively the case, that the calculations are performed using the dimensional regularization. Similarly, the default factorization scheme is the so-called $\overline{\textbf{MS}}$ **scheme** in which $f^{ij}_{\text{scheme}} = 0$. In this scheme the $\mathcal{O}(\alpha_s)$ expressions for the DIS structure function F_2 are:

$$\begin{aligned}&\frac{1}{x}F_2(x,Q^2) = \\ &\sum_{q,\bar{q}} e_q^2 f_q(Q_f^2) \otimes \left\{1 - \frac{\alpha_s}{2\pi}\log\left(\frac{Q_f^2}{Q^2}\right)P_{qq} + \frac{\alpha_s}{2\pi}C_q\right\} \\ +2&\sum_q e_q^2 f_g(Q_f^2) \otimes \left\{\quad -\frac{\alpha_s}{2\pi}\log\left(\frac{Q_f^2}{Q^2}\right)P_{qg} + \frac{\alpha_s}{2\pi}C_g\right\},\end{aligned} \tag{129}$$

where

$$C_q(z) \equiv C_F\left\{(1+z^2)\left[\frac{\log(1-z)}{1-z}\right]_+ - \frac{3}{2}\frac{1}{(1-z)_+} - \frac{1+z^2}{1-z}\log z + 3 + 2z - \left(\frac{9}{2} + \frac{\pi^2}{3}\right)\delta(1-z)\right\} \tag{130}$$

$$C_g(z) \equiv P_{qg}(z)\log\left(\frac{1-z}{z}\right) + T_R 6z(1-z) - P_{qg}(z). \tag{131}$$

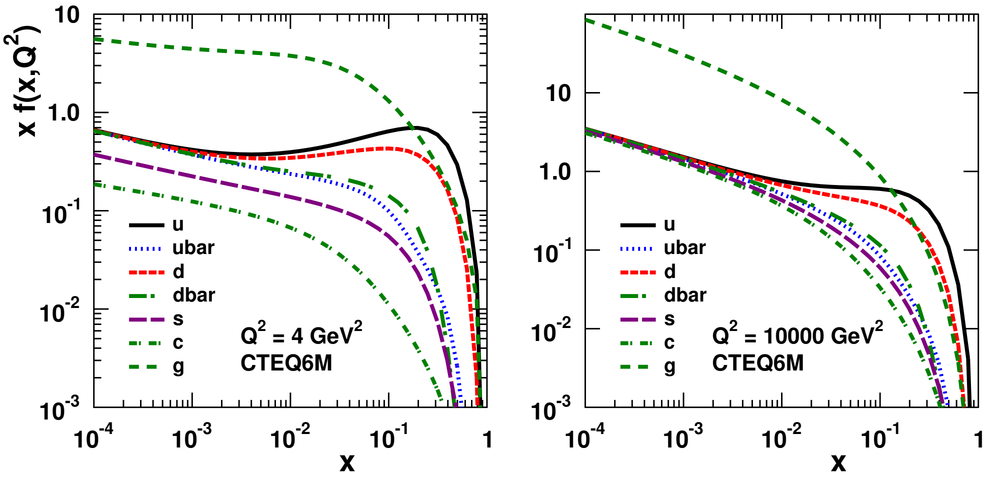

Figure 18: The (archaeological) CTEQ6M partons [24].

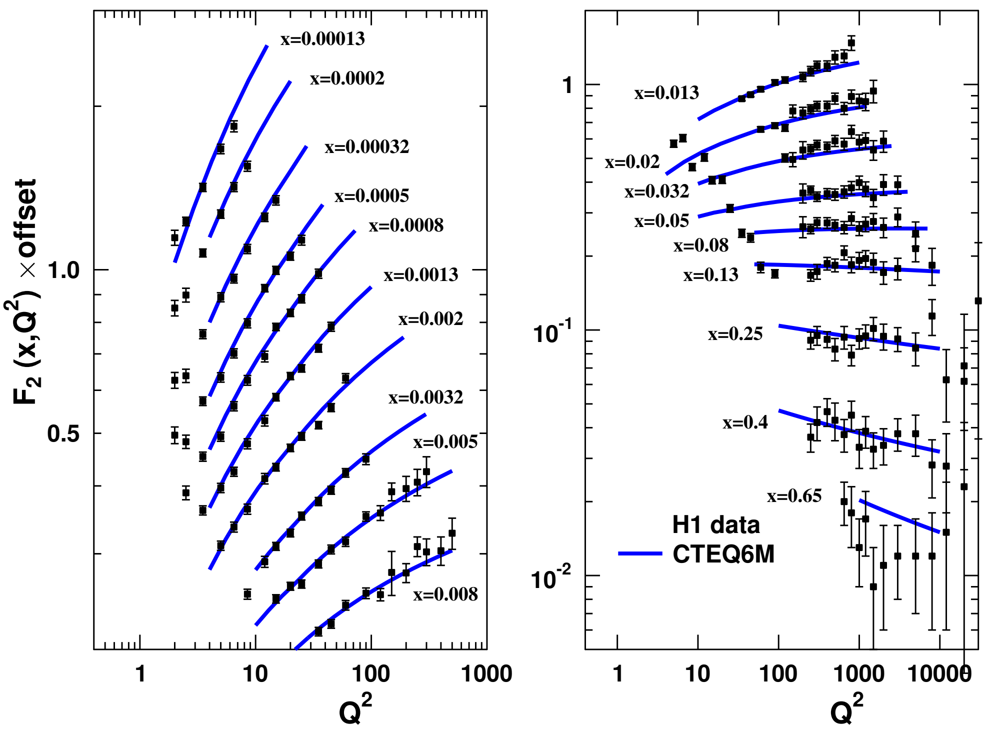

Figure 19: Experimental data for proton structure function F_2 from H1 experiment [25, 26] compared with the CTEQ6M PDFs [24].

4 Solving DGLAP at small x: The Double Asymptotic Scaling

In general, the DGLAP equations have to be solved numerically. However, it is still possible to find some enlightening properties in a closed form. One of the most striking features that can be found "by hand" is the so-called **Double Asymptotic Scaling** [27, 28], related to the behaviour of the DIS structure functions at small-x and high Q^2.

Let us first introduce the concept of **Mellin transform**. We define the Mellin transform of a PDF as

$$f_i(N, Q^2) \equiv \int_0^1 dx x^{N-1} f_i(x, Q^2)\,. \tag{132}$$

The inverse transform from the "Mellin N space" back to the x space can be obtained as

$$f_i(x, Q^2) = \frac{1}{2\pi i} \int_{a-i\infty}^{a+i\infty} dN x^{-N} f(N, Q^2)\,, \tag{133}$$

where the contour of integration has to lie to the right of all the poles the integrand may contain. The Mellin moments of the splitting functions are often called **anomalous dimensions**,

$$\gamma(N)_{ij}^{(n)} \equiv \int_0^1 dx x^{N-1} P_{ij}^{(n)}(x)\,. \tag{134}$$

The power/usefulness of the Mellin transform is, that in the Mellin space the DGLAP equations become just ordinary differential equations. For example, the evolution of the singlet-quark and gluon distributions,

$$\begin{aligned} Q^2 \frac{\Sigma(x,\zeta)}{dQ^2} &= \frac{\alpha_s(Q^2)}{2\pi} \int_x^1 \frac{dz}{z} \left[P_{qq}(z) \Sigma\left(\frac{x}{z}, Q^2\right) + 2n_f P_{qg}(z) f_g\left(\frac{x}{z}, Q^2\right)\right]\,, \\ Q^2 \frac{f_g(x,Q^2)}{dQ^2} &= \frac{\alpha_s(Q^2)}{2\pi} \int_x^1 \frac{dz}{z} \left[P_{gg}(z) f_g\left(\frac{x}{z}, Q^2\right) + P_{gq}(z) \Sigma\left(\frac{x}{z}, Q^2\right)\right]\,. \end{aligned} \tag{135}$$

turns into

$$Q^2 \frac{d}{dQ^2} \begin{bmatrix} \Sigma(N,Q^2) \\ f_g(N,Q^2) \end{bmatrix} = \frac{\alpha_s(Q^2)}{2\pi} \begin{pmatrix} \gamma_{qq} & 2n_f \gamma_{qg} \\ \gamma_{gq} & \gamma_{gg} \end{pmatrix} \begin{bmatrix} \Sigma(N,Q^2) \\ f_g(N,Q^2) \end{bmatrix}\,, \tag{136}$$

by taking the Mellin transform on both sides of Eq. (135). To leading order, the (integer N) anomalous dimensions are

$$\gamma_{qq}^{(0)}(N) = C_F \left[-\frac{1}{2} + \frac{1}{N(N+1)} - 2\sum_{k=2}^{N} \frac{1}{k} \right]\,, \tag{137}$$

$$\gamma_{qg}^{(0)}(N) = T_f \left[\frac{2+N+N^2}{N(N+1)(N+2)} \right]\,, \tag{138}$$

$$\gamma_{gq}^{(0)}(N) = C_F \left[\frac{2+N+N^2}{N(N^2-1)} \right]\,, \tag{139}$$

$$\gamma_{gg}^{(0)}(N) = 2C_A \left[-\frac{1}{12} + \frac{1}{N(N-1)} + \frac{1}{(N+1)(N+2)} - \sum_{k=2}^{N} \frac{1}{k} \right] - \frac{n_f}{3}\,. \tag{140}$$

Towards small x, the most relevant part of the leading-order splitting functions behave as $1/x$. Now, since

$$\int_0^1 dx x^{N-1} \frac{1}{x} = \frac{1}{N-1}\,, \tag{141}$$

we see that towards small x, the $N \approx 1$ region is the interesting one in the Mellin space. Thus, taking the $N \to 1$ limit, we find

$$\gamma_{qq}^{(0)}(N) \xrightarrow{N\to 1} 0\,, \tag{142}$$

$$\gamma_{qg}^{(0)}(N) \xrightarrow{N\to 1} T_f \frac{2}{3}\,, \tag{143}$$

$$\gamma_{gq}^{(0)}(N) \xrightarrow{N\to 1} C_F \left[\frac{2}{N-1} - \frac{3}{2}\right]\,, \tag{144}$$

$$\gamma_{gg}^{(0)}(N) \xrightarrow{N\to 1} 2C_A \left[\frac{1}{N-1} - \frac{11}{12}\right] - \frac{n_f}{3}\,. \tag{145}$$

The inverse transform back to the x space gives,

$$P_{qq}^{(0)}(z) \xrightarrow{z\to 0} 0\,, \tag{146}$$

$$P_{qg}^{(0)}(z) \xrightarrow{z\to 0} T_f \frac{2}{3}\delta(1-z)\,, \tag{147}$$

$$P_{gq}^{(0)}(z) \xrightarrow{z\to 0} \frac{2C_F}{z} - \frac{3C_F}{2}\delta(1-z)\,, \tag{148}$$

$$P_{gg}^{(0)}(z) \xrightarrow{z\to 0} \frac{2C_A}{z} - \left[\frac{11C_A}{6} + \frac{n_f}{3}\right]\delta(1-z)\,. \tag{149}$$

Let us now define a new variable

$$\zeta = \frac{2}{\beta_0}\log\left(\frac{t}{t_0}\right), \quad t \equiv \log(Q^2/\Lambda_{\rm QCD}^2), \quad t_0 \equiv \log(Q_0^2/\Lambda_{\rm QCD}^2)\,, \tag{150}$$

where Q_0^2 is the initial scale for evolution. Trading the Q^2 derivative in the DGLAP equations with ζ, using

$$\frac{d\zeta}{dQ^2} = \frac{\alpha_s(Q^2)}{2\pi}\frac{1}{Q^2} \tag{151}$$

we have

$$\frac{\Sigma(x,\zeta)}{d\zeta} = \int_x^1 \frac{dz}{z}\left[P_{qq}(z)\Sigma\left(\frac{x}{z},\zeta\right) + 2n_f P_{qg}(z) f_g\left(\frac{x}{z},\zeta\right)\right]\,, \tag{152}$$

$$\frac{f_g(x,\zeta)}{d\zeta} = \int_x^1 \frac{dz}{z}\left[P_{gg}(z) f_g\left(\frac{x}{z},\zeta\right) + P_{gq}(z)\Sigma\left(\frac{x}{z},\zeta\right)\right]\,. \tag{153}$$

Neglecting the quark part in the gluon evolution, the evolution equation for the gluon becomes homogeneous,

$$\frac{f_g(x,\zeta)}{d\zeta} = \int_x^1 \frac{dz}{z}\left[P_{gg}(z) f_g\left(\frac{x}{z},\zeta\right)\right]\,. \tag{154}$$

Multiplying by x, and defining $G(x,\zeta) \equiv x f_g(x,\zeta)$, we have

$$\frac{G(x,\zeta)}{d\zeta} = \int_x^1 \frac{dz}{z}\left[zP_{gg}(z)\right] G\left(\frac{x}{z},\zeta\right)\,. \tag{155}$$

Taking now the Mellin transform,

$$\frac{G(N,\zeta)}{d\zeta} = G(N,\zeta) \times \int_0^1 dz z^{N-1}\left[zP_{gg}(z)\right]\,, \tag{156}$$

and using the $x \to 0$ limit for the splitting function in Eq. (149), we get

$$\frac{G(N,\zeta)}{d\zeta} = G(N,\zeta) \times \left[\frac{2C_A}{N} - \left(\frac{11C_A}{6} + \frac{n_f}{3}\right)\right] . \tag{157}$$

The solution is easily seen to be,

$$G(N,\zeta) = G(N,0) \exp\left[\zeta\left(\frac{2C_A}{N} - \frac{11C_A}{6} - \frac{n_f}{3}\right)\right] . \tag{158}$$

We will consider an initial condition $G(x,0) = \mathcal{N}$, where $\mathcal{N}$ is just a normalization constant. The Mellin moments are now $G(N,0) = \mathcal{N}/N$, such that

$$G(N,\zeta) = \frac{\mathcal{N}}{N} \exp\left[\zeta\left(\frac{2C_A}{N} - \frac{11C_A}{6} - \frac{n_f}{3}\right)\right] . \tag{159}$$

To revert the obtained gluon distribution back to the x space, we must take the inverse Mellin transformation Eq. (133),

$$\begin{aligned} G(x,\zeta) &= \frac{1}{2\pi i}\int_{a-i\infty}^{a+i\infty} dN x^{-N} G(N,\zeta) = \frac{1}{2\pi i}\int_{a-i\infty}^{a+i\infty} dN x^{-N}\frac{\mathcal{N}}{N}\exp\left[\zeta\left(\frac{2C_A}{N} - \frac{11C_A}{6} - \frac{n_f}{3}\right)\right] \\ &= \mathcal{N}\exp\left[-\zeta\left(\frac{11C_A}{6} + \frac{n_f}{3}\right)\right] \times \frac{1}{2\pi i}\int_{c-i\infty}^{c+i\infty}\frac{dN}{N}\exp\left[\frac{2\zeta C_A}{N} + N\log(1/x)\right] , \end{aligned} \tag{160}$$

where now $c > 0$. The above integral can be evaluated in terms of modified Bessel functions I_n, using an integral representation,

$$I_n(z) \equiv \frac{1}{2\pi i}\oint \exp\left[\frac{z}{2}\left(t + \frac{1}{t}\right)\right] t^{-n-1} dt\,, \tag{161}$$

where the integration contour encloses the origin. The result is

$$G(x,\zeta) = \exp\left[-\zeta\left(\frac{11C_A}{6} + \frac{n_f}{3}\right)\right] \times I_0\left(2\sqrt{2C_A\zeta\log(1/x)}\right) . \tag{162}$$

Using the asymptotic expansion of the Bessel function

$$I_n(z) \xrightarrow{z\to\infty} \frac{e^z}{\sqrt{2\pi z}}, \tag{163}$$

the gluon distribution $G(x,\zeta)$ can be written, in the limit $\zeta \gg 1$ and $x \ll 1$ (large Q^2, small x),

$$G(x,\zeta) \to \mathcal{N}\exp\left[-\zeta\left(\frac{11C_A}{6} + \frac{n_f}{3}\right)\right] \times \frac{e^{2\sqrt{2C_A\zeta\log(1/x)}}}{\sqrt{4\pi\sqrt{2C_A\zeta\log(1/x)}}} . \tag{164}$$

Defining now two new variables,

$$\sigma \equiv \left[\log\left(\frac{1}{x}\right)\log\left(\frac{t}{t_0}\right)\right]^{1/2}, \quad \rho \equiv \left[\frac{\log(1/x)}{\log(t/t_0)}\right]^{1/2} , \tag{165}$$

we find

$$G(\sigma,\rho) \to \frac{\mathcal{N}}{\sqrt{4\pi\gamma\sigma}}\exp\left(2\gamma\sigma - \frac{\delta\sigma}{\rho}\right) \times \left[1 + \mathcal{O}\left(\frac{1}{\sigma}\right)\right] , \tag{166}$$

where $\gamma \equiv \sqrt{4C_A/\beta_0}$ and $\delta \equiv 2(11C_A/6 + n_f/3)/\beta_0$. Although we have derived this result with a specific boundary condition $G(x, t_0) = constant$, the found asymptotic behaviour is not particulary sensitive to this choice as far as the boundary conditions are reasonably soft.

Having a result for the gluon distribution is of course nice, but in order to directly compare with the DIS data, we must still relate it to the quark distributions. In the $x \to 0$ limit, the evolution for the singlet quark momentum distribution $Q(x, Q^2) = x\Sigma(x, Q^2)$ reads

$$\frac{dQ(x,\zeta)}{d\zeta} = x\int_x^1 \frac{dz}{z}\left[2n_f P_{qg}(z) f_g\left(\frac{x}{z},\zeta\right)\right] = x\int_x^1 \frac{dz}{z} 2n_f \left[T_f \frac{2}{3}\delta(1-z)\right] f_g\left(\frac{x}{z},\zeta\right) \tag{167}$$

$$= x\frac{4T_f n_f}{3} f_g(x,\zeta) = \frac{4T_f n_f}{3} G(x,\zeta)\ . \tag{168}$$

By the chain rule,

$$\frac{dQ(\sigma,\rho)}{d\zeta} = \frac{d\sigma}{d\zeta}\frac{dQ(\sigma,\rho)}{d\sigma} + \frac{d\rho}{d\zeta}\frac{dQ(\sigma,\rho)}{d\rho} = \left(\frac{3\rho}{\gamma^2}\right)\frac{dQ(\sigma,\rho)}{d\sigma} - \left(\frac{\gamma^2\rho^2}{12\sigma}\right)\frac{dQ(\sigma,\rho)}{d\rho}\,, \tag{169}$$

In the $\sigma \to \infty$ limit, the second term can be dropped, so that

$$\frac{Q(\sigma,\rho)}{d\sigma} = \frac{\gamma^2}{3\rho}\frac{4T_f n_f}{3} G(\sigma,\rho)\,, \tag{170}$$

and the singlet quark momentum distribution can be obtained simply as an integral,

$$Q(\sigma,\rho) = Q(0,\rho) + \frac{\gamma^2}{3\rho}\frac{4T_f n_f}{3}\int_0^\sigma d\sigma'\, G\left(\sigma',\rho\right)\ . \tag{171}$$

It is easy to show that

$$\int_0^\sigma d\sigma'\, G\left(\sigma',\rho\right) = \frac{\mathcal{N}}{2\gamma}\frac{1}{\sqrt{4\pi\gamma\sigma}}\exp\left(2\gamma\sigma - \frac{\delta\sigma}{\rho}\right) \times \left[1 + \mathcal{O}\left(\frac{1}{\rho}\right) + \mathcal{O}\left(\frac{1}{\sigma}\right)\right]\,, \tag{172}$$

such that

$$Q(\sigma,\rho) \approx \frac{1}{6}\left(\frac{\gamma}{\rho}\right)\frac{4T_f n_f}{3} G(\sigma,\rho)\ . \tag{173}$$

To leading order, the structure function F_2 now becomes

$$F_2(\sigma,\rho) = \sum_i e_i^2 x\left(f_i + f_{\bar{i}}\right) \approx \left(\frac{1}{n_f}\sum_i^{n_f} e_i^2\right) Q(\sigma,\rho) = \langle e^2\rangle Q(\sigma,\rho)\,, \tag{174}$$

where the average squared fractional quark charge is

$$\langle e^2\rangle \equiv \left(\frac{1}{n_f}\sum_i^{n_f} e_i^2\right) = \left\{\begin{array}{ll} 5/18 & \text{for 4 flavours} \\ 11/45 & \text{for 5 flavours}\end{array}\right.\ . \tag{175}$$

Thus, and to summarize, we find the following:

$$\boxed{\begin{aligned} F_2(\sigma,\rho) &\xrightarrow{\sigma,\rho\to\infty} \langle e^2\rangle \frac{2T_f n_f}{9}\left(\frac{\gamma}{\rho}\right) G(\sigma,\rho)\ , \qquad (176)\\ G(\sigma,\rho) &= \mathcal{N}\frac{1}{\sqrt{4\pi\gamma\sigma}}\exp\left(2\gamma\sigma - \frac{\delta\sigma}{\rho}\right)\ , \qquad (177)\\ &\text{where } \gamma \equiv \sqrt{4C_A/\beta_0} \text{ and } \delta \equiv 2(11C_A/6 + n_f/3)/\beta_0. \end{aligned}}$$

In Refs. [27, 28] the value of δ is slightly different than what we have here. This comes from accounting also for the quarks in the evolution. However, this affects only the subasymptotic behaviour.

We can now see that the asymptotic results for F_2 and G exhibit a particularly simple scaling both in σ and ρ:

For fixed ρ: $\log F_2(\sigma,\rho) \sim$ linear in σ

For fixed σ: $\log F_2(\sigma,\rho) \sim$ independent of ρ

For $\sigma,\rho\to\infty$: $\sigma^{-1}\log F_2(\sigma,\rho) \sim$ independent of both σ and ρ

The latter property is called the **double asymptotic scaling**. The following figures compare the expected behaviour with the data from HERA experiment. In Figure 20, the F_2 data has been rescaled by a factor of

$$R'_F(\sigma,\rho) = R\times\exp\left[\frac{\delta\sigma}{\rho} + \frac{\log\sigma}{2} + \log\left(\frac{\rho}{\gamma}\right)\right]\ , \qquad (178)$$

such that the prediction is

$$R'_F(\sigma,\rho)F_2(\sigma,\rho) \propto \exp(2\gamma\sigma)\ . \qquad (179)$$

Plotted with a logaritmic y axis, we thus expect a straight line as a function of σ with a slope of 2γ. The data clearly agrees with this expectation.

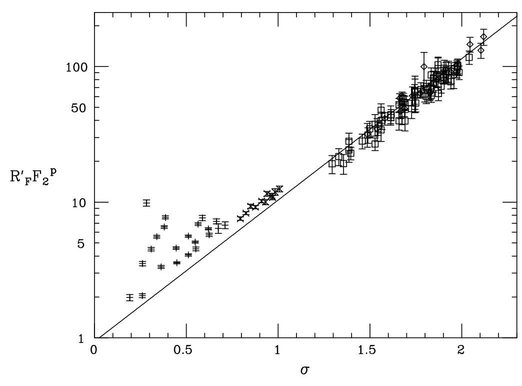

Fig. 1

Figure 20: Tests of the double asymptotic scaling with early HERA data. Figure from Ref. [28].

Scaling the F_2 data with another factor

$$R_F(\sigma,\rho) = R \times \exp\left[-2\gamma\sigma\frac{\delta\sigma}{\rho} + \frac{\log\sigma}{2} + \log\left(\frac{\rho}{\gamma}\right)\right], \tag{180}$$

we would expect

$$R_F(\sigma,\rho)F_2(\sigma,\rho) = \text{constant } + \mathcal{O}\left(\frac{1}{\sigma}\right) + \mathcal{O}\left(\frac{1}{\rho}\right). \tag{181}$$

Examples are shown in Figure 21. The data indicate that the double asymptotic scaling is an excellent approximation.

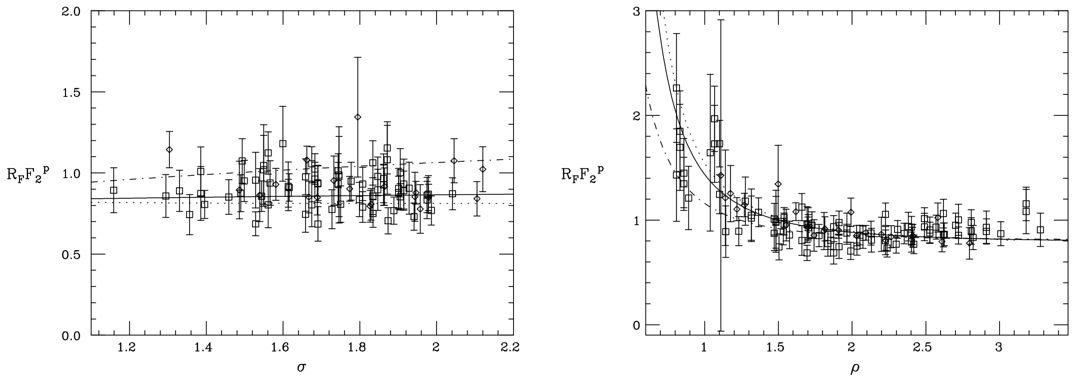

Fig. 2a

Fig. 2b

Figure 21: Tests of the double asymptotic scaling with early HERA data. Figures from Ref. [28].

In the present approximation we ignored the P_{qq} and P_{gq} splitting functions. That is, in terms of parton ladders, we omit the $q \to qg$ splittings. Thus, the diagrams that get resummed in the double asymptotic approximation to F_2, are pure gluon ladders, which end up with a $g \to q\overline{q}$ splitting, see Figure 22.

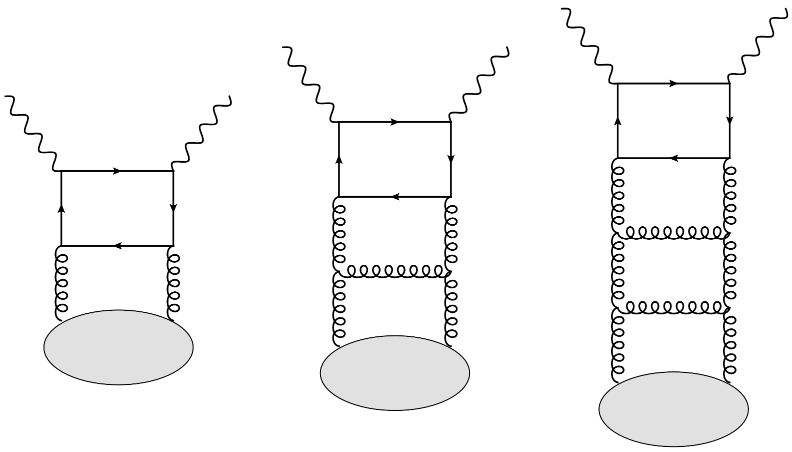

Figure 22: Ladder diagrams that yield the asymptotic behaviour of F_2 at the doubly asymptotic limit $\sigma, \rho \to \infty$.

5 Principles of General-Mass Variable Flavour Number scheme

Up to now, we have implicitly considered PDFs of only gluons and massless quarks. In the younger days of PDF analysis, a pragmatic way of dealing with massive (charm and bottom) quarks was the so-called **zero-mass variable flavour number scheme** (ZM-VFNS). In its simplicity, below the mass threshold $Q^2 < m_{\rm H}^2$ (H=charm, bottom), the heavy quark was considered as non-existing, but above the mass threshold $Q^2 > m_{\rm H}^2$, the heavy quark was included in the calculations (matrix elements, PDF evolution, running of α_s), treating it as a massless quark. At high scales $Q^2 \gg m_{\rm H}^2$ this is perfectly OK, as the $m_{\rm H}^2/Q^2$ terms in the coefficient functions die away. Near the threshold $Q^2 \sim m_{\rm H}^2$, however, the zero-mass approximation is somewhat vague. To overcome this, a consistent framework to deal with heavy quarks, the so-called **general-mass variable flavour number scheme** (GM-VFNS) has been developed.

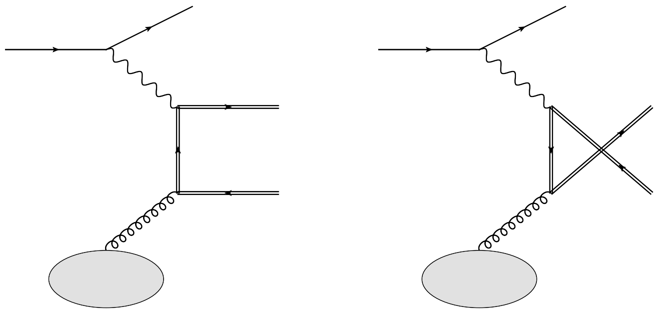

Figure 23: The two diagrams for DIS heavy-quark production in FFNS.

To get started, let us look at the process of heavy-quark production in DIS in an approximation that the proton does not contain a significant quantity of heavy quarks. Indeed, because of the heavy-quark mass $m_{\rm H}^2$, the radiation of heavy quarks in the parton ladder is suppressed in comparison to the massless partons as there is no strict collinear divergence. In this case, the heavy quarks are produced only dynamically by partonic processes. Such a framework in which the heavy quarks are not considered as active partons is often called a **fixed flavour number scheme** (FFNS). Figure 23 shows the two Feynman diagrams for heavy-quark production in DIS to first order in α_s. The resulting expression for the structure function $F_2^{\rm H}$ is [29],

$$\frac{1}{x}F_2^{\rm H}(x,Q^2) = 2e_{\rm H}^2 \int_\chi^1 \frac{dz}{z} C_2^{\rm H}\left(\frac{\chi}{z}, \frac{m_{\rm H}}{Q^2}\right) f_g(z,Q^2)\,, \tag{182}$$

where the coefficient function $C_2^{\rm H}$ reads

$$C_2^{\rm H}\left(z, \frac{m_{\rm H}}{Q^2}\right) = \frac{\alpha_s}{2\pi}\left\{ v\left[4z(1-z) - \frac{1}{2} - 2\left(\frac{m_{\rm H}^2}{Q^2}\right) z(1-z)\right]\right. \tag{183}$$

$$\left. + \left[\!\!\left[\frac{1}{2}\left[z^2+(1-z)^2\right] + 2\left(\frac{m_{\rm H}^2}{Q^2}\right) z(1-3z) - 4\left(\frac{m_{\rm H}^4}{Q^4}\right) z^2 \right]\!\!\right] \log\frac{1+v}{1-v}\right\}\,, \tag{184}$$

and

$$v = \sqrt{1 - \frac{4m_{\rm H}^2}{Q^2}\frac{z}{1-z}}, \quad \chi = x\left(1 + \frac{4m_{\rm H}^2}{Q^2}\right)\,. \tag{185}$$

In comparison to the zero-mass case, an important aspect here is that lower limit for the convolution integral is not x but χ. This accounts for the extra energy required to produce the heavy quark-antiquark pair. Towards high Q^2, $\chi \to x$, so that the massless kinematics is recovered, but at low Q^2 the effect is significant. Recalling that the PDFs are typically rather steep functions of x, even small shifts in the probed momentum fraction may result as significant differences in the cross section. Figure 24 illustrates the situation.

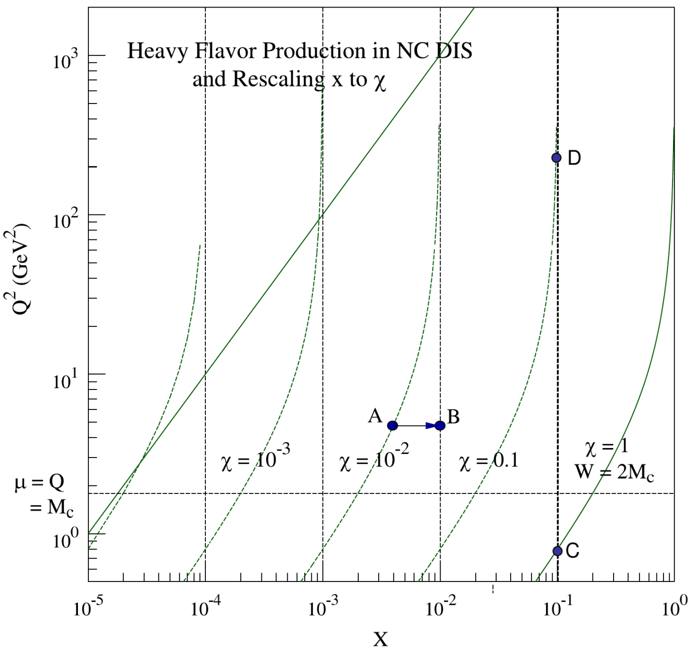

Figure 24: Zero-mass vs. heavy-flavour kinematics in DIS. Figure from Ref. [30]

In the $m_{\rm H} \to 0$ limit, the coefficient function above behaves as

$$C_2^{\rm H}\left(\frac{x}{z}, \frac{m_{\rm H}}{Q^2}\right) \xrightarrow{m_{\rm H}\to 0} \frac{\alpha_s}{2\pi}\frac{1}{2}\left[z^2+(1-z)^2\right]\log\left(\frac{Q^2}{m_{\rm H}}\right) = \frac{\alpha_s}{2\pi}P_{qg}(z)\log\left(\frac{Q^2}{m_{\rm H}^2}\right), \tag{186}$$

which should look familiar to you — it's the same (collinear logarithm)×(splitting function) structure we derived earlier using the Sudakov decomposition. Let us now write

$$\begin{aligned}\frac{1}{x}F_2^{\rm H}(x,Q^2) = 2e_{\rm H}^2\Bigg[&\int_\chi^1 \frac{dz}{z}C_2^{\rm H}\left(\frac{\chi}{z}, \frac{m_{\rm H}^2}{Q^2}\right)f_g(z,Q^2) - \frac{\alpha_s}{2\pi}\log\left(\frac{\mu^2}{m_{\rm H}^2}\right)\int_\chi^1\frac{dz}{z}P_{qg}\left(\frac{\chi}{z}\right)f_g(z,Q^2) \\ &+ \frac{\alpha_s}{2\pi}\log\left(\frac{\mu^2}{m_{\rm H}^2}\right)\int_\chi^1\frac{dz}{z}P_{qg}\left(\frac{\chi}{z}\right)f_g(z,Q^2)\Bigg].\end{aligned} \tag{187}$$

Based on the discussion in the previous sections we understand that, to $\mathcal{O}(\alpha_s)$, we can define the heavy-quark PDF as,

$$f_{{\rm H},\overline{\rm H}}(\chi,\mu^2) = \frac{\alpha_s}{2\pi}\log\left(\frac{\mu^2}{m_{\rm H}^2}\right)\int_\chi^1\frac{dz}{z}P_{qg}(z)f_g\left(\frac{\chi}{z},Q^2\right)+\mathcal{O}(\alpha_s^2), \tag{188}$$

where μ is the factorization scale. Thus, we have

$$\frac{1}{x}F_2^{\rm H}(x,Q^2) = 2e_{\rm H}^2\left[\int_\chi^1\frac{dz}{z}\tilde{C}_2^{\rm H}\left(\frac{\chi}{z},\frac{m_{\rm H}}{Q^2}\right)f_g(z,Q^2)\right] + e_{\rm H}^2\left[f_{\rm H}(\chi,Q^2)+f_{\overline{\rm H}}(\chi,Q^2)\right]+\mathcal{O}(\alpha_s^2), \tag{189}$$

with

$$\tilde{C}_2^{\rm H}\left(z,\frac{m_{\rm H}}{Q^2}\right)=C_2^{\rm H}\left(z,\frac{m_{\rm H}}{Q^2}\right)-\frac{\alpha_s}{2\pi}\log\left(\frac{Q^2}{m_{\rm H}^2}\right)P_{qg}\left(z\right)\,. \tag{190}$$

Note now that the coefficient function $\tilde{C}_2^{\rm H}$ is no longer divergent in the $m_{\rm H}\to 0$ limit — the logarithmic divergence has been resummed to the heavy-quark PDFs $f_{\rm H,\overline{H}}$ and the subtracted from the original coefficient function $C_2^{\rm H}$ to avoid double counting. The last two terms in Eq. (189) are just the leading-order contributions to the F_2 and they are exactly of the same form as for massless quarks. Formally, Eq. (182) and Eq. (189) are the same up to corrections of the order of $\mathcal{O}(\alpha_s^2)$. However, only Eq. (189) is well-behaved at high Q^2. The question of when to change from Eq. (182) (accurate at low Q^2) to Eq. (189) (well-behaved at high Q^2) is ambiguous. The scale at which this change is made is called **transition scale** $Q_{\rm t}$. At this stage, it appears advantageous to take $Q_{\rm t}=m_{\rm H}^2$ since with choice the coefficient function is continuous across the transition scale, and the heavy-quark PDFs starts its DGLAP evolution from zero,

$$\tilde{C}_2^{\rm H}(z,m_{\rm H}^2/Q^2)=C_2^{\rm H}(z,m_{\rm H}^2/Q^2),\quad f_{\rm H}(z,Q^2)=0,\ \text{at } Q^2=m_{\rm H}^2\,.$$

At one power higher in α_s the "best choice" is no longer this obvious [31].

Based on discussions in the earlier sections, it should not be surprising that the definition of heavy-quark PDF in Eq. (188) is not unique, but scale-independent terms defining the scheme are still allowed. These constant terms can be fixed by requiring that the resulting F_2 approaches asymptotically the $\overline{\rm MS}$ results. In the present case, it is easy to check that

$$\tilde{C}_2^{\rm H}\left(z,\frac{m_{\rm H}}{Q^2}\right)\xrightarrow{m_{\rm H}\to 0}\frac{\alpha_s}{2\pi}\left[P_{qg}(z)\log\left(\frac{1-z}{z}\right)+4z(1-z)-\frac{1}{2}\right]=C_2^{\overline{\rm MS}}\left(z\right)\,, \tag{191}$$

where $C_2^{\overline{\rm MS}}\left(z\right)$ is the same as in Eq. (131). That is, the $m_{\rm H}\to 0$ limit is exactly that of $\overline{\rm MS}$ scheme with massless quarks, and no scheme-dependent terms are required. At higher orders this is no longer true, and in order to recover the $\overline{\rm MS}$ results at high Q^2, the added and subtracted piece in Eq. (187) must also contain additional terms. These terms become then the scheme-dependent part in the definition of PDFs. Making sure that the $\overline{\rm MS}$ results for the coefficient functions are asymptotically recovered then also ensures that the PDFs evolve according to the $\overline{\rm MS}$ splitting functions above the transition scale.

5.1 Additional scheme dependence in GM-VFNS

There's yet another scheme dependence in GM-VFNS. This scheme dependence does not affect the definition or evolution of the PDFs, but it's of different nature. In Eq. (187) we "added zero" to the original $\tilde{C}_2^{\rm H}$ by adding and subtracting a certain logarithmic term. However, we can also include arbitrary $m_{\rm H}^2$-dependent terms as well,

$$\begin{aligned}
&\frac{\alpha_s}{2\pi}\log\left(\frac{\mu^2}{m_{\rm H}^2}\right)\int_\chi^1\frac{dz}{z}P_{qg}\left(\frac{\chi}{z}\right)f_g(z,Q^2)\\
&\Longrightarrow\\
&\frac{\alpha_s}{2\pi}\log\left(\frac{\mu^2}{m_{\rm H}^2}\right)\left[1+f(\chi,m_{\rm H}^2)\right]\int_\chi^1\frac{dz}{z}P_{qg}\left(\frac{\chi}{z}\right)f_g(z,Q^2)\,,
\end{aligned} \tag{192}$$

where $f(\chi, m_{\rm H})$ is an arbitrary $m_{\rm H}^2$-dependent function such that $f(\chi, m_{\rm H}^2) \to 0$ as $m_{\rm H} \to 0$. The function $f(\chi, m_{\rm H})$ then appears in the final expression of F_2 as

$$\begin{aligned}\frac{1}{x} F_2^{\rm H}(x, Q^2) = 2e_{\rm H}^2 &\left[\int_\chi^1 \frac{dz}{z} \tilde{C}_2^{\rm H}\left(\frac{\chi}{z}, \frac{m_{\rm H}^2}{Q^2}\right) f_g(z, Q^2)\right] \\ &+ e_{\rm H}^2\left[1 + f(\chi, m_{\rm H}^2)\right]\left[f_{\rm H}\left(\chi, Q^2\right) + f_{\overline{\rm H}}\left(\chi, Q^2\right)\right] ,\end{aligned} \tag{193}$$

where now

$$\tilde{C}_2^{\rm H}\left(\frac{\chi}{z}, \frac{m_{\rm H}}{Q^2}\right) = C_2^{\rm H}\left(\frac{\chi}{z}, \frac{m_{\rm H}^2}{Q^2}\right) - \frac{\alpha_s}{2\pi}\log\left(\frac{Q^2}{m_{\rm H}^2}\right)\left[1 + f(\chi, m_{\rm H}^2)\right] P_{qg}\left(\frac{\chi}{z}\right) . \tag{194}$$

In other words, we can essentially decide what is the $m_{\rm H}^2$ dependence of the coefficient functions for contributions with heavy-quarks in the initial state. In addition, we could also replace χ by x. This is the scheme dependence of GM-VFNS. The difference between different schemes (=different definitions of $f(\chi, m_{\rm H})$) are again formally higher order in α_s. However, using the χ variable in the convolution integral instead of x has a special role in the sense that its origin is in the momentum conservation (the extra energy needed to create a pair quark-antiquark pair).

It is possible to use the scheme dependence of GM-VFNS to make calculations as easy as possible. Indeed, we can define a scheme in which all the heavy-quark initiated processes are computed with zero-mass $\overline{\rm MS}$ coefficient functions. This scheme is known as simplified Aivazis-Collins-Olness-Tung scheme or just **SACOT scheme**. Above, this is achieved by simply setting $f(\chi, m_{\rm H}) = 0$. Correspondingly, the α_s coefficient function would be that of Eq. (130), derived with zero-mass quarks. This scheme is clearly the most simplest one, and as accurate as any other. It's the default one in CTEQ (or CT-TEA) collaboration's PDFs. Before writing down the final expression, there's still one more thing to discuss...

5.2 Matching of strong coupling α_s

In the standard $\overline{\rm MS}$ scheme with massless quarks, the renormalization of the strong coupling α_s is, in practice, achieved by replacing the "bare" coupling α_s^0 in the calculations by the physical coupling $\alpha_s(\mu_{\rm ren}^2)$

$$\begin{aligned}\alpha_s^{\overline{\rm MS}}(\mu_{\rm ren}^2) &= \alpha_s^0\left(1 + \alpha_s^0 B^{\overline{\rm MS}}\right) \\ B^{\overline{\rm MS}} &= \frac{1}{4\pi}\left[\frac{4}{3}T_f n_f - \frac{11}{3}C_A\right]\left[\frac{1}{\hat\epsilon} + \log\left(\frac{\mu_{\rm ren}^2}{\mu^2}\right)\right] ,\end{aligned} \tag{195}$$

where $1/\hat\epsilon = 1/\epsilon + \log(4\pi) - \gamma_E$, n_f refers to the number of light quarks. Taking the derivative gives the usual beta function,

$$\mu_{\rm ren}^2 \frac{d\alpha_s^{\overline{\rm MS}}(\mu_{\rm ren}^2)}{d\mu_{\rm ren}^2} = \frac{d\alpha_s^{\overline{\rm MS}}(\mu_{\rm ren}^2)}{d\log(\mu_{\rm ren}^2)} = -b_0\left[\alpha_s^{\overline{\rm MS}}(\mu_{\rm ren}^2)\right]^2, \quad b_0 = \frac{11C_A - 4T_f n_f}{12\pi} . \tag{196}$$

The calculations in FFNS are usually performed in a different scheme, the so-called **decoupling scheme**. In this scheme, the light-quark and gluon loops are treated as in the $\overline{\rm MS}$ scheme, but the divergences from the heavy-quarks loops are subtracted at zero momentum. In practice, this amounts to a slightly different definition of the strong coupling,

$$\begin{aligned}\alpha_s^{\rm DC}(\mu_{\rm ren}^2) &= \alpha_s^0\left(1 + \alpha_s^0 B^{\rm DC}\right) \\ B^{\rm DC} &= \frac{1}{4\pi}\left[\frac{4}{3}T_f n_{\ell f} - \frac{11}{3}C_A\right]\left[\frac{1}{\hat\epsilon} + \log\left(\frac{\mu_{\rm ren}^2}{\mu^2}\right)\right] + \frac{4}{3}T_f\left[\frac{1}{\hat\epsilon} + \log\left(\frac{\mu_{\rm ren}^2}{\mu^2}\right) - \log\left(\frac{\mu_{\rm ren}^2}{m^2}\right)\right] ,\end{aligned} \tag{197}$$

where $n_{\ell f}$ refers to the number of light quarks. In other words, an additional term $(4T_f/3)\log\left(\mu_{\rm ren}^2/m^2\right)$ is included in the definition (which then appears in the coefficient functions). The point is that the α_s now runs as,

$$\frac{d\alpha_s^{\rm DC}(\mu_{\rm ren}^2)}{d\log(\mu_{\rm ren}^2)} = -b_0'\left[\alpha_s^{\rm DC}(\mu_{\rm ren}^2)\right]^2, \quad b_0' = \frac{11C_A - 4T_f n_{\ell f}}{12\pi}, \tag{198}$$

which agrees with the usual $\overline{\rm MS}$ beta function, but only the number of light quarks $n_{\ell f}$ appears. That is, the heavy quarks decouple from the evolution of α_s. The calculations in this renormalization scheme and α_s can thus be consistently used with PDFs that involve $n_{\ell f}$ light flavours in the evolution. Above the transition scale Q_t^2, where the heavy-quark is also considered as an active parton in the evolution, one simply increments $n_{\ell f}$ by one in the beta function. As for PDFs, also α_s may be discontinuous across the transition scale Q_t^2. Indeed, from Eq. (195) and Eq. (197) it follows that

$$\alpha_s^{\overline{\rm MS}}\left(\mu_{\rm ren}^2\right) = \alpha_s^{\rm DC}\left(\mu_{\rm ren}^2\right)\left[1 + \frac{\alpha_s^{\rm DC}\left(\mu_{\rm ren}^2\right)}{3\pi}T_f\log\left(\frac{\mu_{\rm ren}^2}{m^2}\right)\right] + \mathcal{O}(\alpha_s^3), \tag{199}$$

such that depending on Q_t^2, there may be a discontinuity (for $Q_t^2 = m^2$ there is none). If the $\mathcal{O}(\alpha_s^3)$ terms are included, there will be a discontinuity regardless of Q_t^2.

5.3 Explicit NLO expression for $F_2^{\rm H}$ in the SACOT scheme

Altogether, taking the transition scale to be $Q_t^2 = m_{\rm H}^2$, the explicit NLO formulae for heavy-quark structure function in SACOT scheme are:

At $\mathbf{Q_f^2} < \mathbf{m_{\rm H}^2}$: $\alpha_s(n_f)$

$$\frac{1}{x}F_2^{\rm H}(x,Q^2) \;=\; 2e_{\rm H}^2\int_\chi^1\frac{dz}{z}f_g(z,Q_f^2)\left\{\frac{\alpha_s}{2\pi}C_2^{g\to{\rm H}}\left(\frac{\chi}{z},\frac{m_{\rm H}^2}{Q^2}\right)\right\}$$

At $\mathbf{Q_f^2} > \mathbf{m_{\rm H}^2}$: $\alpha_s(n_f+1)$, H introduced as a new parton in DGLAP evolution

$$\begin{aligned}\frac{1}{x}F_2^{\rm H}(x,Q^2) = 2e_{\rm H}^2\int_\chi^1\frac{dz}{z}f_g(z,Q_f^2)&\left[-\frac{\alpha_s}{2\pi}\log\left(\frac{Q_f^2}{m_{\rm H}^2}\right)P_{qg}\left(\frac{\chi}{z}\right) + \frac{\alpha_s}{2\pi}C_2^{g\to{\rm H}}\left(\frac{\chi}{z},\frac{m_{\rm H}^2}{Q^2}\right)\right], \\ +e_{\rm H}^2\int_\chi^1\frac{dz}{z}\left[f_{\rm H}(z,Q_f^2)+f_{\overline{\rm H}}(z,Q_f^2)\right]&\left[1-\frac{\alpha_s}{2\pi}\log\left(\frac{Q_f^2}{Q^2}\right)P_{qq}\left(\frac{\chi}{z}\right)+\frac{\alpha_s}{2\pi}C_{2,q\to q}^{\overline{\rm MS}}\left(\frac{\chi}{z}\right)\right]\end{aligned}$$

The $\log(Q_f^2/m_{\rm H}^2)P_{qg}$ term is often called the **subtraction term** in the literature. On one hand, it avoids the double counting when the contributions from heavy-quark PDFs are included. On the other hand, it makes the cross section IR safe at large Q^2.

Whether we should refer to the above example as being "NLO" is not unique: For $Q_f^2 > m_{\rm H}^2$ there are clearly both $\mathcal{O}(\alpha_s^0)$ and $\mathcal{O}(\alpha_s)$ contributions, so we may say the calculation is an NLO one. However, for $Q_f^2 < m_{\rm H}^2$ there is only $\mathcal{O}(\alpha_s)$ term present, and as this is the first non-zero term, it can be seen to be a LO approximation. In other words, the counting of orders in not unique, and there is some variation among independent groups. If the contribution of $F_2^{\rm H}$ is just part of the inclusive (anything in the final state) then there's no ambiguity.

Beyond $\mathcal{O}(\alpha_s)$, the notion of "heavy-quark structure function" is not theoretically well defined: cross sections containing at least one heavy-quark in the final state still retain $\log(m_{\rm H}^2/Q^2)$ type of terms (even after subtracting the logs which are resummed into the heavy-quark PDFs). In inclusive cross sections (anything in the final state) they cancel against virtual corrections with heavy-quark loops. On the other hand, cross sections in which the photon couples to the heavy quark are finite, and in phenomenological studies this is usually how the "heavy-quark structure function" is defined beyond $\mathcal{O}(\alpha_s)$.

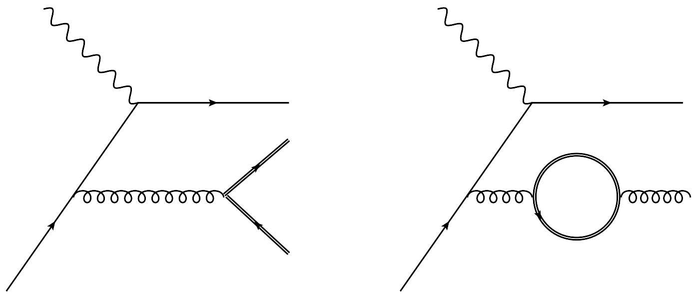

Figure 25: An NNLO diagram for heavy-quark production and a virtual correction involving a heavy-quark loop.

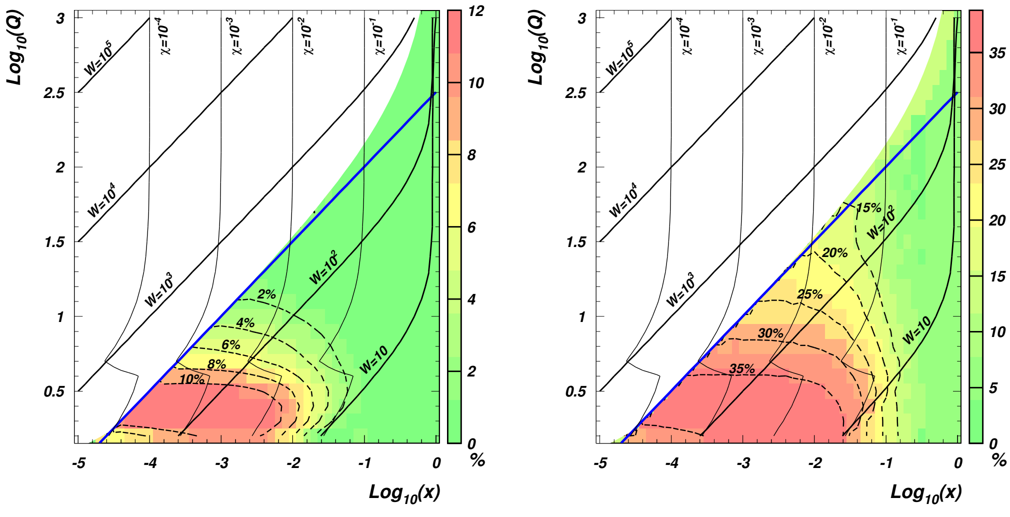

Figure 26: GM-VFNS vs. ZM-VFNS for F_2 (left) and F_L (right). Figure from Ref. [30]

5.4 Miscellaneous ZM-VFNS vs. GM-VFNS effects

Figure 26 demonstrates the size of the relative difference between GM-VFNS and ZM-VFNS schemes for $F_2(x,Q^2)$ and $F_L(x,Q^2) \equiv F_2(x,Q^2) - 2xF_1(x,Q^2)$ in the case of charm-quarks. The effect is most significant at small x and low Q^2. The GM-VFNS also does quantitatively better in global fits. Figure 27 illustrates this in the context of CTEQ6.6 NLO global analysis. For ~3000 data points the χ^2 is 300 units lower for GM-VFNS analysis than for ZM-VFNS.

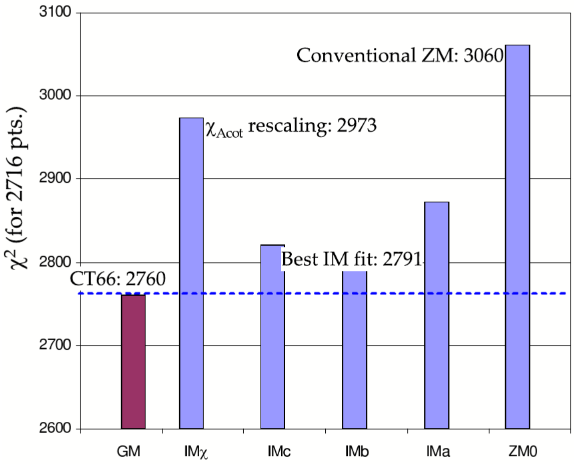

Figure 27: The effect of ZMVFNS vs. GMVFNS in a global fit. Figure from Ref. [32]

6 Practicalities of PDF analysis

The industry of extracting PDFs from experimental data is big, and there are several groups involved each with somewhat different approaches. The idea of **global analysis** is to use as much data as possible. To give an idea Figure 28 shows a table of the data included in the MMHT2014 analysis [33]. There are around 3000 data points from DIS, Drell-Yan, W, Z, jets and top-quark production. The kinematic coverage (in terms of probed x and Q^2 in PDFs) is also wide as shown in Figure 29 in the case of NNPDF3.1 fit [34]. The scales Q^2 reach now up to 1 TeV, and x below 10^{-4} is reach within the perturbative domain.

Apart from the NNPDF group's approach, the PDFs are usually parametrized at **parametrization scale** $Q^2_{\rm param} \sim 1\,{\rm GeV}$ by some functional form,

$$f_i(x, Q^2_{\rm param}) = x^{a_1^i}(1-x)^{a_2^i} \times F_i(x, a_3^i, \ldots, a_n^i)\,, \tag{200}$$

where $F_i(x, a_3, \ldots, a_n)$ is a suitable, flexible enough function. Usually, the parametrized PDF components are gluons the light-flavour quarks (the heavy-flavour is generated perturbatively by the DGLAP evolution). However, the new NNPDF analysis (NNPDF3.1) now also parametrizes the charm quarks. The typical amount of free parameters is 20 to 30 in global analyses. After defining this initial condition, the PDFs can be obtained at the entire (x, Q^2) plane by solving the DGLAP equations. The PDFs so obtained are then used to compute theory predictions for the observables included in the analysis.

Data set	LO	NLO	NNLO
BCDMS μp F_2 [125]	162 / 153	176 / 163	173 / 163
BCDMS μd F_2 [19]	140 / 142	143 / 151	143 / 151
NMC μp F_2 [20]	141 / 115	132 / 123	123 / 123
NMC μd F_2 [20]	134 / 115	115 / 123	108 / 123
NMC $\mu n/\mu p$ [21]	122 / 137	131 / 148	127 / 148
E665 μp F_2 [22]	59 / 53	60 / 53	65 / 53
E665 μd F_2 [22]	52 / 53	52 / 53	60 / 53
SLAC ep F_2 [23, 24]	21 / 18	31 / 37	31 / 37
SLAC ed F_2 [23, 24]	13 / 18	30 / 38	26 / 38
NMC/BCDMS/SLAC/HERA F_L [20, 125, 24, 63, 64, 65]	113 / 53	68 / 57	63 / 57
E866/NuSea pp DY [88]	229 / 184	221 / 184	227 / 184
E866/NuSea pd/pp DY [89]	29 / 15	11 / 15	11 / 15
NuTeV νN F_2 [29]	35 / 49	39 / 53	38 / 53
CHORUS νN F_2 [30]	25 / 37	26 / 42	28 / 42
NuTeV νN xF_3 [29]	49 / 42	37 / 42	31 / 42
CHORUS νN xF_3 [30]	35 / 28	22 / 28	19 / 28
CCFR $\nu N \to \mu\mu X$ [31]	65 / 86	71 / 86	76 / 86
NuTeV $\nu N \to \mu\mu X$ [31]	53 / 40	38 / 40	43 / 40
HERA e^+p NC 820 GeV[61]	125 / 78	93 / 78	89 / 78
HERA e^+p NC 920 GeV[61]	479 /330	402 /330	373/ 330
HERA e^-p NC 920 GeV [61]	158/ 145	129/ 145	125 /145
HERA e^+p CC [61]	41 / 34	34 / 34	32 / 34
HERA e^-p CC [61]	29 / 34	23 / 34	21 / 34
HERA ep F_2^{charm} [62]	105 /52	72 / 52	82 / 52
H1 99–00 e^+p incl. jets [126]	77 / 24	14 / 24	—
ZEUS incl. jets [127, 128]	140/60	45 / 60	—
DØ II $p\bar{p}$ incl. jets [119]	125 / 110	116 / 110	119 / 110
CDF II $p\bar{p}$ incl. jets [118]	78 / 76	63 / 76	59 / 76
CDF II W asym. [66]	55 / 13	32 / 13	30 / 13
DØ II $W \to \nu e$ asym. [67]	47 / 12	28 / 12	27 / 12
DØ II $W \to \nu\mu$ asym. [68]	16 / 10	19 / 10	21 / 10
DØ II Z rap. [90]	34 / 28	16 / 28	16 / 28
CDF II Z rap. [70]	95 / 28	36 / 28	40 / 28
ATLAS W^+, W^-, Z [10]	94/30	38/30	39/30
CMS W asymm $p_T > 35$ GeV [9]	10/11	7/11	9/11
CMS asymm $p_T > 25$ GeV, 30 GeV[77]	7/24	8/24	10/24
LHCb $Z \to e^+e^-$ [79]	76/9	13/9	20/9
LHCb W asymm $p_T > 20$ GeV[78]	27/10	12/10	16/10
CMS $Z \to e^+e^-$ [84]	46/35	19/35	22/35
ATLAS high-mass Drell-Yan [83]	42/13	21/13	17/13
CMS double diff. Drell-Yan [86]	—	372/132	149/132
Tevatron, ATLAS, CMS $\sigma_{t\bar{t}}$ [91]–[97]	53/13	7/13	8/13
ATLAS jets (2.76 TeV+7 TeV)[108, 107]	162/116	106/116	—
CMS jets (7 TeV) [106]	150/133	138/133	—
All data sets	**3706 / 2763**	**3267 / 2996**	**2717 / 2663**

Figure 28: The data in MMHT2014 global fit. Figure from Ref. [33]

6.1 χ^2 figure-of-merit function and the importance of correlations

In one way or another, the optimal correspondence between set of PDFs $f_{i=g,q,\bar{q}}$ depending on a set of parameters $\{a\}$ is almost always defined as the minimum of the global χ^2 function. In its

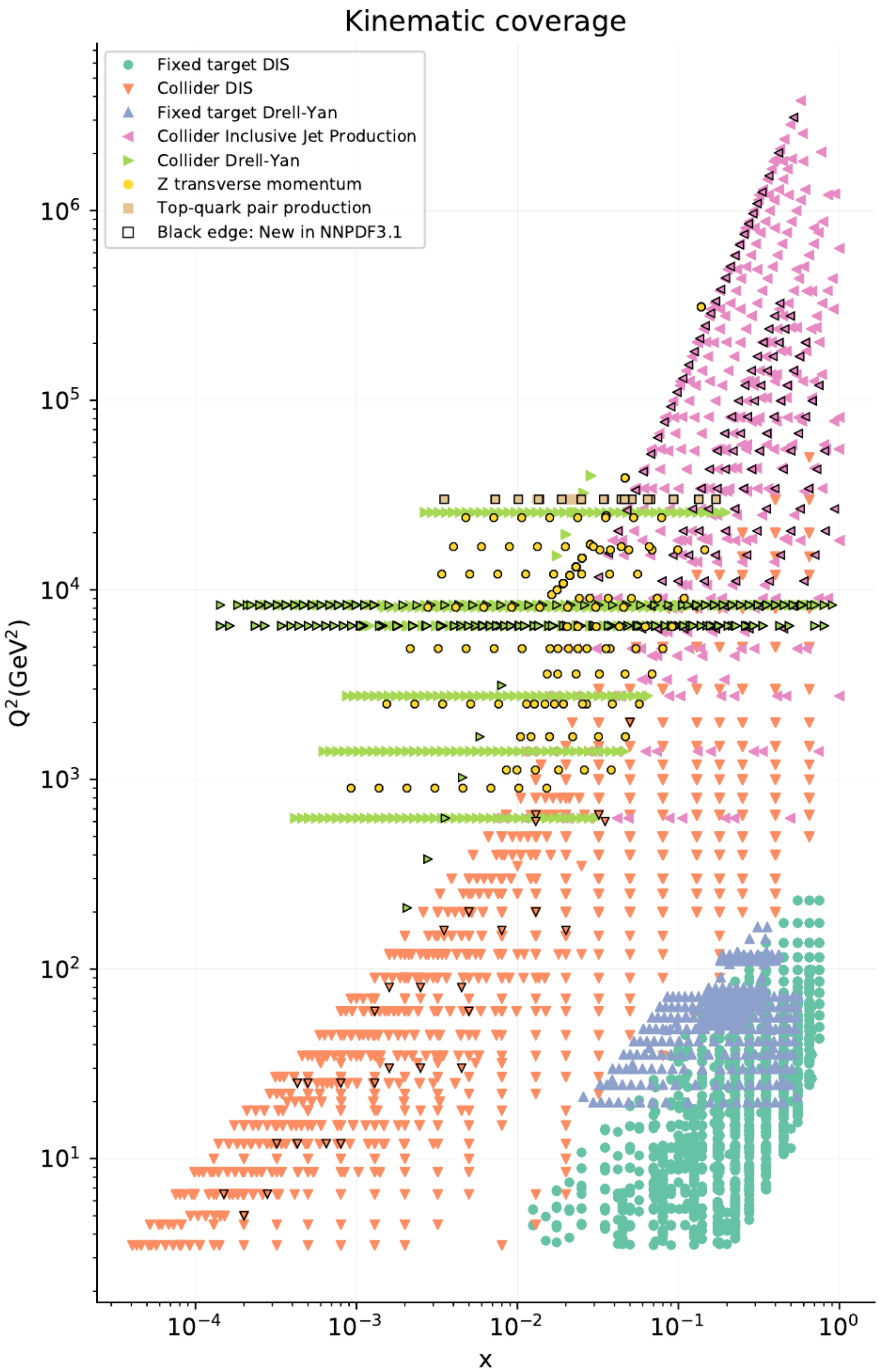

Figure 29: The kinematic coverage NNPDF3.1 global fit. Figure from Ref. [34]

most simple form, we can write it as

$$\chi^2[f(\{a\})] = \sum_k \left[\frac{y_k^{\text{theory}}[f(\{a\})] - y_k^{\text{data}}}{\delta_k^{\text{data}}} \right]^2 , \tag{201}$$

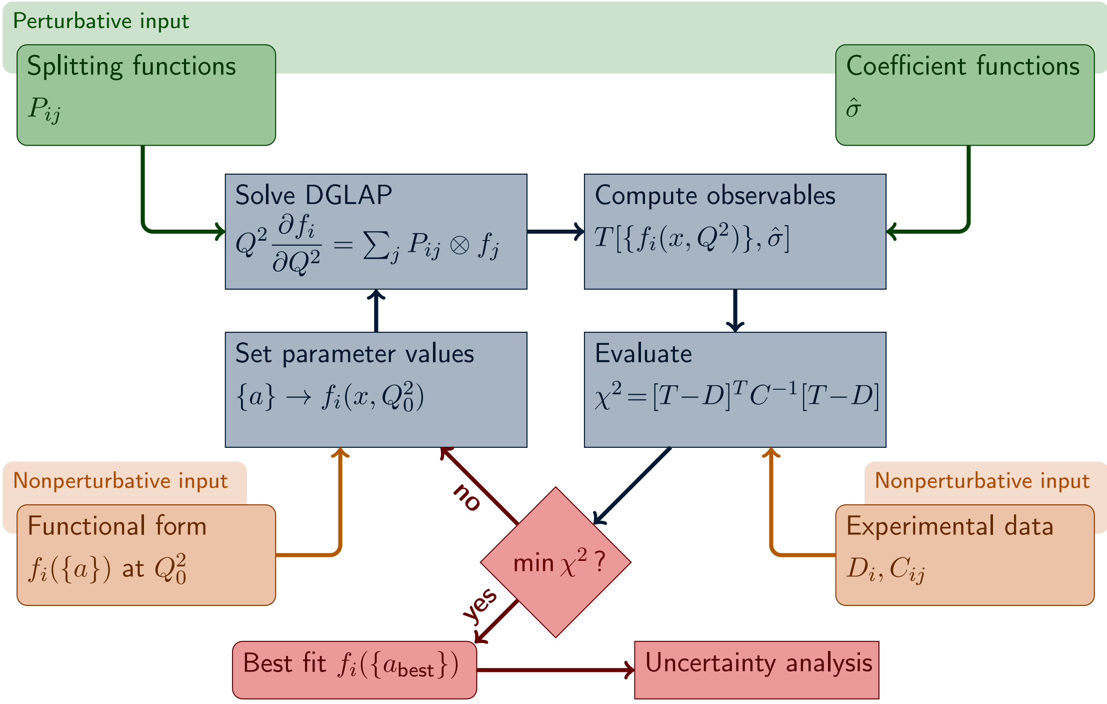

Figure 30: Elements and flow of a global PDF analysis. Figure from Ref. [35]

where $y_k^{\text{theory}}[f(\{a\})]$ are the theory predictions depending on the PDFs. The corresponding experimental values are denoted by y_k^{data} and their **uncorrelated** uncertainties by δ_k^{data}. This simple form of the χ^2 function has, however, become largely inadequate for the precision PDF analysis. This is because the uncertainties of the data points are often mutually **correlated**. The simplest example is the luminosity $\mathcal{L}$, which affects the cross-section extraction as,

$$\text{number of events} = \mathcal{L} \times (\text{cross section}) \, . \tag{202}$$

We can account for the correlated systematic errors by constructing a **covariance matrix**. To be specific, we define the elements of the covariance matrix C by

$$C_{ij} = \delta_{ij} \, (\sigma_i^{\text{uncorr}})^2 + \sum_k \beta_i^k \beta_j^k \, , \tag{203}$$

where σ_i^{uncorr} is the uncorrelated error of data point i, and β_i^k denotes the absolute shift of this data point corresponding to 1-sigma deviation of the systematic parameter k. In other words, the data point y_i^{data} is considered to lie in the region

$$y_i^{\text{data}} - \beta_i^k < y_i^{\text{data}} < y_i^{\text{data}} + \beta_i^k \tag{204}$$

with 68% probability, due to uncertainties in the kth systematic source. Typical sources of correlated uncertainties include luminosity, unfolding and jet energy scale uncertainties. The χ^2 function generalizes to

$$\chi^2 = \sum_{i,j=1}^{N_{\text{data}}} \left(y_i^{\text{theory}}[f] - y_i^{\text{data}}\right) C_{ij}^{-1} \left(y_j^{\text{theory}}[f] - y_j^{\text{data}}\right) \, . \tag{205}$$

Calculating the χ^2 in this way is equivalent to (see e.g. [36, 37, 38]) minimizing

$$\chi^2 = \sum_i \left[\frac{y_i^{\text{theory}} - y_i^{\text{data}} - \sum_k s_k \beta_i^k}{\sigma_i^{\text{uncorr}}} \right]^2 + \sum_k s_k^2, \tag{206}$$

with respect to the systematic parameters s_k. Effectively, this corresponds to assuming that the systematic uncertainties obey a Gaussian probability distribution. The minimum occurs with the parameter values

$$s_k^{\min} = \sum_j \left[\beta_j^k - \sum_{i,\ell,s} \beta_i^k C_{i\ell}^{-1} \beta_\ell^s \beta_j^s \right] \frac{y_j^{\text{theory}} - y_j^{\text{data}}}{(\sigma_j^{\text{uncorr}})^2}, \tag{207}$$

and

$$-\sum_k s_k^{\min} \beta_i^k \tag{208}$$

is the net systematic shift for the data point y_i^{data}. This shift can sometimes be significant. To see this concretely Figure 31 shows a comparison between the CMS 7 TeV jet data [39] and a NLO QCD prediction using CTEQ6.6 PDFs [40]. The left-hand panel shows the ratio to the central CTEQ6.6 prediction without applying the systematic shifts on the data — the data-vs-theory correspondence does not look particularly good, does it?. The right-hand panel shows the result after applying the optimal systematic shift on the data — this brings the data to a much better agreement with the prediction. The importance of the correlated systematic uncertainties is on the level that if the experiment does not provide these correlations, the PDF fitters are hesitant to include the data into their fits. However, this is not all. Above we have implicitly considered the systematic uncertainties as being **additive**. However, they can be **multiplicative** as well (given as percents to the measured data value). In principle, it's up to the experiments to say which kind of uncertainties they provide. An improper use of uncertainties can lead to so-called **D'Agostini bias** [41].

6.2 PDF uncertainties in the Hessian method

In the Hessian approach to quantify the PDF errors [43], the behaviour of χ^2 around the best fit S_0 is approximated by a second order polynomial in the space of fit parameters $\{a\}$

$$\chi^2\{a\} \approx \chi_0^2 + \sum_{ij} \delta a_i H_{ij} \delta a_j, \qquad H_{ij} \equiv \frac{1}{2} \frac{\partial^2 \chi^2}{\partial a_i \partial a_j}, \tag{209}$$

where $\delta a_j \equiv a_j - a_j^0$ are the excursions from the best-fit values and χ_0^2 is the minimum value of χ^2. The terms linear in δa_j are absent since the first derivatives are zero at the minimum. Being symmetric, the Hessian matrix H_{ij} has N_{eig} orthonormal eigenvectors $\mathbf{v}^{(k)}$ and eigenvalues ϵ_k satisfying

$$H_{ij} v_j^{(k)} = \epsilon_k v_i^{(k)}, \tag{210}$$

$$\sum_j v_j^{(k)} v_j^{(\ell)} = \sum_j v_k^{(j)} v_\ell^{(j)} = \delta_{k\ell}. \tag{211}$$

At the minimum of χ^2 the eigenvalues are positive definite $\epsilon_k > 0$ for $\forall\, k$, and we can define a new set of variables as

$$z_k \equiv \sqrt{\epsilon_k} \sum_j v_j^{(k)} \delta a_j. \tag{212}$$

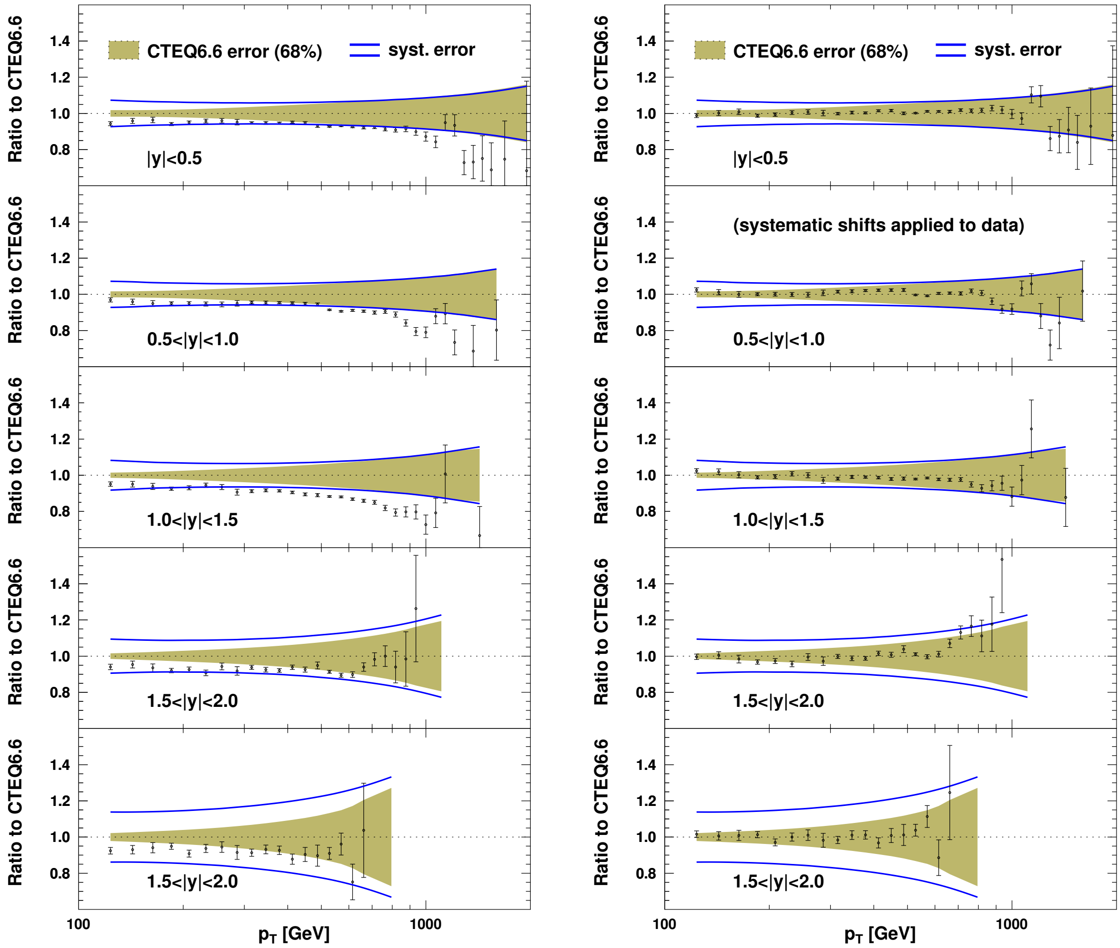

Figure 31: **Left-hand panels:** The CMS inclusive jet cross sections for the five rapidity intervals compared to the NLO calculation with CTEQ6.6 PDFs and taking $\mu_f = \mu_r = p_T/2$. The error bars in the data points show the statistical uncertainty, while the total systematic error is indicated by the blue lines. The colored bands show the CTEQ6.6 PDF uncertainty. **Right-hand panels:** As the left-hand panels, but after applying the systematic shifts. Figure from Ref. [42].

One then easily finds that

$$\chi^2\{a\} \approx \chi_0^2 + \sum_i z_i^2. \tag{213}$$

That is, the transformation in Eq. (212) diagonalizes the Hessian matrix. Figure 32 illustrates the transformation graphically. In the original variables, the constant-χ^2 surfaces are ellipses (for any pair of parameters). The Eq. (212) transforms these into circles. In other words, the χ^2 increases uniformly to an arbitrary direction in the z space — the z_i coordinates are uncorrelated. On paper this is all simple. In practice, it can be numerically rather challenging to obtain a reliable Hessian matrix. One of the reason is that the χ^2 may not be as smooth as one would think, but it may contain discontinuities. This is related to the limited precision to which the DGLAP equations are numerically solved and to the finite accuracy of the integrals required in computation of the observables. Also, if some fit parameters are not particularly well constrained, the higher-order terms in the expansion of the χ^2 function may be relevant which complicates

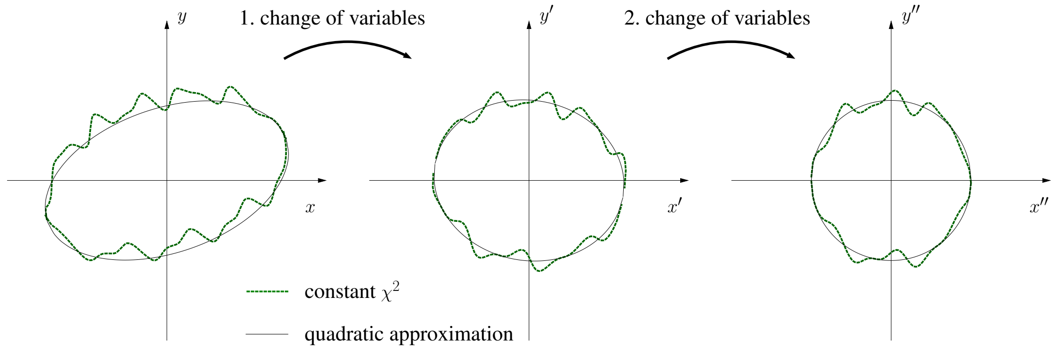

Figure 32: Diagonalization of the Hessian graphically.

the computation of the second derivatives. A typical situation is that even if the minimization algorithm cannot find a lower χ^2, some of the eigenvalues of the Hessian may come out negative. One possibility is to use the **linearized Hessian matrix**

$$H_{ij}^{\text{linearized}} = \sum_k \left(\frac{\partial y_k^{\text{theory}}[f(\{a\})]}{\partial a_i} \right) \left(\frac{\partial y_k^{\text{theory}}[f(\{a\})]}{\partial a_j} \right) \frac{1}{\delta_k^{\text{data}}}, \tag{214}$$

which can be obtained from Eq. (201) discarding the double derivatives. Since this involves only single derivatives, it's computation is somewhat easier than when also the double derivatives are kept. The most appealing property of $H_{ij}^{\text{linearized}}$ is, that it is positive definite. That is, it's eigenvalues are all positive — always. Recalling from calculus that the eigenvalues of the Hessian matrix should be positive definite only when the χ^2 is at its minimum, shows that using $H_{ij}^{\text{linearized}}$ some information is clearly lost.

6.2.1 Error propagation

Let us now consider any quantity X that depends on the PDFs, that is $X \equiv X(\{z\})$. In a linear approximation, X may be expanded in the vicinity of its central value $X_0 \equiv X(\{z = 0\})$ as

$$X \approx X_0 + \underbrace{\sum_j \left(\frac{\partial X}{\partial z_j} \right) \delta z_j}_{\Delta X}. \tag{215}$$

How large can the deviation ΔX be if we require that χ^2 grows from its best-fit value χ_0^2 by some fixed amount $\Delta\chi^2$? Since χ^2 grows uniformly in all z-space directions, the z-space vector that extremizes ΔX for a given $\Delta\chi^2$, is in the direction of the gradient of X and has a length of $\sqrt{\Delta\chi^2}$. The components of this vector are

$$\delta z_i = \sqrt{\Delta\chi^2} \underbrace{\left(\frac{\partial X}{\partial z_i} \right) \left(\sum_j \left(\frac{\partial X}{\partial z_j} \right)^2 \right)^{-1/2}}_{i\text{th component of the gradient vector of length 1}}, \tag{216}$$

giving

$$(\Delta X)^2_{\text{extremum}} \approx \Delta\chi^2 \sum_j \left(\frac{\partial X}{\partial z_j} \right)^2. \tag{217}$$

In order to facilitate the computation of the derivatives $\partial X/\partial z_k$ in Eq. (217), we define a collection of auxiliary PDFs in several z-space coordinates:

$$\begin{aligned}
S_0 &= (0,0,0,\ldots,0) \\
S_1^{\pm} &= \pm\sqrt{\Delta\chi^2}\,(1,0,0,\ldots,0) \\
S_2^{\pm} &= \pm\sqrt{\Delta\chi^2}\,(0,1,0,\ldots,0) \\
&\vdots \\
S_{N-1}^{\pm} &= \pm\sqrt{\Delta\chi^2}\,(0,0,\ldots,1,0) \\
S_N^{\pm} &= \pm\sqrt{\Delta\chi^2}\,(0,0,\ldots,0,1).
\end{aligned} \tag{218}$$

Using these PDF sets, the derivatives $\partial X/\partial z_k$ can be approximated by a finite difference

$$\frac{\partial X}{\partial z_k} \approx \frac{X(S_k^{\pm}) - X(S_0)}{\pm\sqrt{\Delta\chi^2}} \approx \frac{X(S_k^{+}) - X(S_k^{-})}{2\sqrt{\Delta\chi^2}}, \tag{219}$$

where $X(S_k^{\pm})$ denotes the value of X computed with the PDF set $S_k^{\pm}$. Using these in Eq. (217) we get

$$(\Delta X)^2_{\text{extremum}} \approx \sum_k \left(X(S_k^{\pm}) - X(S_0)\right)^2 \approx \frac{1}{4}\sum_k \left(X(S_k^{+}) - X(S_k^{-})\right)^2. \tag{220}$$

These are the simplest equations by which the PDF uncertainties are propagated to any quantity X. They can also be generalized to asymmetric errors [44], though their mathematical meaning is not as clear as here. The PDF sets defined in Eq. (218) are referred to as **PDF error sets** and they are usually distributed along with the central set. The tolerance $\Delta\chi^2$ required to define the uncertainty levels are usually taken to be much larger than unity. The tolerance can also be different for each eigendirection.

6.3 Monte-Carlo techniques

The Monte-Carlo techniques are used particularly in PDF analyses of the NNPDF collaboration. Although there are different variants of the method, the basic idea is, in fact, quite much simpler than the Hessian one. In principle, one prepares several replicas $k = 1,\ldots,N_{\text{replica}}$ of the original data values y_i^{data} by the transformation

$$y_i^{\text{data}}(k) \to y_i^{\text{data}}\left[1 + \delta y_i^{\text{data}}\, R_i(k)\right], \quad i = 1,\ldots,N_{\text{data}}\,, \tag{221}$$

where $R_i(k)$ is a random number drawn from a Gaussian distribution centered at 0 and with unit variance. Changes to the equation above are necessary if the uncertainties are correlated (also whether the uncertainties are additive or multiplicative, counts). After the a set of data has been prepared, the PDFs are fitted to these data. Thus, one obtain a collection of N_{replica} PDFs, $f_{k=1,\ldots,N_{\text{replica}}}$. From these PDF replicas one can then compute the expectation value $\langle\mathcal{O}\rangle$ and variance $\delta\langle\mathcal{O}\rangle$ for an observable $\mathcal{O}$ as

$$\langle\mathcal{O}\rangle = \frac{1}{N_{\text{replica}}}\sum_{k=1}^{N_{\text{replica}}} \mathcal{O}\left[f_k\right], \tag{222}$$

$$\delta\langle\mathcal{O}\rangle = \sqrt{\frac{1}{N_{\text{rep}}}\sum_{k=1}^{N_{\text{replica}}} \left(\mathcal{O}\left[f_k\right] - \langle\mathcal{O}\rangle\right)^2}. \tag{223}$$

It can be shown that the obtained PDFs are distribute according $e^{-\chi^2/2}$-like distribution and the variance corresponds to $\Delta\chi^2 = 1$ in the Hessian approximation (when the approximations required for the Hessian method to be reliable, are valid). By increasing the variance of the Gaussian distribution from which the random numbers $R_i(k)$ are drawn from, also higher tolerance levels (corresponding to $\Delta\chi^2 > 1$) can be set. Although simple, robust and easy to implement, the problem is that in order to get enough statistics, hundreds (or thousands) of separate PDF fits are required.

6.4 Proton PDF sets: NNPDF3.1 vs. CT14 vs. MMHT14

A comparison of the latest global PDF fits by NNPDF, CTEQ, and MMHT collaborations is shown in Figure 33. Despite the different details (schemes, fitting methodology,...) all are pretty much compatible.

6.5 Nuclear PDFs

All PDFs are hadron specific (though universal in all processes that hadron is involved). That is, the PDFs of protons, neutrons, pions, kaons, etc. are different. It has also been noticed that the PDFs of bound nucleons appear different than their free counterparts (though experiments with free neutrons are a bit difficult to do...). This observation stems from the experimental findings — like those shown in Figure 34 — which clearly indicate that the DIS structure functions are modified in lepton-nucleus scattering. At small-x the ratio F_2^A/F_2^p is less than unity, which is often called **nuclear shadowing**. Around $x \sim 0.1$ the ratio is above unity (**antishadowing**). Towards larger x the ratio goes below unity again, which is known as **EMC effect**. At very high x the ratio rises again strongly (**Fermi motion**).
Often, the bound proton PDFs, or just **nuclear PDFs**, are written as

$$f_i^{\text{proton},A}(x, Q^2) = R_i^A(x, Q^2) \times f_i^{\text{proton}}(x, Q^2), \tag{224}$$

where A refers to the mass number of the nucleus. The factors $R_i^A(x, Q^2)$ are nuclear modifications to the free-proton PDFs. The nuclear $f_i^{\text{proton},A}(x, Q^2)$ and free-proton $f_i^{\text{proton}}(x, Q^2)$ PDF obey the same DGLAP equations, and thereby also the nuclear modification is Q^2 dependent. The nuclear PDFs can be extracted essentially the same way as the free proton PDFs, though the available data are much more scarce (no "nuclear HERA" data). The two most recent global fits are EPPS16 [45] and nCTEQ15 [46]. The nuclear modifications from these two are compared in Figure 34 at $Q^2 = 10\,\text{GeV}^2$.

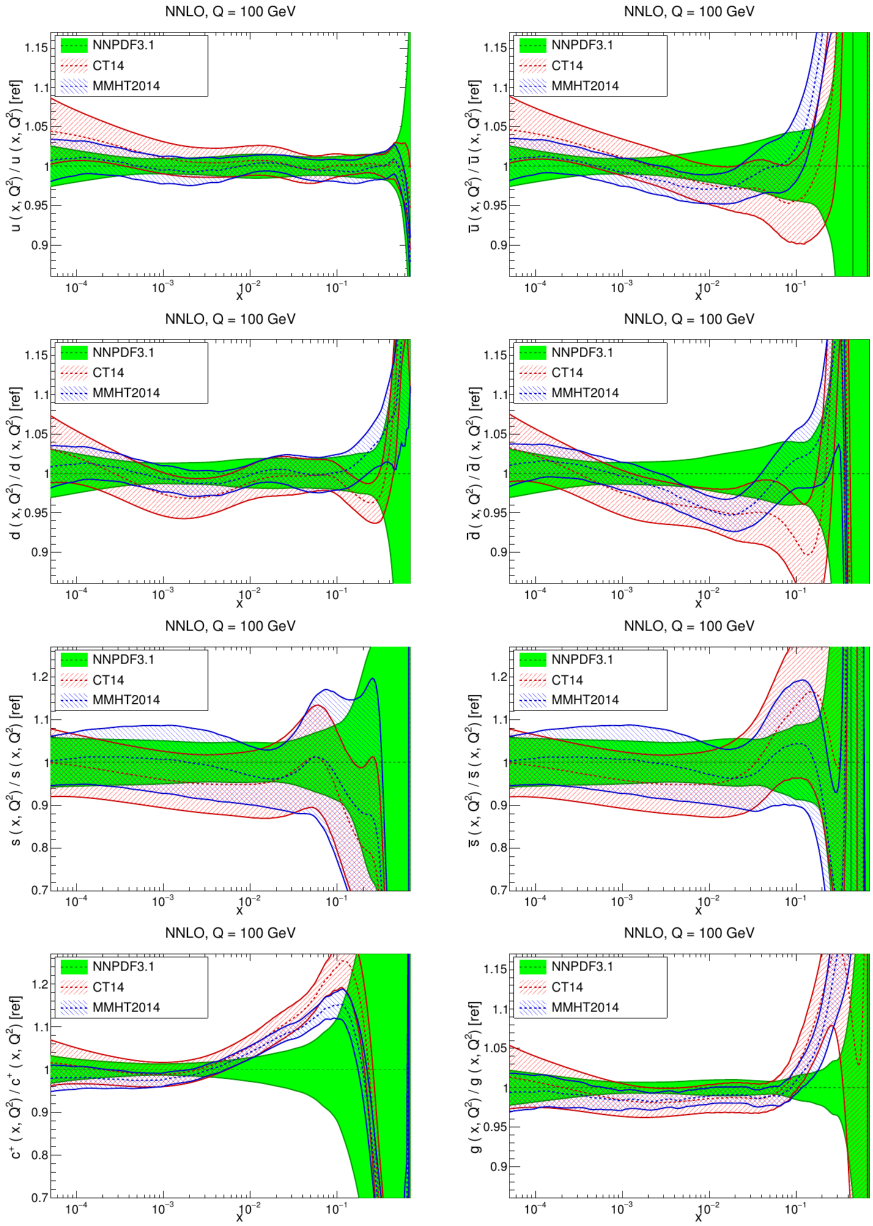

Figure 33: A comparison between NNPDF3.1, CT14, and MMHT2014 PDFs [34].

7 Photons in protons

Until now, we have only considered the QCD part of PDFs. However, as well as quarks can radiate gluons, they may also radiate photons, and photons may split into leptons. Thus, the partonic content of protons is more than just quarks and gluons. We will discuss the photon PDFs here. The QED coupling $\alpha_{\rm em}$ is of course much smaller than QCD coupling α_s, so the photon distribution will be much smaller than e.g. that of gluons. However, at 3-loop QCD level (NNLO PDFs, the current standard) the LO QED effects begin to compete with QCD: At $Q = 10\,\mathrm{GeV}$, $\alpha_s(Q) \approx 0.2$ we have $\alpha_s^3(Q) \approx 0.008$, which is of the same order as the QED coupling $\alpha_{\rm em} \approx 1/137 \approx 0.007$. Furthermore, for some processes at the LHC the photon-photon

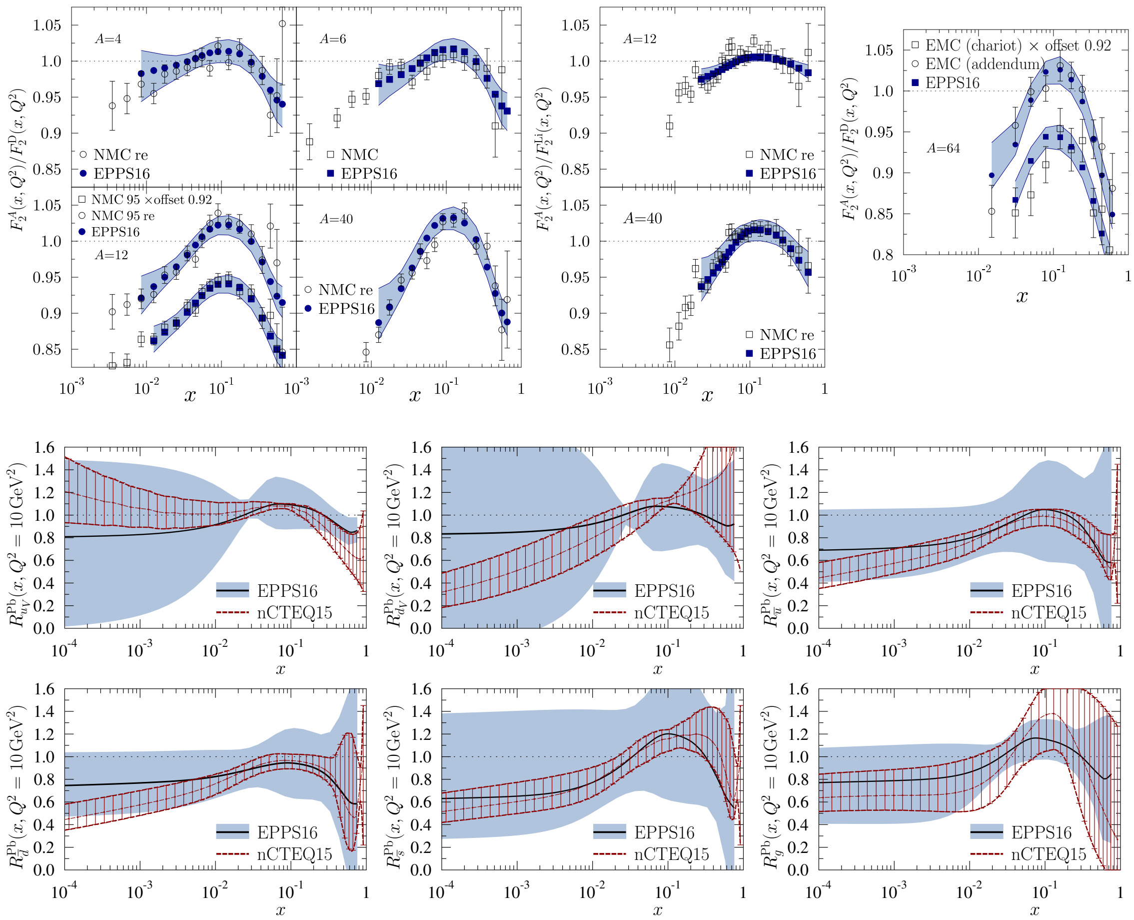

Figure 34: Up: Structure functions measured on a heavy nucleus divided by deuteron structure functions. Down: Nuclear modifications from EPPS16 and nCTEQ15 global fits. Figs. from Ref. [45].

channels can be important for other reasons. For example, in the Drell-Yan dilepton production, the $q\bar{q}$ channel is significantly suppressed at high invariant masses $M_{\ell^+\ell^-} \gg M_{\rm Z}$ due to the $\sim 1/M^2_{\ell^+\ell^-}$ behaviour of the s-channel propagator. In contrast, the photon-photon channel proceeds via t/u channels which are not similarly suppressed.

7.1 Evolution with QED corrections

The DGLAP equations are readily generalized to include QED effects. They can be written, using the convolution notation, e.g. as

$$\frac{dg}{dt} = \sum_j P_{gq_j} \otimes q_j + \sum_j P_{g\bar{q}_j} \otimes \bar{q}_j + P_{gg} \otimes g + P_{g\gamma} \otimes \gamma\,, \tag{225}$$

$$\frac{d\gamma}{dt} = \sum_j P_{\gamma q_j} \otimes q_j + \sum_j P_{\gamma\bar{q}_j} \otimes \bar{q}_j + P_{\gamma g} \otimes g + P_{\gamma\gamma} \otimes \gamma\,, \tag{226}$$

$$\frac{dq_i}{dt} = \sum_j P_{q_i q_j} \otimes q_j + \sum_j P_{q_i\bar{q}_j} \otimes \bar{q}_j + P_{q_i g} \otimes g + P_{q_i\gamma} \otimes \gamma\,, \tag{227}$$

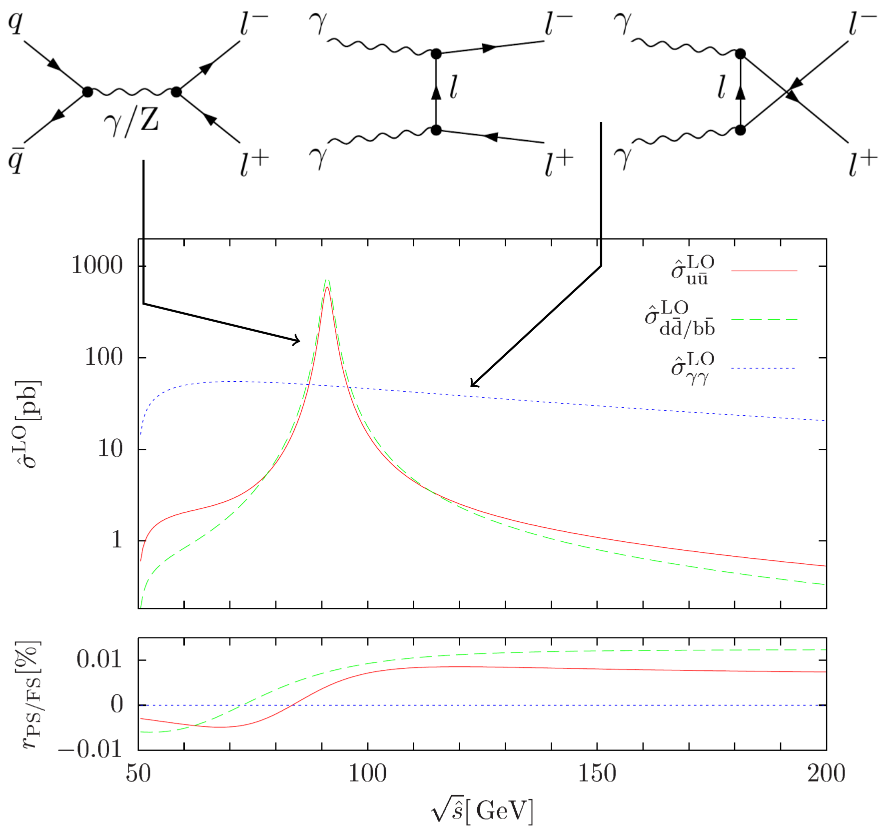

where $t = \ln \mu^2$. The splitting functions involve pure QCD, pure QED, plus mixed terms,

$$P_{ij} = \left(\frac{\alpha_s}{2\pi}\right) P_{ij}^{(1,0)} + \left(\frac{\alpha_s}{2\pi}\right)^2 P_{ij}^{(2,0)} + \left(\frac{\alpha_s}{2\pi}\right)^3 P_{ij}^{(3,0)} + \left(\frac{\alpha_{\mathrm{em}}}{2\pi}\right) P_{ij}^{(0,1)} + \left(\frac{\alpha_{\mathrm{em}}}{2\pi}\right)\left(\frac{\alpha_s}{2\pi}\right) P_{ij}^{(1,1)} + \ldots . \quad (228)$$

The QCD $\mathcal{O}(\alpha_s)$ kernels were discussed in Section 2. The pure QED splitting functions are

$$P_{qq}^{(0,1)}(x) = e_q^2 \left[\frac{1+x^2}{(1-x)_+} + \frac{3}{2}\delta(1-x)\right], \quad (229)$$

$$P_{q\gamma}^{(0,1)}(x) = N_C\, e_q^2 \left[x^2 + (1-x)^2\right], \quad (230)$$

$$P_{\gamma q}^{(0,1)}(x) = e_q^2 \left[\frac{1+(1-x)^2}{x}\right], \quad (231)$$

$$P_{\gamma\gamma}^{(0,1)}(x) = -\frac{2}{3}\sum_f e_f^2\, \delta(1-x), \quad (232)$$

entailing some interesting features. The splitting functions involving quarks depend explicitly on the electromagnetic charge. This means that the upper (up, charm, top) and lower (down, strange, bottom) quarks no longer evolve with equal pace. This also explicitly destroys the **isospin symmetry** between up and down quarks,

$$f_u^{\mathrm{proton}}(x, Q^2) \neq f_d^{\mathrm{neutron}}(x, Q^2)$$
$$f_d^{\mathrm{proton}}(x, Q^2) \neq f_u^{\mathrm{neutron}}(x, Q^2),$$

which would be an exact symmetry in (massless) QCD. The $\gamma \to \gamma$ splitting function involves a sum over fermion charges,

$$\sum_f e_f^2 = N_C \sum_q^{n_F} e_q^2 + \sum_l^{n_L} e_l^2 \,, \tag{233}$$

where n_F and n_L are the number of quark and lepton flavours. In comparison to QCD case, only δ-function part is present, as photons do not self-interact.

The effect of isospin violation in two different PDFs including photon component are shown in Figure (35). Apart from the photon distribution, the isospin-breaking effects are some at the level of percents, (the input parametrization is isospin symmetric in NNPDF2.3QED). The lower photon content of the neutron can be understood on the basis of lower effective charge of the neutron,

$$\begin{aligned} \text{Proton} :& \sum e_u^2 + e_u^2 + e_d^2 = 1 \\ \text{Neutron} :& \sum e_d^2 + e_d^2 + e_u^2 = 2/3 \,. \end{aligned}$$

Thus, to first approximation $f_\gamma^{\text{neutron}}/f_\gamma^{\text{proton}} \approx 2/3 \approx 0.7$. This is in qualitative agreement with Figure (35).

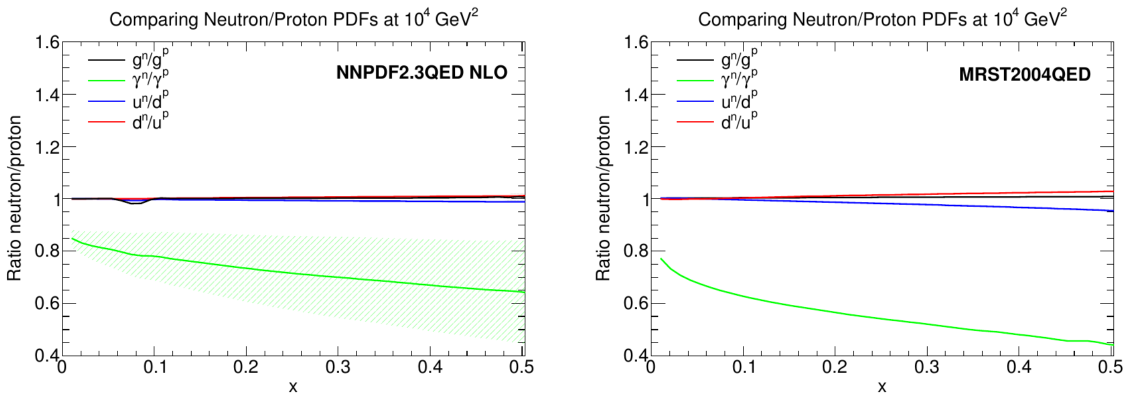

Figure 35: Figure from Ref. [47].

Along with the increasingly precise LHC data, the role of photon PDFs has become more and more important and several data-driven analyses have tried to pin down the photon PDFs. Out of the LHC data, the high-mass Drell-Yan is indeed one of the most constraining ones. Figure 36 below shows some recent ATLAS data up to TeV mass range. These data can put constraints for the photon PDF as illustrated in Figure 37 below. However, a recent theory breakthrough which we now consider in some detail, has now revolutionized the way the photon PDFs are extracted.

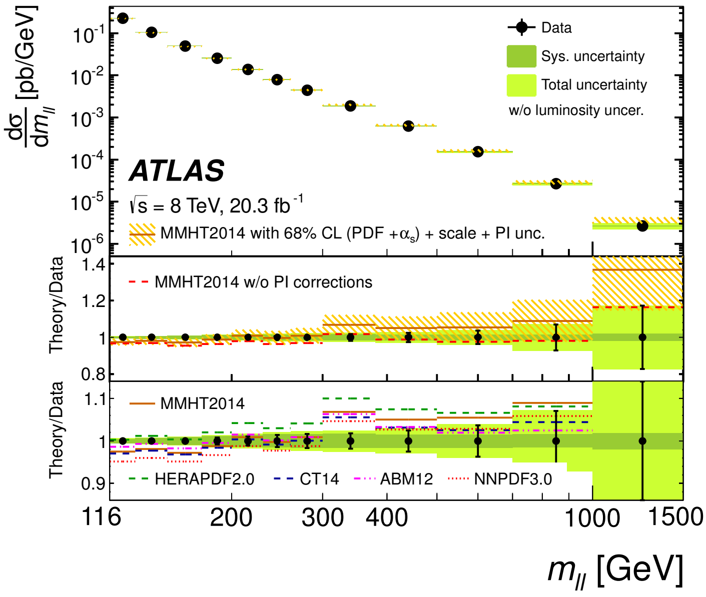

Figure 36: Figure from Ref. [48]

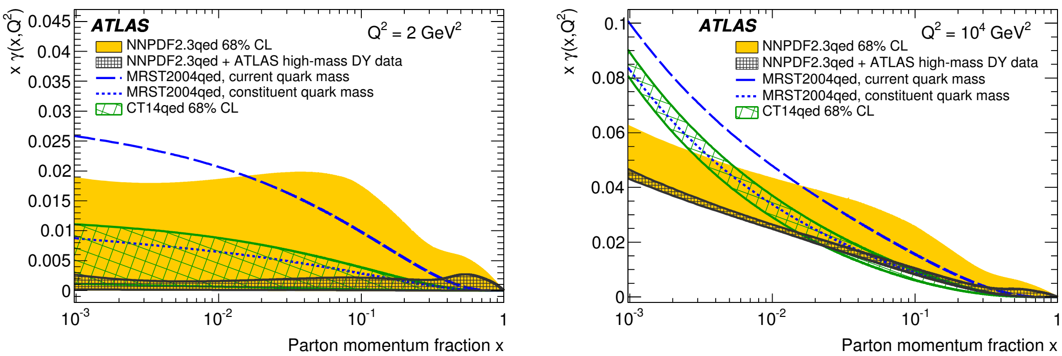

Figure 37: Figure from Ref. [48]

7.2 Calculation of the photon PDF in terms of F_2 and F_L

Here, we will go through (in a bit simplified way) the method introduced in Refs. [49, 50], of how to relate the photon PDFs and the usual F_2 and F_L DIS structure functions. The starting point here is a hypothetical Beyond-Standard-Model (BSM) probe that couples to the Standard-Model particles only via photon exchange. What one assumes here are two spin-1/2 leptons, incoming ℓ an outgoing L, where the former is massless, $M_\ell = 0$, and the latter is heavy $M_{\rm L} \gg M_{\rm p}$. The interaction term introduced in the Lagrangian is

$$\left(\frac{e}{\Lambda}\right) \overline{L} \sigma^{\mu\nu} \ell F_{\mu\nu}, \tag{234}$$

where $\sigma^{\mu\nu} = \dfrac{i}{2}[\gamma^\mu, \gamma^\nu]$, and $F_{\mu\nu}$ is the electromagnetic tensor. The electromagnetic coupling is e and the scale Λ is introduced for dimensional reasons. The limit $\Lambda \to \infty$ will be assumed throughout the calculation. The corresponding vertex factor reads

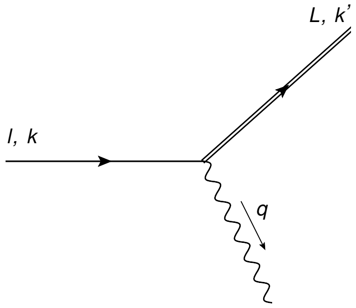

$$\propto i\left(\frac{e}{\Lambda}\right)\sigma^{\mu\nu}q_\mu$$

7.2.1 General expression

The general diagram for scattering of lepton ℓ off a proton is show in Figure 38. First, considering

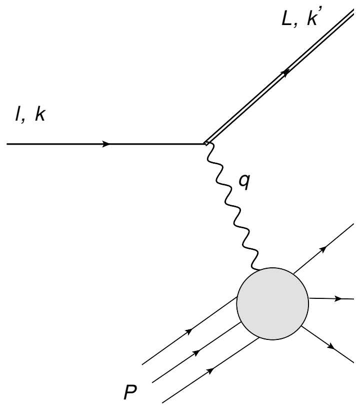

Figure 38: Probing the proton in a $\ell + \text{proton} \to L + X$ process.

such a BSM probe may appear as an extra complication. However, the advantage lies in taking the $\Lambda \to \infty$ limit. In this limit all the corrections to the incoming and outgoing lepton lines (as well as multi-photon exchange) will be suppressed by additional inverse powers of Λ and they disappear in the considered limit. Thus, the QED corrections for the process in Figure 38 are restricted to the virtual photon self-energy corrections. One subtlety here is whether part of these self-energy loops should be included in the definition of the hadronic part. Here, the definition of the hadronic tensor is taken to be such that it does not contain any of these. In other words, at partonic level, the diagrams entering the hadronic tensor are all one-photon-irreducible. The matrix element for the process in Figure 38 can be written as,

$$\mathcal{M} = \left[\overline{u}(k', s')(-i\frac{e}{\Lambda}\sigma^{\mu\alpha}q_\alpha)u(k,s)\right]\left(-\frac{ig_{\mu\nu}}{q^2}\right)\langle \text{out}| - ie\hat{J}_\mu(0)|(P,\sigma), \text{in}\rangle\,. \tag{235}$$

Squaring and averaging over the spins, gives,

$$\begin{aligned}\overline{|M|^2} = \frac{e^4}{q^4}\ &\underbrace{\frac{1}{\Lambda^2}\frac{1}{2}\sum_{s,s'}\left[\overline{u}(k',s')\sigma^{\mu\alpha}q_\alpha u(k,s)\right]\left[\overline{u}(k',s')\sigma^{\nu\beta}q_\beta u(k,s)\right]^*}_{L^{\mu\nu}} \\ &\times \frac{1}{2}\sum_\sigma \langle n, \text{out}|\hat{J}_\mu(0)|(P,\sigma),\text{in}\rangle\langle n,\text{out}|\hat{J}_\nu(0)|(P,\sigma),\text{in}\rangle^*\end{aligned} \tag{236}$$

so that, as in Section 1.1, the cross section is

$$d\sigma = \frac{1}{4P\cdot k}\frac{e^4}{q^4}\frac{d^3\mathbf{k}'}{(2\pi)^3 2E'}L^{\mu\nu}\times \overbrace{\boxed{\begin{array}{l}\displaystyle\frac{1}{2}\sum_{\sigma}\sum_{n}\int\prod_{i=1}^{n}\frac{d^3\mathbf{k_i}}{(2\pi)^3 2k_i^0}(2\pi)^4\delta^{(4)}(P+q-\sum_{j=1}^{n}k_j)\\ \langle n,\mathrm{out}|\hat{J}_\mu(0)|(P,\sigma),\mathrm{in}\rangle\langle n,\mathrm{out}|\hat{J}_\nu(0)|(P,\sigma),\mathrm{in}\rangle^*\,.\end{array}}}^{4\pi M_\mathrm{p}W_{\mu\nu}\text{ “hadronic tensor“}} \tag{237}$$

Here, the leptonic tensor is

$$\begin{aligned}L^{\mu\nu} &\equiv \frac{1}{\Lambda^2}\frac{1}{2}\mathrm{Tr}\left[\left(\not{k}'+M_\mathrm{L}\right)\sigma^{\mu\alpha}\not{k}\sigma^{\nu\beta}\right]q_\alpha q_\beta \\ &= \frac{1}{\Lambda^2}\left(M_\mathrm{L}^2+Q^2\right)\left(q^\mu q^\nu - M_\mathrm{L}^2 g^{\mu\nu}\right)+4Q^2k^\mu k^\nu - 2\left(M_\mathrm{L}^2+Q^2\right)\left(k^\mu q^\nu + k^\nu q^\mu\right)\,.\end{aligned} \tag{238}$$

The total cross section can thus be written as

$$\sigma = \frac{4\pi M_\mathrm{p}}{4P\cdot k}\int\frac{e_\mathrm{ph}^4(q^2)}{q^4}\frac{d^4q}{(2\pi)^3}\left[L^{\mu\nu}W_{\mu\nu}\right]\theta\left(k'^0\right)\theta\left(p^0+q^0\right)\theta\left[(p+q)^2-M_\mathrm{p}^2\right]\delta\left(k'^2-M_\mathrm{L}^2\right), \tag{239}$$

where we have traded the k' integral with a q integral. The θ functions impose the positivity of the final state energies, and that the final-state invariant mass is at least the proton mass (proton is the lightest baryon and the baryon number is conserved). The inclusion of loop corrections to the intermediate photon line results in replacing the constant QED coupling e by the physical running coupling $e_\mathrm{ph}(q^2)$. In what follows, we will use the notation $e(-q^2) = e(Q^2) \equiv e_\mathrm{ph}(q^2)$. The phase space integral can be written as

$$\int\frac{d^4q}{(2\pi)^3}\theta\left(k'^0\right)\theta\left(p^0+q^0\right)\theta\left[(p+q)^2-M_\mathrm{p}^2\right]\delta\left(k'^2-M_\mathrm{L}^2\right) \tag{240}$$

$$= \frac{1}{16\pi^2 M_\mathrm{L}^2}\int_\eta^{1-\frac{2\eta M_\mathrm{p}}{M_\mathrm{L}}}dz\int_{Q^2_\mathrm{min}}^{Q^2_\mathrm{max}}Q^2dQ^2\,, \tag{241}$$

where

$$\eta \equiv \frac{M_\mathrm{L}^2}{2P\cdot k} = \frac{M_\mathrm{L}^2}{s-M_\mathrm{p}},\qquad z\equiv\frac{\eta}{x}\,, \tag{242}$$

and x is the usual Bjorken variable $x = Q^2/(2P\cdot q)$. Neglecting terms which are suppressed by powers of $M_\mathrm{p}^2/M_\mathrm{L}^2$, the integration limits for the Q^2 integral can be shown to be,

$$Q^2_\mathrm{min} = \frac{M_\mathrm{p}^2\eta^2}{1-z},\qquad Q^2_\mathrm{max} = \frac{M_\mathrm{L}^2(1-z)}{z}\,. \tag{243}$$

In Section 1.1 we argued that the general structure (which is of relevance here) for the hadronic tensor is

$$W_{\mu\nu} = -\frac{F_1(x,Q^2)}{M_\mathrm{p}}\left(g_{\mu\nu}-\frac{q_\mu q_\nu}{q^2}\right)+\frac{2x}{Q^2}\frac{F_2(x,Q^2)}{M_\mathrm{p}}\left(P_\mu-\frac{P\cdot q}{q^2}q_\mu\right)\left(P_\nu-\frac{P\cdot q}{q^2}q_\nu\right), \tag{244}$$

where we have already included Q^2 as a an argument of $F_{1,2}$ as we know that they are also functions of Q^2. The contraction $L^{\mu\nu}W_{\mu\nu}$ gives,

$$\begin{aligned}L^{\mu\nu}W_{\mu\nu} = \frac{1}{\Lambda^2}\frac{M_\mathrm{L}^4}{z\eta M_\mathrm{p}}&\left[\left(-z^2-\frac{z^2Q^2}{2M_\mathrm{L}^2}+\frac{z^2Q^4}{2M_\mathrm{L}^4}\right)F_L(x,Q^2)\right.\\ &\left.+\left(2-2z+z^2+\frac{2\eta^2M_\mathrm{p}^2}{Q^2}-\frac{2zQ^2}{M_\mathrm{L}^2}+\frac{z^2Q^2}{M_\mathrm{L}^2}-\frac{2\eta^2M_\mathrm{p}^2Q^2}{M_\mathrm{L}^4}\right)F_2(x,Q^2)\right],\end{aligned} \tag{245}$$

where the longitudinal structure function is, with finite target mass,

$$F_{\rm L}(x,Q^2) \equiv \left(1+\frac{4x^2M_{\rm p}^2}{Q^2}\right)F_2(x,Q^2) - 2xF_1(x,Q^2)\,. \tag{246}$$

The total cross section thus becomes,

$$\sigma = \frac{2\pi}{\Lambda^2}\int\frac{dz}{z}\int_{Q^2_{\rm min}}^{Q^2_{\rm max}}\frac{dQ^2}{Q^2}\alpha^2(Q^2)\left[\left(-z^2-\frac{z^2Q^2}{2M_{\rm L}^2}+\frac{z^2Q^4}{2M_{\rm L}^4}\right)F_L\left(\frac{\eta}{z},Q^2\right)\right. \tag{247}$$
$$\left.+\left(2-2z+z^2+\frac{2\eta^2M_{\rm p}^2}{Q^2}-\frac{2zQ^2}{M_{\rm L}^2}+\frac{z^2Q^2}{M_{\rm L}^2}-\frac{2\eta^2M_{\rm p}^2Q^2}{M_{\rm L}^4}\right)F_2\left(\frac{\eta}{z},Q^2\right)\right]\,.$$

For future convenience, we write the front factor as

$$\frac{2\pi}{\Lambda^2} = \frac{2\pi e^2(\mu^2)}{\Lambda^2e^2(\mu^2)} = \frac{2\pi e^2(\mu^2)}{4\pi\Lambda^2\alpha^2(\mu^2)} = \frac{\pi e^2(\mu^2)}{\Lambda^2}\frac{1}{2\pi\alpha(\mu^2)} = \sigma_0\times\frac{1}{2\pi\alpha(\mu^2)} \tag{248}$$

$$\sigma_0 = \frac{\pi e^2(\mu^2)}{\Lambda^2}\,. \tag{249}$$

Let us now split the equation for the cross section as,

$$\sigma = \frac{\sigma_0}{2\pi\alpha(\mu^2)}\int_\eta^1\frac{dz}{z}\int_{Q^2_{\rm min}}^{Q^2_{\rm max}}\frac{dQ^2}{Q^2}\alpha^2(Q^2) \tag{250}$$
$$\left[-z^2F_L\left(\frac{\eta}{z},Q^2\right)+\left(2-2z+z^2+\frac{2\eta^2M_{\rm p}^2}{Q^2}\right)F_2\left(\frac{\eta}{z},Q^2\right)\right]$$
$$+\frac{\sigma_0}{2\pi\alpha(\mu^2)}\int_\eta^1\frac{dz}{z}\int_{Q^2_{\rm min}}^{Q^2_{\rm max}}\frac{dQ^2}{Q^2}\alpha^2(Q^2)$$
$$\left[\left(-\frac{z^2Q^2}{2M_{\rm L}^2}+\frac{z^2Q^4}{2M_{\rm L}^4}\right)F_L\left(\frac{\eta}{z},Q^2\right)+\left(-\frac{2zQ^2}{M_{\rm L}^2}+\frac{z^2Q^2}{M_{\rm L}^2}-\frac{2\eta^2M_{\rm p}^2Q^2}{M_{\rm L}^4}\right)F_2\left(\frac{\eta}{z},Q^2\right)\right]\,.$$

The lower part is suppressed at low Q^2 by additional factors of Q^2, whereas the upper part gets contributions from all Q^2. In the lower part we may drop the F_L term as it's higher order in QCD and QED couplings, $F_L = \mathcal{O}(\alpha_s)+\mathcal{O}(\alpha)$. In the upper part we cannot do the same for the logarithmic Q^2 integral which leads to a $\log(\alpha_s)$ behaviour as we saw in Section 2.5. In the lower part we may also write

$$F_2\left(\frac{\eta}{z},Q^2\right) = F_2\left(\frac{\eta}{z},\mu^2\right)+\mathcal{O}(\alpha_s)+\mathcal{O}(\alpha)\,,$$
$$\alpha^2(Q^2) = \alpha^2(\mu^2)+\mathcal{O}(\alpha)\,. \tag{251}$$

These approximations render the Q^2 integral in the lower part trivial, and the above expression simplifies to

$$\sigma = \sigma_0\left\{\frac{1}{2\pi\alpha(\mu^2)}\int_\eta^1\frac{dz}{z}\int_{Q^2_{\rm min}}^{Q^2_{\rm max}}\frac{dQ^2}{Q^2}\alpha^2(Q^2)\right. \tag{252}$$
$$\left[-z^2F_L\left(\frac{\eta}{z},Q^2\right)+\left(zp_{\gamma q}(z)+\frac{2\eta^2M_{\rm p}^2}{Q^2}\right)F_2\left(\frac{\eta}{z},Q^2\right)\right]$$
$$\left.+\frac{\alpha(\mu^2)}{2\pi}\int_\eta^1\frac{dz}{z}\left[(1-z)(2-z)F_2\left(\frac{\eta}{z},\mu^2\right)\right]\right\}\,,$$

where $p_{\gamma q}(z) = [1+(1-x)^2]/x = P_{\gamma q}(z)/e_q^2$. We now split the remaining Q^2 integral into ”low-Q^2“ and ”high-Q^2“ parts,

$$
\begin{aligned}
\sigma = \sigma_0 \Bigg\{ & \frac{1}{2\pi\alpha(\mu^2)} \int_\eta^1 \frac{dz}{z} \int_{Q^2_{\min}}^{\frac{\mu^2}{1-z}} \frac{dQ^2}{Q^2} \alpha^2(Q^2) \left[-z^2 F_L\left(\frac{\eta}{z}, Q^2\right) + \left(z p_{\gamma q}(z) + \frac{2\eta^2 M_{\mathrm{p}}^2}{Q^2} \right) F_2\left(\frac{\eta}{z}, Q^2\right) \right] \\
& + \frac{1}{2\pi\alpha(\mu^2)} \int_\eta^1 \frac{dz}{z} \int_{\frac{\mu^2}{1-z}}^{Q^2_{\max}} \frac{dQ^2}{Q^2} \alpha^2(Q^2) \left[-z^2 F_L\left(\frac{\eta}{z}, Q^2\right) + \left(z p_{\gamma q}(z) + \frac{2\eta^2 M_{\mathrm{p}}^2}{Q^2} \right) F_2\left(\frac{\eta}{z}, Q^2\right) \right] \\
& + \frac{\alpha(\mu^2)}{2\pi} \int_\eta^1 \frac{dz}{z} \left[(1-z)(2-z) F_2\left(\frac{\eta}{z}, \mu^2\right) \right] \Bigg\} \,,
\end{aligned}
$$

In the second line we may again replace the Q^2 in the arguments of α and F_2 by μ^2, as well as throw away the F_L and $2\eta^2 M_{\mathrm{p}}^2/Q^2$ terms. Performing the Q^2 integral gives finally,

$$
\begin{aligned}
\sigma = \sigma_0 \Bigg\{ & \frac{1}{2\pi\alpha(\mu^2)} \int_\eta^1 \frac{dz}{z} \int_{Q^2_{\min}}^{\frac{\mu^2}{1-z}} \frac{dQ^2}{Q^2} \alpha^2(Q^2) \left[-z^2 F_L\left(\frac{\eta}{z}, Q^2\right) + \left(z p_{\gamma q}(z) + \frac{2\eta^2 M_{\mathrm{p}}^2}{Q^2} \right) F_2\left(\frac{\eta}{z}, Q^2\right) \right] \\
& + \frac{\alpha(\mu^2)}{2\pi} \int_\eta^1 \frac{dz}{z} \left[(1-z)(2-z) + z p_{\gamma q}(z) \log\left(\frac{M_{\mathrm{L}}^2 (1-z)^2}{z\mu^2} \right) \right] F_2\left(\frac{\eta}{z}, \mu^2\right) \Bigg\} \,. \qquad (253)
\end{aligned}
$$

7.2.2 QCD-improved parton-model result

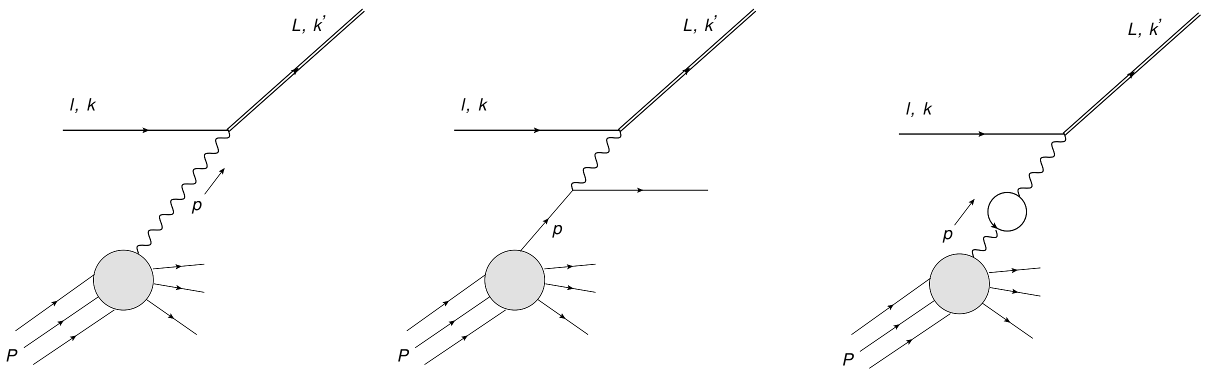

Figure 39: Diagrams for $\ell + \text{proton} \to L + X$ process in parton-level calculation.

As in Section 1.2, we now need the parton-model counter part to compare with the general expression Eq. (253). To $\mathcal{O}(\alpha)$, there are three diagrams to consider, as shown in Figure 39. The leftmost graph corresponds to the leading-order contribution. The matrix elements for this process can be written as

$$
\mathcal{M} = \left[\overline{u}(k', s')(-i\frac{e}{\Lambda}\sigma^{\mu\alpha}(-p_\alpha))u(k,s) \right] \epsilon_\mu(p, \lambda) \,. \qquad (254)
$$

Squaring and averaging/summing over the spins/polarization, we have

$$
\overline{|\mathcal{M}|^2} = \frac{e^2}{4\Lambda^2} \mathrm{Tr}\left[\left(\not{k}' + M_{\mathrm{L}} \right) \sigma^{\mu\alpha} \not{k} \sigma^{\nu\beta} \right] p_\alpha p_\beta \times \underbrace{\sum_\lambda \epsilon_\mu(p,\lambda)\epsilon_\nu^*(p,\lambda)}_{-g_{\mu\nu}} = \frac{e^2 \hat{s}^2}{\Lambda^2} \,. \qquad (255)
$$

The corresponding LO partonic cross section is then

$$\hat{\sigma}^{(0)} = \frac{1}{\hat{s}} \int \frac{d^3k'}{2E'(2\pi)^3} \overline{|\mathcal{M}|^2} (2\pi)^4 \delta^{(4)} \left(p + k - k'\right) = \frac{\pi}{\hat{s}} \frac{e^2 \hat{s}^2}{\Lambda^2} \delta \left(\hat{s} - M_{\rm L}^2\right) = \sigma_0 \times M_{\rm L}^2 \delta \left(\hat{s} - M_{\rm L}^2\right) . \tag{256}$$

The hadronic cross section is obtained by folding the partonic results with the photon PDFs,

$$\begin{aligned} \sigma^{(0)} &= \int d\xi \hat{\sigma}^{(0)} f_\gamma(\xi, \mu^2) = \sigma_0 \times M_{\rm L}^2 \int d\xi \delta \left(\hat{s} - M_{\rm L}^2\right) = \sigma_0 \times \frac{M_{\rm L}^2}{s} \int d\xi \delta \left(\xi - \frac{M_{\rm L}^2}{s}\right) f_\gamma(\xi, \mu^2) \\ &= \sigma_0 \times \eta f_\gamma(\eta, \mu^2) . \end{aligned} \tag{257}$$

The second graph in Figure 39 contains a collinear singularity when the quark from the proton spits a photon along its line of path. There, we also meet again the just-derived leading-order result. Within the dimensional regularization, the resulting partonic cross section reads,

$$\hat{\sigma}^{(1)} = \sigma_0 e_q^2 \left\{ \frac{\alpha}{2\pi} \left(-\frac{1}{\hat{\epsilon}} + \log \frac{M_{\rm L}^2}{\mu_D^2} \right) z p_{\gamma q}(z) + \frac{\alpha}{2\pi} h(z) \right\} \tag{258}$$

$$h(z) = -2 + 3z + z p_{\gamma q}(z) \log \frac{(1-z)^2}{z} , \tag{259}$$

where $z \equiv M_{\rm L}^2/\hat{s} = \eta/\xi$. The corresponding hadronic cross section then becomes

$$\sigma^{(1)} = \sum_q \int_\eta^1 d\xi \hat{\sigma}^{(1)} f_q(\xi, \mu^2) \tag{260}$$

$$= \sigma_0 \sum_q e_q^2 \int_\eta^1 \frac{d\xi}{\xi} \left\{ \frac{\alpha}{2\pi} \left(-\frac{1}{\hat{\epsilon}} + \log \frac{M_{\rm L}^2}{\mu_D^2} \right) z p_{\gamma q}(z) + \frac{\alpha}{2\pi} h(z) \right\} \xi f_q(\xi, \mu^2) . \tag{261}$$

As in Section 3.5, we can write the photon PDF, to first order in α in the $\overline{\rm MS}$ scheme as,

$$f_\gamma(\eta, \mu^2) = \int_\eta^1 \frac{d\xi}{\xi} \left(\frac{\alpha}{2\pi}\right) \left[-\frac{1}{\hat{\epsilon}} - \log \left(\frac{\mu_D^2}{\mu^2}\right) \right] \sum_q P_{\gamma q} \left(\frac{\eta}{\xi}\right) f_q \left(\xi, \mu^2\right) , \tag{262}$$

or, multiplying by $\eta = z\xi$,

$$\eta f_\gamma(\eta, \mu^2) = \int_\eta^1 \frac{d\xi}{\xi} \left(\frac{\alpha}{2\pi}\right) \left[-\frac{1}{\hat{\epsilon}} - \log \left(\frac{\mu_D^2}{\mu^2}\right) \right] \sum_q z P_{\gamma q} \left(z\right) \xi f_q \left(\xi, \mu^2\right) . \tag{263}$$

Thus,

$$\begin{aligned} \sigma^{(1)} &= \sum_q \int_\eta^1 d\xi \hat{\sigma}^{(1)} f_q(\xi, \mu^2) = \sigma_0 \times \eta f_\gamma(\eta, \mu^2) \\ &+ \sigma_0 \int_\eta^1 \frac{d\xi}{\xi} \frac{\alpha}{2\pi} \left\{ \log \frac{M_{\rm L}^2}{\mu^2} z p_{\gamma q}(z) + h(z) \right\} \times \sum_q e_q^2 \xi f_q(\xi, \mu^2) . \end{aligned} \tag{264}$$

Recalling that to leading order $F_2(x, \mu^2) = \sum_q e_q^2 x f_q(x, \mu^2)$, we can write the above expression as,

$$\sigma^{(1)} = \sigma_0 \left\{ \eta f_\gamma(\eta, \mu^2) + \int_\eta^1 \frac{dz}{z} \frac{\alpha(\mu^2)}{2\pi} \left[\log \frac{M_{\rm L}^2 (1-z)^2}{z \mu^2} z p_{\gamma q}(z) - 2 + 3z \right] F_2 \left(\frac{\eta}{z}, \mu^2\right) . \right\} \tag{265}$$

The rightmost diagram in Figure 39 involving an on-shell photon, is zero in the $\overline{\rm MS}$ scheme with massless fermions. In any case, we would not contribute to the hadronic tensor, as it's one-photon reducible. Thus, Eq. (265) is our final parton-model result.

7.2.3 Combination of the general and parton-model expressions

Expressions in Eq (253) and Eq. (265) represent the same cross section, so they are equal. By equating the two,

$$\sigma^{\text{parton model}} = \sigma^{\text{general}} \, ,$$

we see that the front factors σ_0 as well as $\log(M_{\text{L}}^2(1-z)^2)/(z\mu^2)$ terms cancel. What is left is,

$$\boxed{\begin{aligned} \eta f_\gamma(\eta,\mu^2) = {} & \frac{1}{2\pi\alpha(\mu^2)} \int_\eta^1 \frac{dz}{z} \int_{\frac{M_{\text{p}}^2\eta^2}{1-z}}^{\frac{\mu^2}{1-z}} \frac{dQ^2}{Q^2} \alpha^2(Q^2) \left[-z^2 F_L\left(\frac{\eta}{z}, Q^2\right) \right. \\ & \left. + \left(z p_{\gamma q}(z) + \frac{2\eta^2 M_{\text{p}}^2}{Q^2} \right) F_2\left(\frac{\eta}{z}, Q^2\right) \right] - \frac{\alpha(\mu^2)}{2\pi} \int_\eta^1 \frac{dz}{z} \left[z^2 F_2\left(\frac{\eta}{z}, \mu^2\right) \right] \, . \end{aligned}} \qquad (266)$$

This is the final result for the photon distribution. It does not depend on any of the parameters of the considered BSM process. This is how it must be as required by the universality of the PDFs. We see that if we know the structure functions F_2 and F_L accurately enough, we also know the photon content of the proton. This formula is included as a theoretical constraint e.g. in the recenr NNPDF3.1luxQED [51] global fit of PDFs.

7.3 Photons in global fits

To evaluate Eq. (266) numerically, one needs to consider a wide range in x and Q^2. However, all regions are either covered by data or they can be computed from PDFs, as illustrated in Figure 40. Note that there are contributions from low-W resonanace region, $(M_{\text{p}} + M_\pi)^2 < W^2 < 3.5\,\text{GeV}^2$, low-$W$ continuum $W^2 > 3.5\,\text{GeV}^2$, as well as the elastic region $F_{2,L}(x=1, Q^2)$. As shown in Figure 40, it's necessary to account for all these regions. The additional theory constraint of Eq. (266) leads to a significantly more precise photon PDF that when it's extracted directly from the data by conventional methods. Figure 41 shows the effect within the context of NNPDF3.1 global analysis. The fraction of the proton's momentum carried by the photon is always small, $< 1\%$, see Figure 42. As already discussed, the contributions of photon-photon channels can become important in particular at high-invariant masses – some examples are shown in Figure 43.

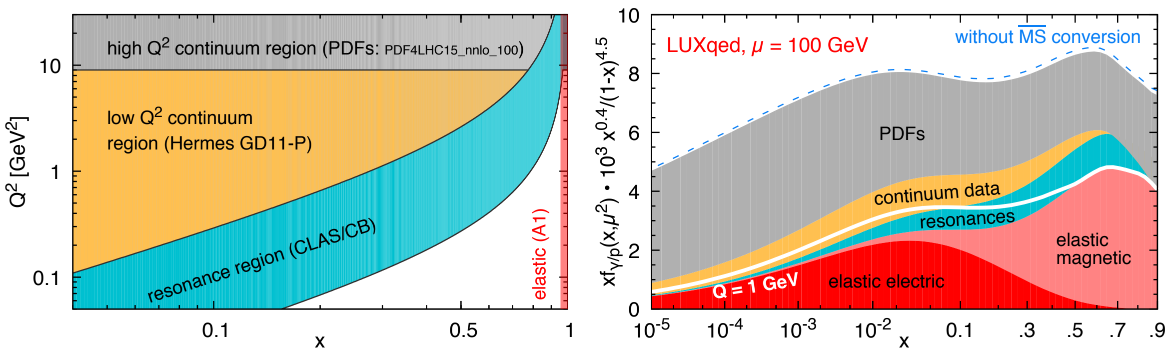

Figure 40: Figure from Ref. [49].

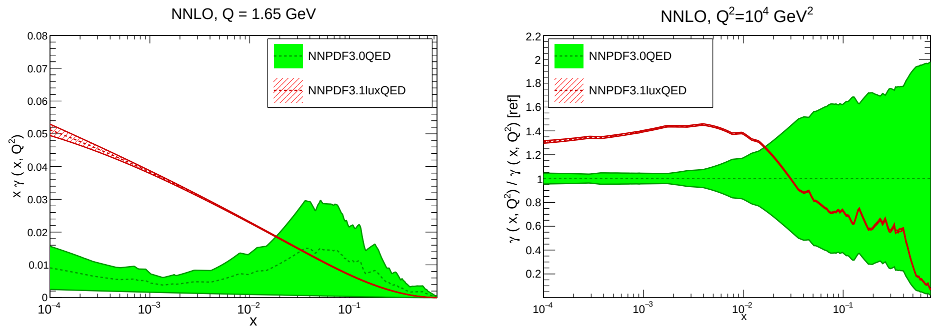

Figure 41: Photon PDF and its uncertainty in NNPDF3.0 and NNPDF3.1luxQED fits. The latter one includes the theory input of Eq. (266). Figure from Ref. [51].

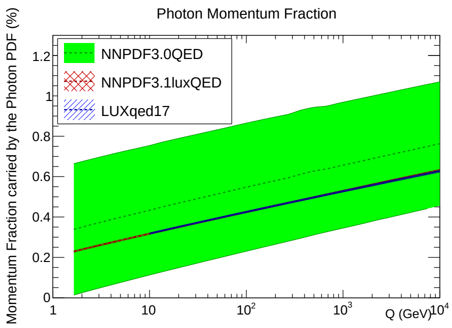

Figure 42: Momentum of the proton carried by the photons. Figure from Ref. [51].

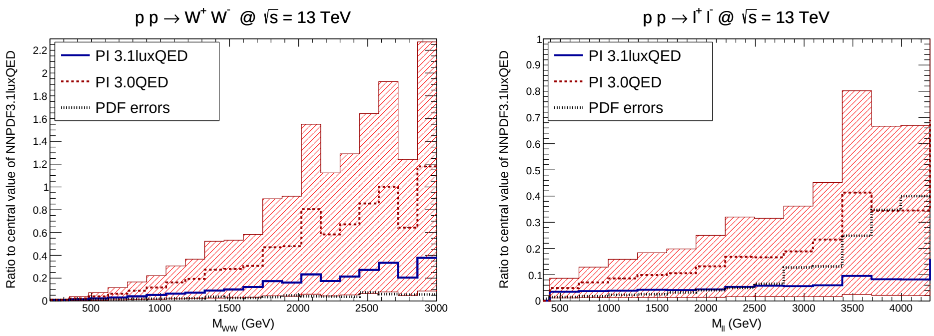

Figure 43: Contributions of $\gamma + \gamma$ initial state at high invariant mass. Figure from Ref. [51].

References

[1] R. P. Feynman, Phys. Rev. Lett. **23** (1969) 1415. doi:10.1103/PhysRevLett.23.1415

[2] J. D. Bjorken and E. A. Paschos, Phys. Rev. **185** (1969) 1975. doi:10.1103/PhysRev.185.1975

[3] Phys. Rev. D 98, 030001 (2018).

[4] R. Brock *et al.* [CTEQ Collaboration], Rev. Mod. Phys. **67** (1995) 157. doi:10.1103/RevModPhys.67.157

[5] V. V. Sudakov, Sov. Phys. JETP **3** (1956) 65 [Zh. Eksp. Teor. Fiz. **30** (1956) 87].

[6] Y. L. Dokshitzer, Sov. Phys. JETP **46** (1977) 641 [Zh. Eksp. Teor. Fiz. **73** (1977) 1216];

[7] V. N. Gribov and L. N. Lipatov, Yad. Fiz. **15** (1972) 781 [Sov. J. Nucl. Phys. **15** (1972) 438];

[8] V. N. Gribov and L. N. Lipatov, Yad. Fiz. **15** (1972) 1218 [Sov. J. Nucl. Phys. **15** (1972) 675];

[9] G. Altarelli and G. Parisi, Nucl. Phys. B **126** (1977) 298. doi:10.1016/0550-3213(77)90384-4

[10] D. J. Pritchard and W. J. Stirling, Nucl. Phys. B **165** (1980) 237. doi:10.1016/0550-3213(80)90086-3

[11] W. J. Stirling, DAMTP 79/5.

[12] R. D. Field, Front. Phys. **77** (1989) 1.

[13] M. Kaku, New York, USA: Oxford Univ. Pr. (1993) 785 p

[14] W. Furmanski and R. Petronzio, Phys. Lett. **97B** (1980) 437. doi:10.1016/0370-2693(80)90636-X

[15] G. Curci, W. Furmanski and R. Petronzio, Nucl. Phys. B **175** (1980) 27. doi:10.1016/0550-3213(80)90003-6

[16] A. Vogt, S. Moch and J. A. M. Vermaseren, Nucl. Phys. B **691** (2004) 129 doi:10.1016/j.nuclphysb.2004.04.024 [hep-ph/0404111].

[17] S. Moch, J. A. M. Vermaseren and A. Vogt, Nucl. Phys. B **688** (2004) 101 doi:10.1016/j.nuclphysb.2004.03.030 [hep-ph/0403192].

[18] J. Davies, A. Vogt, B. Ruijl, T. Ueda and J. A. M. Vermaseren, Nucl. Phys. B **915** (2017) 335 doi:10.1016/j.nuclphysb.2016.12.012 [arXiv:1610.07477 [hep-ph]].

[19] M. Bonvini, S. Marzani and T. Peraro, Eur. Phys. J. C **76** (2016) no.11, 597 doi:10.1140/epjc/s10052-016-4445-6 [arXiv:1607.02153 [hep-ph]].

[20] H. Abramowicz *et al.* [H1 and ZEUS Collaborations], Eur. Phys. J. C **75** (2015) no.12, 580 doi:10.1140/epjc/s10052-015-3710-4 [arXiv:1506.06042 [hep-ex]].

[21] R. D. Ball, V. Bertone, M. Bonvini, S. Marzani, J. Rojo and L. Rottoli, Eur. Phys. J. C **78** (2018) no.4, 321 doi:10.1140/epjc/s10052-018-5774-4 [arXiv:1710.05935 [hep-ph]].

[22] R. K. Ellis, H. Georgi, M. Machacek, H. D. Politzer and G. G. Ross, Nucl. Phys. B **152** (1979) 285. doi:10.1016/0550-3213(79)90105-6

[23] J. C. Collins, D. E. Soper and G. F. Sterman, Adv. Ser. Direct. High Energy Phys. **5** (1989) 1 doi:10.1142/9789814503266_0001 [hep-ph/0409313].

[24] D. Stump, J. Huston, J. Pumplin, W. K. Tung, H. L. Lai, S. Kuhlmann and J. F. Owens, JHEP **0310** (2003) 046 doi:10.1088/1126-6708/2003/10/046 [hep-ph/0303013].

[25] C. Adloff *et al.* [H1 Collaboration], Eur. Phys. J. C **13** (2000) 609 doi:10.1007/s100520000316 [hep-ex/9908059].

[26] C. Adloff *et al.* [H1 Collaboration], Eur. Phys. J. C **21** (2001) 33 doi:10.1007/s100520100720 [hep-ex/0012053].

[27] R. D. Ball and S. Forte, Phys. Lett. B **335** (1994) 77 doi:10.1016/0370-2693(94)91561-X [hep-ph/9405320].

[28] R. D. Ball and S. Forte, Phys. Lett. B **336** (1994) 77 doi:10.1016/0370-2693(94)00956-2 [hep-ph/9406385].

[29] M. Gluck and E. Reya, Phys. Lett. **83B** (1979) 98. doi:10.1016/0370-2693(79)90898-0

[30] W. K. Tung, H. L. Lai, A. Belyaev, J. Pumplin, D. Stump and C.-P. Yuan, JHEP **0702** (2007) 053 doi:10.1088/1126-6708/2007/02/053 [hep-ph/0611254].

[31] V. Bertone *et al.* [The xFitter Developers Team], Eur. Phys. J. C **77** (2017) no.12, 837 doi:10.1140/epjc/s10052-017-5407-3 [arXiv:1707.05343 [hep-ph]].

[32] P. M. Nadolsky and W. K. Tung, Phys. Rev. D **79** (2009) 113014 doi:10.1103/PhysRevD.79.113014 [arXiv:0903.2667 [hep-ph]].

[33] L. A. Harland-Lang, A. D. Martin, P. Motylinski and R. S. Thorne, Eur. Phys. J. C **75** (2015) no.5, 204 doi:10.1140/epjc/s10052-015-3397-6 [arXiv:1412.3989 [hep-ph]].

[34] R. D. Ball *et al.* [NNPDF Collaboration], Eur. Phys. J. C **77** (2017) no.10, 663 doi:10.1140/epjc/s10052-017-5199-5 [arXiv:1706.00428 [hep-ph]].

[35] P. Paakkinen, arXiv:1802.05927 [hep-ph].

[36] J. Gao *et al.*, Phys. Rev. D **89** (2014) no.3, 033009 doi:10.1103/PhysRevD.89.033009 [arXiv:1302.6246 [hep-ph]].

[37] D. Stump, J. Pumplin, R. Brock, D. Casey, J. Huston, J. Kalk, H. L. Lai and W. K. Tung, Phys. Rev. D **65** (2001) 014012 doi:10.1103/PhysRevD.65.014012 [hep-ph/0101051].

[38] S. Albino, B. A. Kniehl and G. Kramer, Nucl. Phys. B **803** (2008) 42 doi:10.1016/j.nuclphysb.2008.05.017 [arXiv:0803.2768 [hep-ph]].

[39] S. Chatrchyan *et al.* [CMS Collaboration], Phys. Rev. D **87** (2013) no.11, 112002 Erratum: [Phys. Rev. D **87** (2013) no.11, 119902] doi:10.1103/PhysRevD.87.112002, 10.1103/PhysRevD.87.119902 [arXiv:1212.6660 [hep-ex]].

[40] P. M. Nadolsky, H. L. Lai, Q. H. Cao, J. Huston, J. Pumplin, D. Stump, W. K. Tung and C.-P. Yuan, Phys. Rev. D **78** (2008) 013004 doi:10.1103/PhysRevD.78.013004 [arXiv:0802.0007 [hep-ph]].

[41] G. D'Agostini, Nucl. Instrum. Meth. A **346** (1994) 306. doi:10.1016/0168-9002(94)90719-6

[42] H. Paukkunen and P. Zurita, JHEP **1412** (2014) 100 doi:10.1007/JHEP12(2014)100 [arXiv:1402.6623 [hep-ph]].

[43] J. Pumplin, D. Stump, R. Brock, D. Casey, J. Huston, J. Kalk, H. L. Lai and W. K. Tung, Phys. Rev. D **65** (2001) 014013 doi:10.1103/PhysRevD.65.014013 [hep-ph/0101032].

[44] P. M. Nadolsky and Z. Sullivan, eConf C **010630** (2001) P510 [hep-ph/0110378].

[45] K. J. Eskola, P. Paakkinen, H. Paukkunen and C. A. Salgado, Eur. Phys. J. C **77** (2017) no.3, 163 doi:10.1140/epjc/s10052-017-4725-9 [arXiv:1612.05741 [hep-ph]].

[46] K. Kovarik *et al.*, Phys. Rev. D **93** (2016) no.8, 085037 doi:10.1103/PhysRevD.93.085037 [arXiv:1509.00792 [hep-ph]].

[47] R. D. Ball *et al.* [NNPDF Collaboration], Nucl. Phys. B **877** (2013) 290 doi:10.1016/j.nuclphysb.2013.10.010 [arXiv:1308.0598 [hep-ph]].

[48] G. Aad *et al.* [ATLAS Collaboration], JHEP **1608** (2016) 009 doi:10.1007/JHEP08(2016)009 [arXiv:1606.01736 [hep-ex]].

[49] A. Manohar, P. Nason, G. P. Salam and G. Zanderighi, Phys. Rev. Lett. **117** (2016) no.24, 242002 doi:10.1103/PhysRevLett.117.242002 [arXiv:1607.04266 [hep-ph]].

[50] A. V. Manohar, P. Nason, G. P. Salam and G. Zanderighi, JHEP **1712** (2017) 046 doi:10.1007/JHEP12(2017)046 [arXiv:1708.01256 [hep-ph]].

[51] V. Bertone *et al.* [NNPDF Collaboration], SciPost Phys. **5** (2018) 008 doi:10.21468/SciPostPhys.5.1.008 [arXiv:1712.07053 [hep-ph]].